UiT The Arctic University of Norway

Faculty of Health Science
Department of Clinical Medicine

Advanced methods in reproductive medicine: Application of optical nanoscopy, artificial intelligence-assisted quantitative phase microscopy and mitochondrial DNA copy numbers to assess human sperm cells

Daria Popova

A dissertation for the degree of Philosophiae Doctor – October 2021

Advanced methods in reproductive medicine: Application of optical nanoscopy, artificial intelligence-assisted quantitative phase microscopy and mitochondrial DNA copy numbers to assess human sperm cells

Daria Popova

A dissertation for the degree of Philosophiae Doctor

Women's Health & Perinatology Research Group
Department of Clinical Medicine
Faculty of Health Science

UiT − The Arctic University of Norway

Tromsø
2021

Acknowledgments

The PhD project was carried out at the Department of Clinical Medicine, Faculty of Health Sciences, and at the Department of Physics and Technology, Faculty of Science and Technology, UiT – The Arctic University of Norway. The UiT Tematiske satsinger program fully funded the research for this project.

This interdisciplinary work is a result of the collaboration of many different people. First and foremost, I would like to thank the supervisory team – **Professor Purusotam Basnet, Professor Ganesh Acharya** and **Professor Balpreet Singh Ahluwalia** – who provided me the opportunity to participate in this work, mentored, and supported me throughout the way of my PhD.

धन्यवाद

I am very thankful to all members of the *wonderful* nanoscopy research group at the UiT. Especially I am profoundly grateful to my closest collaborators: **Ida Oppstad, Vishesh Dubey** and **Ankit Butola,** for their invaluable contributions to this work. It was a great experience to work with you! Thank you for giving me the feeling of cooperativeness and fellowship during and after the research process. My special thank goes to researcher **Deanna Wolfson** for her supportiveness and high expertise in imaging systems.

I wish to express my gratitude to all the Women's Health & Perinatology Research Group members. Special thanks to my lab angel – senior engineer **Åse Vårtun.** Åse, you encouraged me every day with your sunny smile. I am immensely grateful for all the help you gave me during this project! I am extremely grateful to **Mona Nystad** and **Veronika Franeková** for their willingness to help and support me by a good word anytime. I would also like to thank **Dr. Martha Hentemann** and bioengineers: **Ms. Sissel A. Hansen, Ms. Inger K. Olaussen** and **Ms. Sylvi Johansen** at the IVF Clinic, University Hospital of North Norway, Tromsø, for coordinating with the patients.

Sincere thanks to my co-author **Dr. Priya Bride, Dr. Francesco D'Antonio** and senior academic librarian **Eirik Reierth** for their helping hand in the intricate field of systematic review and meta-analysis.

I would like to express my gratitude to **Professor Natasa Škalko-Basnet** and **Dr. Mona Nystad** for valuable comments and proof-reading on the draft of my thesis.

I am thankful to my former colleagues from The International Centre for Reproductive Medicine in St. Petersburg (ICRM), Russia. Thank you for all expertise and skills in the area of male fertility assessment you gave me during the work at your centre.
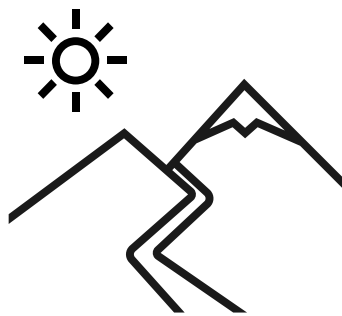
I am profoundly grateful to my former supervisors from the Faculty of Biology, St. Petersburg State University – **Alla Krasikova** and **Natalia Velichko** – my first invaluable teachers. Thank you for giving me a grounding for the rest of my life.

Last but not least, I would express my sincere gratitude to all my friends and family in Norway, Russia, Ukraine and Sweden. Thank you for making my life meaningful!

June 2021, Tromsø   Daria Popova

Table of Contents

List of Figures

List of Tables

Abbreviations

AI	Artificial Intelligence
AOT	Oligoasthenoteratospermia
ART	Assisted Reproductive Technologies
BFM	Bright-Field Microscopy
BSA	Bovine Serum Albumin
CCD	Charge-Coupled Device
CNNs	Convolutional Neural Networks
DGC	Density Gradient Separation
DHM	Digital Holographic Microscopy
DNA	Deoxyribonucleic Acid
DNNs	Deep Neural Networks
EDCs	Endocrine-Disrupting Chemicals
HA	Hyaluronic Acid
ICSI	Intracytoplasmic Sperm Injection
IMSI	Intracytoplasmic Morphologically Selected Sperm Injection
IVF	*In Vitro* Fertilization
MACS	Magnetic Activated Cell Sorting
MSOME	Motile Sperm Organelle Morphology Examination
mtDNAcn	Mitochondrial DNA copy numbers
NP	Non-Progressive Motility
OPD	Optical Path Delay
PICS	Phase Imaging with the Computational Specificity
PICSI	Physiological Intracytoplasmic Sperm Injection
PBS	Phosphate-Buffered Saline
PFA	Paraformaldehyde

PR	Progressive Motility
PSC-DHM	Partially Spatially Coherent Digital Holographic Microscope
RT	Room Temperature
ROS	Reactive Oxygen Species
QPM	Quantitative Phase Microscopy
SIM	Structured Illumination Microscopy
STORM	Stochastic Optical Reconstruction Microscopy
SUZI	Subzonal Insemination Technique
SVM	Support Vector Machine
TIRF	Total Internal Reflection Fluorescence
VAP	Average Path Velocity
VCL	Curvilinear Velocity
VSL	Straight-Line Velocity
WHO	World Health Organization

Glossary

Artificial intelligence

An advanced form of predictive computing commonly used in modern technologies.

Asthenospermia

Percentage of progressively motile spermatozoa below the lower reference limit.

Azoospermia

No spermatozoa in the ejaculate.

Coherent light beams

Beams with identical frequency and waveform.

Dry mass

The density of the cell's non-aqueous content, mainly the proteins, carbohydrates and lipids.

Interference

A phenomenon in which two waves superpose to form a resultant wave of greater, lower, or the same amplitude.

Oligoasthenoteratospermia

Percentages of both progressively motile and morphologically normal spermatozoa below the lower reference limits.

Oligospermia

Total number (or concentration, depending on outcome reported) of spermatozoa below the lower reference limit.

Super-Resolution Microscopy (Nanoscopy)

Optical microscopy that has a resolution on the order of 100 nm or below.

Refractive Index

Measure in optics describes how fast light travels through the material.

Teratospermia

Percentage of morphologically normal spermatozoa below the lower reference limit.

List of Papers

Paper I

Opstad*, I. S., **Popova*, D. A.,** Acharya, G., Basnet, P. & Ahluwalia, B. S. (2018). Live-cell imaging of human spermatozoa using structured illumination microscopy. *Biomedical Optics Express*, *9*(12), 5939-5945.

*Equally contributed

Paper II

Dubey*, V., **Popova*, D.,** Ahmad, A., Acharya, G., Basnet, P., Mehta, D. S. I. & Ahluwalia, B. S. (2019). Partially spatially coherent digital holographic microscopy and machine learning for quantitative analysis of human spermatozoa under oxidative stress condition. *Scientific Reports*, *9*, Article 3564.

*Equally contributed

Paper III

Butola*, A., **Popova*, D.,** Prasad, D. K., Ahmad, A., Habib, A., Tinguely, J. C., Basnet, P., Acharya, G., Senthilkumaran, P., Mehta, D. S. & Ahluwalia, B. S. (2020). High spatially sensitive quantitative phase imaging assisted with deep neural network for classification of human spermatozoa under stressed condition. *Scientific Reports*, *10*(1), Article 13118.

*Equally contributed

Paper IV

Popova*, D., Bhide*, P., D'Antonio, F., Basnet, P. & Acharya, G. (2021). Sperm mitochondrial DNA copy numbers in normal and abnormal semen analysis: a systematic review and meta-analysis (submitted manuscript).

*Equally contributed

Abstract

Declined fertility rate and population is a matter of serious concern, especially in the developed nations. Assisted Reproductive Technologies (ART), including *in vitro* fertilization (IVF), have provided great hope for infertility treatment and maintaining population growth and social structure. With the help of ART, more than 8 million babies have already been born so far. Despite the worldwide expansion of ART, there is a number of open questions on the IVF success rates. Male factors for infertility contribute equally as female factors, however, male infertility is primarily focused on the "semen quality". Therefore, the search of new semen parameters for male fertility evaluation and the exploration of the optimal method of sperm selection in IVF have been included among the top 10 research priorities for male infertility and medically assisted reproduction. The development of imaging systems coupled with image processing by Artificial Intelligence (AI) could be the revolutionary step for semen quality analysis and sperm cell selection in IVF procedures.

For this work, we applied optical nanoscopy technology for the analysis of human spermatozoa, i.e., label-based Structured Illumination Microscopy (SIM) and non-invasive Quantitative Phase Microscopy (QPM). The SIM results demonstrated a prominent contrast and resolution enhancement for subcellular structures of living sperm cells, especially for mitochondria-containing midpiece, where features around 100 nm length-scale were resolved. Further, non-labeled QPM combined with machine learning technique revealed the association between gradual progressive motility loss and the morphology changes of the sperm head after external exposure to various concentrations of hydrogen peroxide. Moreover, to recognize healthy and stress-affected sperm cells, we applied Deep Neural Networks (DNNs) to QPM images achieving an accuracy of 85.6% on a dataset of 10,163 interferometric images of sperm cells. Additionally, we summarized the evidence from published literature regarding the association between mitochondrial DNA copy numbers (mtDNAcn) and semen quality.

To conclude, we set up the high-resolution imaging of living human sperm cells with a remarkable level of subcellular structural details provided by SIM. Next, the morphological changes of sperm heads resulting from peroxidation have been revealed by QPM, which may not be explored by microscopy currently used in IVF settings. Besides, the implementation of DNNs for QPM image processing appears to be a promising tool in the automated classification and selection of sperm cells during IVF procedures. Moreover, the results of our meta-analysis showed an association of mtDNAcn in human sperm cells and semen quality, which seems to be a relevant sperm parameter for routine clinical practice in male fertility assessment.

11

1 INTRODUCTION

1.1 Semen quality

The term «semen» (from the Greek σπέρμα – «seed») refers to ejaculated material comprising a seminal fluid and haploid spermatozoa. The semen quality is a measure of male fertility and is defined by several parameters, including spermatozoa morphology. The mature human sperm cell consists of a head, neck, a midpiece containing the mitochondrial sheath with approximately 10-14 spirals of mitochondria and the longest part – tail (Figure 1). The sperm head includes a nucleus with highly compacted DNA and a cap-like structure called the acrosome, which contains enzymes necessary for the fertilization process (Pitnick *et al.,* 2009).

Figure 1 The structure of human spermatozoon.

(1) The sperm head of a human spermatozoon, **(2)** neck, **(3)** midpiece containing the mitochondrial sheath, **(4)** tail, **(5)** the end piece. **(A)** The acrosome and **(B)** nucleus region. The image was acquired by three-dimensional refractive index tomography.

Since the first study of spermatozoa led by the Dutch businessman and scientist Anton van Leeuwenhoek using a single-lens microscope in 1676, sperm cells appeared to be one of the remarkable cells in the human body with a specific structure conditioned by its pivotal function (Birkhead & Montgomerie 2009). The active development and implementation of medically assisted reproduction have made sperm cell research particularly important in male fertility assessment and infertility treatment.

1.1.1 Assessment of semen quality

Semen analysis is a part of male reproductive health investigation widely and routinely used in fertility assessment. The World Health Organization (WHO) criteria have been considered a gold standard of semen quality analysis since 1980. The lower reference limits of semen measures were revised and scaled-down three times in 1987, 1992 and 2010 (Cooper *et al.*, 2010). The trend is explained by the gradual decline of semen parameters over the last decades due to various reasons (Virtanen *et al.*, 2017). Male reproductive problems such as impaired spermatogenesis, decreased testosterone production, cryptorchidism and testicular cancer may result in reduced semen parameters, which are essential predictors of male fecundity (Skakkebaek *et al.*, 2016). According to the last WHO criteria (2010), the corresponding lower values for the main clinical parameters are listed in Table 1. These reference values reflect the semen parameters of men having children, and thresholds are used to classify patients as subfertile or infertile.

Table 1 Lower reference limits for semen analyses (WHO 2010).

Parameter	Reference value
Semen volume	1.5 ml
Total sperm count	39 million cells per semen volume
Sperm concentration	15 million cells/ml
Progressive motility	32%
Total motility	40%
Vitality	58% of live cells
Morphology	4% of normal form

Following the recommendations of the WHO group on male infertility, which were presented to the WHO Steering Committee Meeting for Guidelines and Nomenclatures in September 2015, the assessment of several semen parameters is a more convenient predictor of male fertility status in comparison to a single parameter (Barratt *et al.*, 2017). Moreover, the high quality of evidence suggests that: *"a single ejaculate is sufficient to establish the most appropriate investigation and treatment pathway. However, a semen analysis can be repeated if one or more abnormalities are found"* (Barratt *et al.*, 2017).

1.1.2 The global decline in semen quality parameters

One of the well-defined and generalized reports on the significant decrease in semen measures was put forward by Carlsen and colleagues (1992). The decrease of seminal volume (3.40 ml to 2.75 ml) and mean sperm cell concentration (113×10^6/ml to 66×10^6/ml) has been shown between 1940 and 1990 from publications covering 20 countries (Carlsen *et al*., 1992). The included studies vary based on analyzed semen parameters, analysis methods, study population, and potential interfering factors. Participants could be healthy or infertile/subfertile partners of infertile/fertile women undergoing ART procedures, semen donors, or participants of unknown fertility. However, the heterogeneous population, including healthy and infertile patients, could result in the study's bias.

The historical review by Carlsen (1992) has initiated the avalanche of retrospective and newly collected prospective studies related to semen quality (Adamopoulous *et al*., 1996; Irvine *et al*., 1996; Younglai *et al*., 1998; Swan *et al*., 2000; Itoh *et al*., 2001; Geoffroy-Siraudin *et al*., 2012; Rolland *et al*., 2013). For instance, male fertility was assessed in the University Hospital of North Norway, Tromsø, from 1993 to 2012 (Basnet *et al*., 2016), where semen samples from 5739 men were analyzed as a part of routine clinical investigation of subfertile and infertile couples. Interestingly, the mean age of men among couples seeking ART treatment increased gradually during the study period from 32.0 years to 35.6 years. In addition, Basnet and colleagues found a gradual decrease in mean seminal fluid volume, mean sperm cell concentration and decrease in total sperm count per ejaculate (by 11.4%, 23.1% and 28.9%, respectively) between two decades of the study (1993-2002 and 2003-2013). Moreover, besides the increase in the number of oligozoospermic patients, the proportion of asthenozoospermic and azoospermic patients, who used ART for infertility treatment, increased dramatically during the study period.

Another study by Auger presents the semen analyses between 1973 and 1992 from healthy 1750 donors who had previously fathered at least one child (Auger *et al*., 1995). Most of the donors lived in the Paris area. In comparison to Basnet's (2016) study from Norway and Carlsen's study from Denmark (1992), seminal fluid's mean volume did not change during the study period. At the same time, the mean sperm concentration decreased from 89×10^6/ml in 1973 to 60×10^6/ml in 1992. Moreover, the level of motile and morphologically normal cells decreased by 0.6% and 0.5% per year, respectively (Auger *et al*., 1995).

The recent large-scale meta-regression analysis of Levine and colleagues (2017) collected information about sperm concentration and total sperm count from 6 continents and

50 countries between 1973 and 2011 (Levine *et al*., 2017). These data indicate a decline in sperm concentration (52.4%) and total sperm count (59.3%) of unselected men in Europe, North America, New Zealand and Australia over the study period. Notably, the analysis did not show the same trend for the studies from South America, Asia and Africa, resulting from limited statistical power or unexplained reasons behind the semen quality decline.

To sum up, over the past 30 years, numerous studies identified a significant decrease in semen quality. Although there is variability in semen parameters between countries, an evident trend of decreasing semen quality is presented. Future studies should be done to prove if this trend is stable or due to random fluctuations.

1.1.3 Probable reasons for adverse semen quality

During the last decades, an adverse trend in male reproductive health has been likely associated with multiple influences both prenatally and in adult life. Following the concept by Skakkebæk (2001), various disorders of the male reproductive system such as reduced semen quality, testicular cancer, testicular maldescent, hypospadias might be interrelated with each other through a testicular dysgenesis syndrome (Figure 2), which is associated with the fetal testis exposure to external adverse factors or resulted from genetic abnormalities (Skakkebæk *et al*., 2001).

There are three early periods in male developmental health that are important for the further normal development and function of reproduction: the intrauterine phase, the neonatal phase in the first months of life, and puberty (Ferlin 2020). An adverse effect acting through the mother during the pregnancy might interfere with normal fetus germ proliferation and differentiation. Thus, environmental pollutants such as endocrine-disrupting chemicals (EDCs) appear to affect the perinatal and adult testes negatively (Hauser *et al*., 2006; Sharpe 2010). EDCs include toxic stable organic pollutants (for ex. polychlorinated biphenyls and their pyrolytic products), non-persistent organic pollutants (phthalates), pesticides, which are known to affect male reproductive health (Dallinga *et al*., 2002; Martenies *et al*., 2013; Chiu *et al*., 2016).

Although environmental factors are one of the probable reasons for deteriorating semen quality (Sharpe *et al*., 1993; Nordkap *et al*., 2012; Bloom *et al*., 2015), the declined semen measures have been detected both in places with heavy industrial pollution (***Japan*** – Itoh *et al*., 2001; ***China*** – Liu *et al*., 2020) and places with little pollution (***France*** – Auger *et al*., 1995; ***Greece*** – Adamopoulos *et al*., 1996; ***United Kingdom*** – Irvine *et al*., 1996; ***Canada*** – Younglai

et al., 1998; ***Norway*** – Basnet *et al*., 2016). That may indirectly suggest the presence of other deteriorating factors to male reproductive health in addition to environmental reasons.
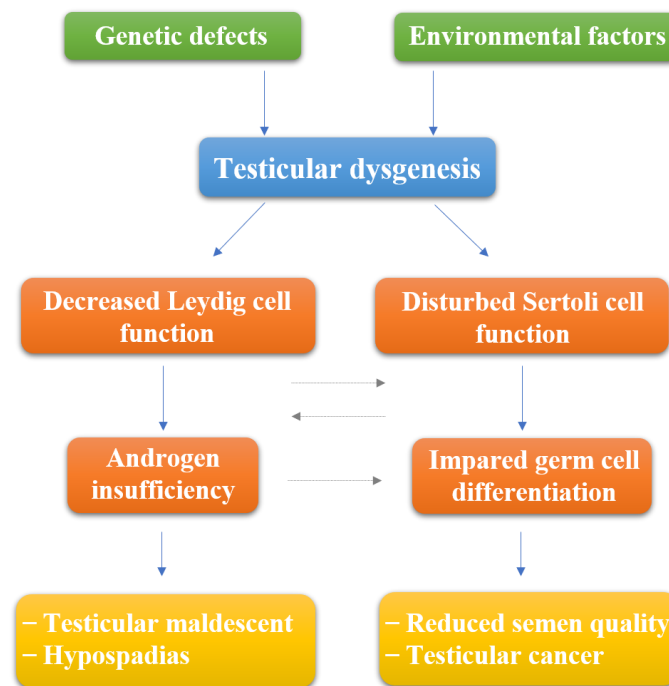
Figure 2 Schematic representation of pathogenic links between the components and clinical manifestations of testicular dysgenesis syndrome. Reduced semen quality could be linked by pathological mechanisms of testicular dysgenesis syndrome to increased incidence of testicular maldescent and hypospadias of newborns, along with testicular cancer of adults. The increased male reproductive health problem is most likely to be a result of genetic and environmental factors.

_____

This figure was adapted from *Human Reproduction*, 16(5), Skakkebaek N. E., Rajpert-De Meyts E. & Main K. M., Testicular dysgenesis syndrome: an increasingly common developmental disorder with environmental aspects, pp. 972-978, (2001).

During the adult period of life, the spermatogenic capacity can be affected by various lifestyle factors such as diet (Afeiche *et al*., 2013; Jensen *et al*., 2013), smoking (Sharma *et al*., 2016), sexually transmitted diseases (Gimenes *et al*., 2014) and obesity, which relates to increased risk of azoospermia and oligospermia (Sermondade *et al*., 2013). Psychological stress can also be included as a reason for worsening semen quality all around the world. For example, it has been shown by Li and colleagues (2011) that different forms of stress derived from job,

life events, or social support-related stress are connected with decreased sperm concentration, progressive motility and increased level of morphologically abnormal sperm forms (Li *et al*., 2011). Nordkap and colleagues (2016) categorize stress more in detail based on a self-reported survey from stress-related parts of the Copenhagen Psychological Questionnaire. The men were categorized as "being distressed," "having the problem in relaxing," "being irritated" and "being tense" all the time or four weeks before the survey. The men with the highest stress level had lower sperm concentration (38%), lower total sperm count (34%) and lower semen volume (15%) than men with medium stress level (Nordkap *et al*., 2016). It is notable that men from the highest stress group were smokers, used marijuana, consumed caffeine and had sexually transmitted diseases compared to men with low stress levels.

Several meta-analyses have revealed the association of reduced sperm motility and viability with acute exposure to radiofrequency fields of cellular phones (Adams *et al*., 2014; Liu et al., 2014). Using the Internet through Wi-Fi connection has also been reported to decrease semen quality (Avendano *et al*., 2012). It has been proposed that the possible reason for the adverse effect of mobile phone expose and wireless Internet is oxidative stress resulted in sperm nuclear DNA fragmentation (Avendano *et al*., 2012).

To conclude, male reproductive health problems can be conditioned by multiple reasons. Some external factors can influence the fertility potential reversibly such as sexual abstinence before the collection of the semen (Auger *et al*., 1995), heating, cigarette smoking, lifestyle and psychology. Other factors affect fertility irreversibly such as age (Auger *et al*., 1995), genetic status (Ferlin *et al*., 2007; Skakkebaek *et al*., 2016) and prenatal exposure to adverse environmental factors. For that reason, prevention of male infertility, starting with life's initial point – the conception, seems to be the most effective way to improve male reproductive health (Ferlin 2020).

1.2 Advances in male reproductive health and infertility treatment

Given the presented worldwide changes in semen quality, the question arises of whether these changes result in infertility. The WHO defines infertility as "*a disease of the reproductive system defined by the failure to achieve a clinical pregnancy after 12 months or more of regular unprotected sexual intercourse*". It has been established that half of a couple's infertility is conditioned by male factors such as poor semen quality, genetic syndromes, cryptorchidism and sexual disorders (Agarwal *et al*., 2021). The invention of ART gives infertile couples a chance to have a genetic offspring. Specifically, historical advances in male reproductive health

such as cryopreservation and Intracytoplasmic Sperm Injection (ICSI) have profoundly impacted the management of couples with male factor infertility.

1.2.1 Cryopreservation of sperm cells

Cryopreservation is a freezing technique to preserve both the genetic material as well as metabolic activity of cells and tissues after storage at extremely low temperatures. This technique has broad clinical applications, including the freezing of blood and cancerous tissue samples, stem cells of different origins for further therapy and autologous transplantations, mesenchymal stromal cells for regenerative medicine and tissue engineering (Jang *et al*., 2017).

Based on cryobiology achievements, human fertility preservation has been carried out as an effective ART service worldwide. For instance, cryopreservation of mature sperm cells is one of the first techniques implemented in the clinical practice providing fertility preservation of adult men (Bunge & Sherman, 1953). Specifically, adolescent men, young adults and adults undergoing chemotherapy or other cytotoxic fertility-dangerous medication can preserve their semen to have offspring in the future (Sanger *et al*., 1992; Rousset-Jablonski *et al*., 2016). Another group of patients who are recommended cryopreservation of sperm cells is azoospermic males undergoing testicular biopsy or aspiration of sperm from the epididymis or testicles (Gangrade, 2013). In addition, the cryopreservation of testicular tissue is a prospective method both for *in vitro* spermatogonial stem cell maturation and for direct autotransplantation of the tissue back into the patient's body after the effective treatment (Onofre *et al*., 2016). Moreover, biobanking has a profound application for the storage of cryopreserved semen of donors.

According to the previous reports, semen can be stored for decades with the subsequent fertilization capacity (Szell *et al*., 2013). Thawed semen can be used for Intrauterine Insemination (IUI), IVF or ICSI. The type of fertilization technique depends on the infertility origin and cryo survival rate of post-thawed semen. Following the concept of «partial survival», freezing and thawing processes lead to a decrease of more than 50% in motility parameters and survivance (Donnelly *et al*., 2001), ultrastructure and cell morphology changes (Woolley & Richardson 1978; Barthelemy 1990; Ozkavukcu *et al*., 2008), mitochondrial activity reduction (O'Connel *et al*., 2002) and damage of sperm DNA (Kopeika *et al*., 2015). The above-mentioned cell changes might be influenced by the cryoprotector, cryopreservation and thawing itself and most of all by characteristics of native semen, such as sperm cell motility and

concentration. Semen samples with a low survival rate are used for fertilization using the ICSI technique when an embryologist selects an individual cell for direct injection into the oocyte.

1.2.2 Intracytoplasmic Sperm Injection

1.2.2.1 Historical background

Until the development of ART, male infertility treatment was limited. For example, oligospermia cases were treated with increasing gonadotropin secretion to stimulate spermatogenesis. Most of the male fertility problems caused by inflammation and infection were medicated with antibiotics and anti-inflammatory drugs. Traditional medicine such as vitamins, herbs, minerals, and so forth was also used to improve semen quality (Kovacs 2020). At the beginning of the "ART era," subfertile men with the decreased number of motile sperms could achieve fertilization of the oocyte using **microdrops** of semen of moderate or mild quality (Figure 3a) (Svalander *et al.,* 1994). Building upon the microdrop technique, it was possible to inseminate the egg and get the first baby with a sperm obtained microsurgically from men with obstructive azoospermia (Temple-Smith *et al.,* 1985).
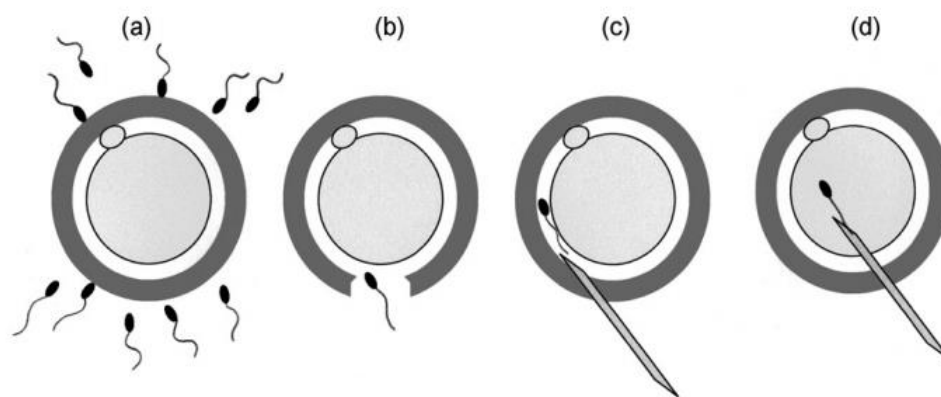
Figure 3 Different micromanipulation techniques to fertilize the egg. **(a)** Microdrop technique (standard IVF), **(b)** Zona Pellucida Drilling (ZD), and Partial Zona Pellucida Dissection (PZD), **(c)** Subzonal Insemination (SUZI) and **(d)** Intracytoplasmic Sperm Injection (ICSI).

_____

This figure was published in *Sperm biology: an evolutionary perspective*, In Birkhead T. R., Hosken D. J., Pitnick S. (Eds.). Pacey A. A., Sperm, human fertility and society, pp. 565-597, *Copyright Academic Press* (2009).

The next step in overcoming male infertility was micromanipulation procedures to achieve the fertilization with the semen of extremely low sperm concentration and motility (Figure 3b-d). For example, **Zona Pellucida (ZP) drilling** involved making a hole in the zona pellucida with subsequent incubation in a sperm suspension (Figure 3b) (Gordon *et al.,* 1988). However, the method did not work successfully in humans. During **Partial Zona Dissection (PZD),** a mechanical slit was made before incubation in a sperm suspension (Malter *et al.,* 1989). Another variant of micromanipulation was the **Subzonal Insemination Technique (SUZI**), involving the embedding of sperm cells into the perivitelline space in between zona pellucida and the oocyte membrane (Figure 3c) (Lawsking *et al.,* 1987; Svalander *et al.,* 1994). Sperms were treated before injection to enhance the acrosome reaction. SUZI was successfully applied on mice, and further, the first clinical trial was performed in humans at the Infertility Medical Centre in 1987 in Australia. The first birth with the help of SUZI-microinjection was reported in 1988 by Ng in Singapore (Kovacs 2020).

The following significant modification of microinjection was ICSI, introduced in 1991 in Brussels at the Centre for Reproductive Medicine of Vrije Universiteit Brussel (Figure 3d). The first ICSI was the failed SUZI case when a microinjector accidentally penetrated the oocyte membrane with one sperm cell. This procedure resulted in the birth of a child in 1992 (Palermo *et al.,* 1992). Further, the results after ICSI were more effective in comparison with SUZI. Due to this fact, the ICSI became the only microinjection technique used to successfully achieve pregnancy from men with severe semen abnormalities (Kovacs 2020).

1.2.2.2   Clinical recommendations to use ICSI

The International Committee for Monitoring Assisted Reproductive Technologies (ICMART) and The European Society of Human Reproduction and Embryology (ESHRE) reproductive organizations reported the increasing global use of ICSI constituting two-thirds of the total number of fresh ART cycles (Dyer *et al.,* 2016; Calhaz-Jorge *et al.,* 2017). Despite the original recommendations of using ICSI, there has been a rise in the use of ICSI for non-severe male factor infertility, non-male factor infertility and fertilization failures (Boulet *et al.,* 2015). For that reason, the American Society for Reproductive Medicine (ASRM) and the Society for Advanced Reproductive Technology (SART) state that ICSI should not be routinely performed for non-male factor infertility cases (Penzias *et al.,* 2020). The use of ICSI should be based on the following clinical evidences:

→ The severe factor of male subfertility such as autoimmune infertility.

→ Cases of failed conventional IVF due to impaired sperm function.

→ Patients with azoospermia who are subjected to surgical recovery of cells from the reproductive tract.

→ Cryopreservation in a limited quantity of sperm cells and decreased survival rate after thawing.

→ Upcoming preimplantation genetic screening. In that case, ICSI prevents contamination with surplus sperm cells attached to the zygote.

→ Fertilization with cryopreserved oocytes. Limited data exist that fusion of the sperm cell and the thawed oocyte might be compromised using conventional IVF (Gook & Edgar, 2007).

1.2.2.3 Effect of ICSI on long- and short-term health in offspring

There have been concerns about the adverse effects of assisted technologies on offspring's wellbeing. A substantial amount of meta-analyses and systematic reviews have demonstrated a link between fertility problems, cardiometabolic diseases and neurodevelopmental disorders among offspring conceived with the help of ART (Catford *et al.,* 2017; Rumbold *et al.,* 2017; Catford *et al.,* 2018; Bay *et al.,* 2019). For instance, Sandin and colleague's extensive spectrum analysis showed that severe male infertility with subsequent surgical sperm extraction increased the risk of mental retardation and autism in offspring (Sandin *et al.,* 2013). Moreover, the results of Berntsen's review (2019) revealed the increased risk of obstetric complications for ART pregnancies, such as hypertensive disorders in pregnancy, placental complications, gestational diabetes and medical interventions (Figure 4) (Berntsen *et al.,* 2019). Based on the Australian data, there is an increased risk of stillbirth, neonatal death, preterm birth, low birth weight and major birth defects using ART (Davies *et al.,* 2012; Marino *et al.,* 2014; Davies 2020).

It is important to note that the early ART protocols included transferring two or more embryos, affecting the reported perinatal outcomes. Presently, elective single embryo transfer is recommended to overcome the problems associated with multiple pregnancies and support maternity and neonatal health care (Martikainen *et al.,* 2001). However, it is still controversial whether the live birth defects of ART conceived children are due to infertility itself or the ART treatments (Figure 4).
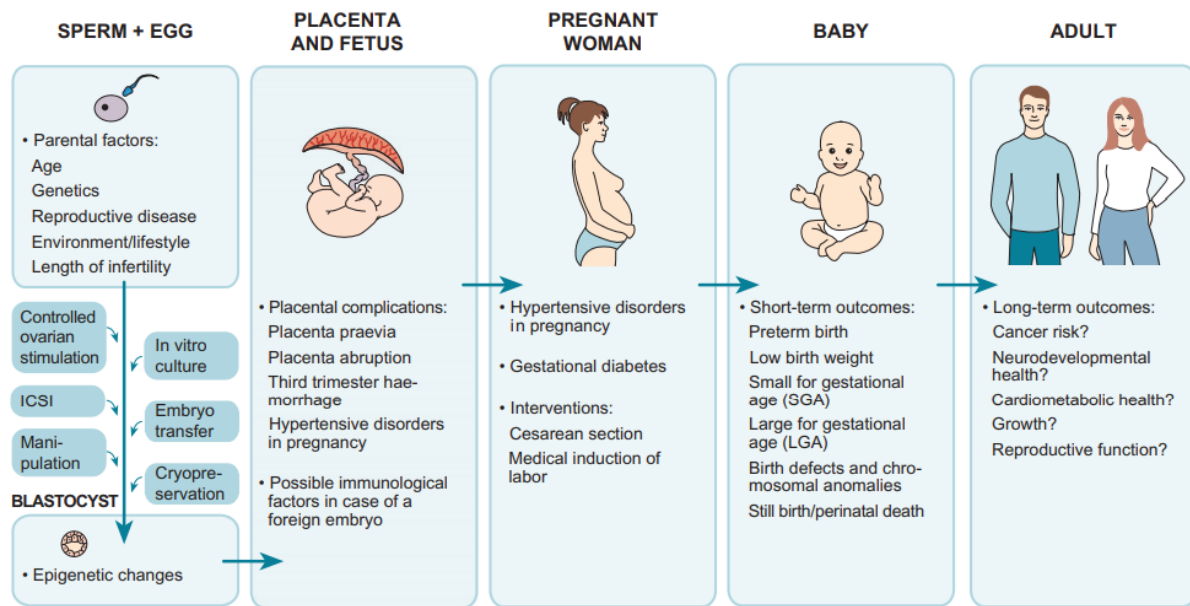
Figure 4 Factors affecting the short- and long-term health in offspring born after ART. The ART outcome is most likely to be a result of a combination of parental factors (age, genetics, reproductive disease, environment/lifestyle, length of infertility) and the ART itself (for ex. controlled ovarian stimulation, ICSI, *in vitro* culture, assisted hatching, trophectoderm biopsy, embryo transfer, cryopreservation). The short-term health effect of ART is manifested on antenatal and neonatal levels, including pregnant women's health. The data on the long-term effect of ART is still too limited to draw a robust conclusion.

_____

Interestingly, it has been reported by a limited number of studies that the fertility of ICSI conceived men is affected (Katagiri *et al.,* 2004; Palermo *et al.,* 2008; Belva *et al.,* 2016; Belva *et al.,* 2017; Rumbold *et al.,* 2019). For instance, the level of serum testosterone and free serum testosterone in ICSI conceived infant boys is decreased by 23% and 27%, respectively. In addition, a 60% reduction in the luteinizing hormone to testosterone ratio compared to infants conceived spontaneously has been detected (Kai *et al.,* 2007). Moreover, the reduced semen quality has been presented on the limited cohort of ICSI conceived males from Belgium at age 18-22 (Belva *et al.,* 2016; Rumbold *et al.,* 2019). In addition, Y-microdeletions are detected in

the ICSI offspring (Katagiri et al., 2004). Despite the presented findings, the adverse effect of ICSI on male fertility of conceived children needs to be confirmed in larger studies.

1.2.2.4   An overview of current sperm cell selection techniques for ICSI

One of the crucial steps in ART is cell selection, which aims to pick up the cell with the highest fertilizing potential. The proper cell selection may guarantee successful fertilization *in vitro,* embryo development and offspring wellbeing. In general, the spermatozoon of high fertilization capacity has a genome with proper integrity and intactness, progressive motility and normal morphology, ability to capacitate and express all of the necessary receptors and enzymes for oocyte fusion (Kravetz 2005). In the case of ICSI, sperm cell overcomes biological requirements essential in fertilization *in vivo*. Hence, the selection process in terms of ICSI is particularly important.

Numerous techniques for sperm cell selection have been introduced recently, but most of them are out of routine clinical use due to high expenses or manpower input (Sakkas 2013). In terms of cost and effectiveness, the optimized **Density Gradient Separation (DGC)** method is currently used for routine sperm purification purposes (Mortimer & Mortimer 2013). The DGC method is based on the high density of human spermatozoa, which is due to highly packaged DNA surrounded by a thin rim of cytoplasm to be remained after cytoplasm elimination during spermiogenesis. After centrifugation in a continuous density gradient, the cells with the greatest densities are placed to the densest layer (Aitken 2020). Another technique is the **swim-up** test based on spermatozoa's intrinsic motility and the ability to penetrate the dense extracellular matrices (Agarwal 2018). The swim-up process involves the layering of a hyaluronate solution, a component of cervical mucus, with subsequent incubation of an hour at 37 °C. Progressive sperm cells migrate directly from semen to medium leaving behind non-progressive cells, debris and somatic cells. Hence, this method has been reported to produce sperm suspension of high quality and motility.

In ICSI, the sperm selection is based on the motility and morphology assessment by conventional light microscope followed by the sperm selection with DGC or swim-up. At the same time, advanced sperm selection techniques are being assessed, which are based on sperm features different from motility and morphology. For example, **electrophoretic sperm separation** is a separation method premised on the negative charge of sperm cells migrating to the anode in the electric field (Ainsworth *et al.,* 2005; Aitken 2020). A separation membrane with a pore size of 5 µm provides the migration of sperm cells but no other cell types. The

constant applied current (75 mA) and a variable voltage (18-21 V) are applied to the reservoir with a semen sample and an electrophoresis buffer. It has been demonstrated that membrane-based electrophoresis is effective as the DGC method regarding isolation of cells with high motility and DNA integrity and lower leukocyte contamination level (Fleming 2008). Moreover, the electrophoretic method provides the minimum risk of oxidative stress because it does not imply centrifugation (Aitken 2020). Despite the apparent success of the electrophoretic method in the separation of high-quality spermatozoa, there were no significant differences in fertilization rate after using DGC-prepared spermatozoa and after sperm separation in the electric field (Fleming 2008).

Sperm-binding to hyaluronic acid (HA) is another method to check the functionality of the sperm cell shortly before fertilization by ICSI. The method is based on the capability of the spermatozoa to bind to the hyaluronic acid-rich matrix of the oocyte using specific receptors (Huszar *et al.,* 2007). The method is marketed as a Physiological Intracytoplasmic Sperm Injection (PICSI®) and SpermSlow® that differs from each other by using immobilized HA or suspended HA, respectively. In PICSI®, mature sperm cells bind to the HA, while the SpermSlow® technique slows down movements of the sperm cell. Several studies have estimated the effectiveness of the sperm-binding to the hyaluronic acid method regarding sperm quality and effects on ART outcome (Parmegiani *et al.,* 2010; Majumdar & Majumdar 2013; Erberelli *et al.,* 2017). The HA method gives less sperm DNA fragmentation compared to DGC. At the same time, it appeared to be no fertilization improvements and pregnancy rates (Beck-Fruchter *et al.,* 2016). More importantly, there is no increase in the likelihood of live birth (McDowell *et al.,* 2014).

Sperm cells with signs of apoptosis have a phosphatidylserine receptor exposed on the plasma membrane, which is an indicator of starting DNA degradation. This feature of sperm cells is used in **Magnetic-Activated Cell Sorting (MACS)** or non-apoptotic sperm selection. Apoptotic sperm cells, which externalize phosphatidylserine on the surface, bind to the annexin V-conjugated paramagnetic microbeads (Said and Land 2011). After the incubation with the microbeads, the sample is allowed to run through the magnet-containing column, leaving the apoptotic cells in the column. Due to the MACS can not eliminate somatic cells from the semen, an additional step of DGC centrifugation is used, which may be detrimental to the cells and sperm count (Said and Land 2011). It has been shown that combined MACS-DGS selects the cells with higher potential of mitochondrial membrane, decreased level of active caspase-3 and phosphatidylserine exposure, normal morphology and better DNA integrity compared with DGS only (Said *et al.,* 2005). However, the positive effect of the method on the ICSI outcomes

is controversial, as reported by several studies and summarized in a systematic review and meta-analysis (Gil *et al.,* 2013).

An advanced high optical magnification method of sperm selection was introduced in 2002 in Israel called **Intracytoplasmic Morphologically selected Sperm Injection (IMSI)** (Bartoov *et al.,* 2002) (Figure 5). In IVF laboratories, the micromanipulation system is equipped with optics giving magnification at ×400. At the same time, IMSI achieves magnification up to ×6600. For IMSI, sperm cells are prepared by routine washing techniques followed by imaging using an inverted light microscope equipped with Nomarski optics with ×100 oil-immersion objective. Finally, digital enhancement by using software is applied to obtain high magnification (Bartoov *et al.,* 2002).
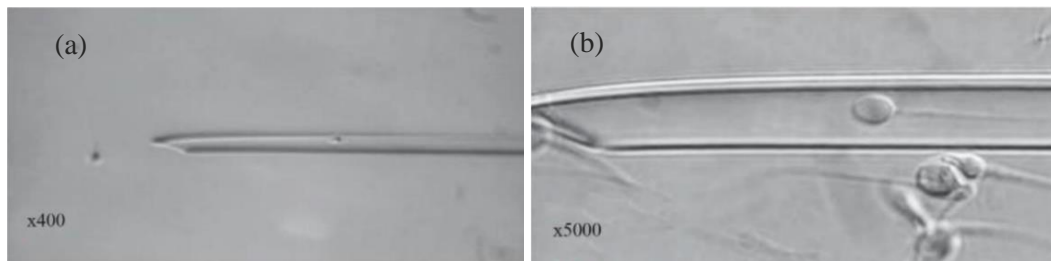
Figure 5 Microinjection pipettes containing sperm cells at different magnification. (a) The ICSI and **(b)** IMSI procedures at the magnification of ×400 and ×5000, respectively.
_____
This figure was published in *Journal of Reproduction & Infertility*, 21(1), Mangoli E., & Khalili M. A., The Beneficial Role of Intra Cytoplasmic Morphologically Selected Sperm Injection (IMSI) in Assisted Reproduction, pp. 3-10, *Open Access Article* (2020).

The **Motile Sperm Organelle Morphology Examination (MSOME)** is performed using IMSI setup to resolve subtle morphology changes in sperm structures such as the acrosome, nucleus, mitochondria, tail, neck and post acrosomal lamina (Berkovitz *et al.,* 2006a). Based on IMSI analysis, it has been shown that the presence of nuclear vacuoles in the sperm head, which conventional ICSI cannot detect, decreased pregnancy rate and increased abortion rate (Berkovitz *et al.,* 2006b). Moreover, a new grading system was established to assess the morphology of spermatozoa, considering the presence, number and size of vacuoles in the head (Bartoov *et al.,* 2002; Vanderzwalmen *et al.,* 2008).

1.3 Prospective methods of sperm cell selection and analysis in ART

Due to the selection of reproductive cells and embryos are performed mainly based on morphology, the development of imaging systems is one of the central issues in ART. Presently, IVF laboratories use differential interference contrast microscopy, phase-contrast microscopy by Zernike, and the Hoffman modulation contrast system (Mirsky *et al.,* 2016). All these methods generate contrast from local variations in refractive index across the cell and do not provide information about the deep morphology and structures of the sample (Hu and Popescu, 2019). Moreover, available 2D information overlaps with the optical aberrations, which might affect the analyzed morphological details. In this regard, IMSI was created to improve the outcome of IVF, as compared with the conventional ICSI. IMSI is an enhanced imaging technique enabling the resolution of subtle sperm morphological structures (Bartoov *et al.,* 2002). However, despite the enhanced magnification and reported success of pregnancy rates using IMSI, the technique is expensive and time-consuming. Moreover, the result of the meta-analysis on comparing the clinical outcomes between ICSI and IMSI does not support the use of IMSI due to the lack of conclusive evidence about live birth outcomes, risks of miscarriage and effect on clinical pregnancy (Teixeira *et al.,* 2013). Thus, new imaging techniques for cell morphology assessment in ART are under a continuous state of exploration. An alternative imaging solution for sperm selection and analysis is QPM, which has been successfully demonstrated to study sperm cell biology.

1.3.1 Quantitative Phase Microscopy

QPM is a method based on an optical phenomenon of interference providing 3D information about the specimen. The digital holography applied to QPM is called Digital Holographic Microscopy (DHM). In contrast to other imaging systems, QPM offers quantitative information about the optical thickness of the sample in a non-labeled manner. QPM has been thoroughly used in basic and clinical science due to its nanoscale sensitivity in 2D, 3D and 4D (time-resolved tomography) without invasion of the biological sample (Park *et al.,* 2018). For example, QPM has been implemented in cancer cells phenotyping (Kemper *et al.,* 2006), in blood cell screening providing information about morphological and biochemical parameters (Shaked *et al.,* 2011), in neurophotonics for the study of live neurons during electrical activity (Marquet *et al.,* 2014), in cell growth regulation of mammalian cells (Mir *et al.,* 2011) and in the analysis of the internal structures of the eukaryotic cell such as condensed

chromosomes in metaphase (Sung *et al.,* 2012). Besides, the combination of QPM with artificial intelligence is a promising tool for automated cell selection, which can be clinically applied in the future.

1.3.1.1 Basic principles of QPM

QPM offers quantitative information of the analyzed sample about information of the refractive index and the cell's local thickness. That means that the QPM data is directly related to the morphological changes of the cells, which cannot be analyzed by bright field microscopy (BFM) commonly used in ART. Basically, QPM records how much light is delayed when passing through the analyzed object. The optical path delay – OPD *(x, y)* is defined as refractive index changes into the sample:

$$OPD\ (x,\ y) = t\ (x,\ y)(n_c\text{-}n_s),$$

where *OPD (x, y)* – the optical path delay at each cell point, *t (x, y)* – the cell thickness, *$(n_c$-$n_s)$* refractive index variation between the cell and surrounding medium.

QPM makes it possible to measure this delay quantitatively and thus acquire an interferogram by recording the interference of the two superimposed coherent beams: one beam passing through the sample and another reference beam that does not come in contact with the object (Figure 6). An experimental setup can be equipped with a different light source, such as coherent laser light or incoherent white light. The hologram is usually acquired by the CCD camera (Charge-Coupled Device), which is a part of the digital holography microscopy system. The digital hologram (interferogram) is mathematically processed to the optical thickness map of the sample (quantitative phase map or phase-contrast map) (Figure 7). The deep red corresponds to the maximum phase, and the deep blue is associated with the zero phase. The phase parameters changes might represent the changes in the morphology of the sample. The number of 2D holographic images at different object planes creates 3D quantitative image, allowing the spatial phase sensitivity to distinguish the tiniest biological structures as the tail part of spermatozoa with a thickness of approximately 100 nm.
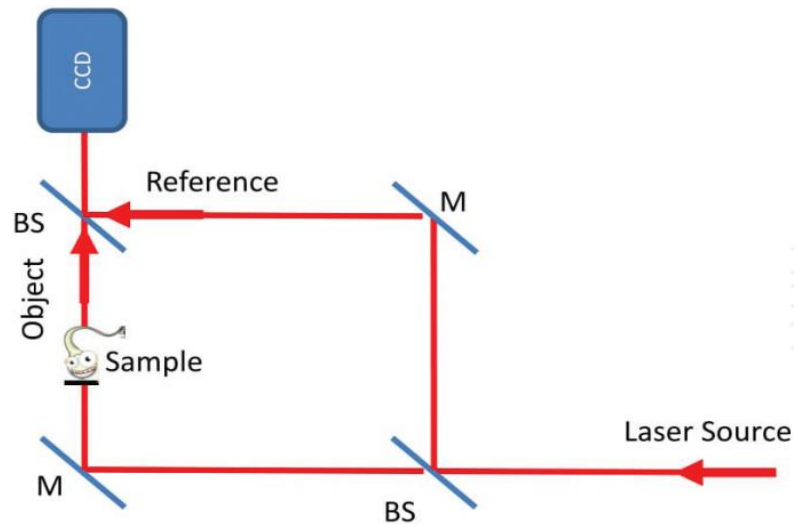
Figure 6 Typical interferometric setup for digital holographic microscopy. The original light source is divided into two coherent beams by a beam splitter. One beam interacts with an object under test, and another reference beam does not contact the object. The resulting quantitative phase map is reconstructed by recording the interferogram of those two superimposed coherent beams. The hologram is acquired by a digital sensor array (for example, CCD camera). BS – beam splitter, M – mirror. Reference- and object beams are highlighted.

_____

This figure was published in *Spermatozoa - Facts and Perspectives*, In Meccariello R., Chianese R. (Eds.). Angelis A. De, Ferrara M. A., Coppola G., & De Luca A. C., Advanced Label-Free Optical Methods for Spermatozoa Quality Assessment and Selection, pp. 219-240, IntechOpen, ***Open access article*** (2018).

1.3.1.2   QPM of human sperm cells

The first imaging of sperm cells by QPM was performed in 2008 by researchers from Spain and Israel on swine spermatozoa (Mico *et al.,* 2008). The capacity of interferogram microscopy for sperm analysis was expanded by Di Caprio and colleagues (2010) on bovine spermatozoa. Later the Israeli research group led by prof. Shaked published a number of studies about QPM of human sperm cells with special emphasis on the application of this technique in ART procedures (Eravuchira *et al.,* 2015; Haifler *et al.,* 2015; Balberg *et al.,* 2017; Barnea *et al.,* 2018; Dardikman-Yoffe *et al.,* 2020).
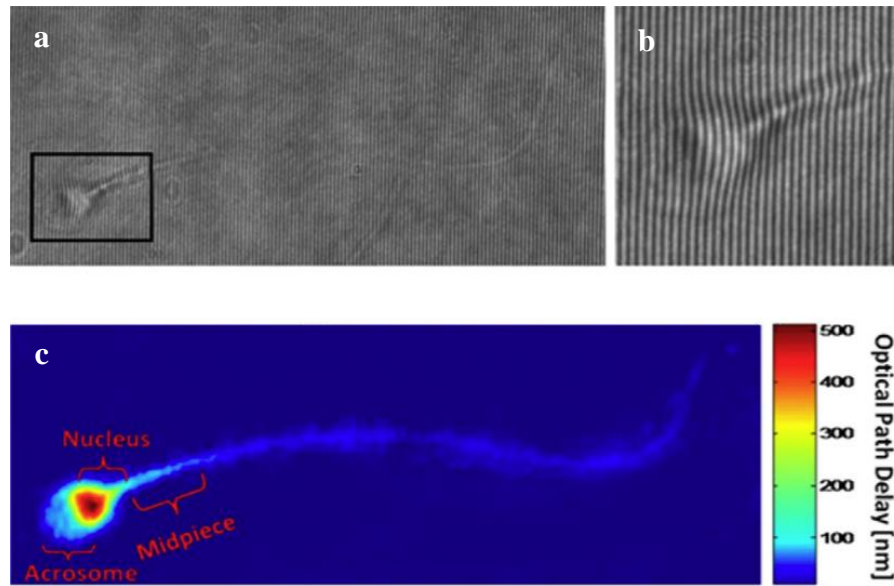
Figure 7 Quantitative Phase Microscopy of human spermatozoa. (a) An interferogram of human sperm cell obtained with QPM. **(b)** The optical path delay is encoded into the bending of the interference fringes. **(c)** The optical thickness map of the sample is digitally calculated from the interferogram.

_____

Assessment of sperm morphology by QPM

   Haifler and colleagues (2015) have demonstrated the QPM's ability to analyze the human sperm morphology in a comparable manner to label-based BFM being used in IVF. There was no statistical difference comparing the main sperm morphological parameters using QPM and label-based BFM using the WHO 2010 criteria (Haifler *et al.,* 2015). The picture showed that morphological features such as vacuoles were seen clearly using both non-labeled QPM and label-based BFM (Figure 8). Moreover, the specificity and sensitivity of head width, acrosome area, and midpiece width imaging using QPM were higher than label-free BFM. Namely, 50% of the vacuoles that label-free BFM missed were detected by QPM.
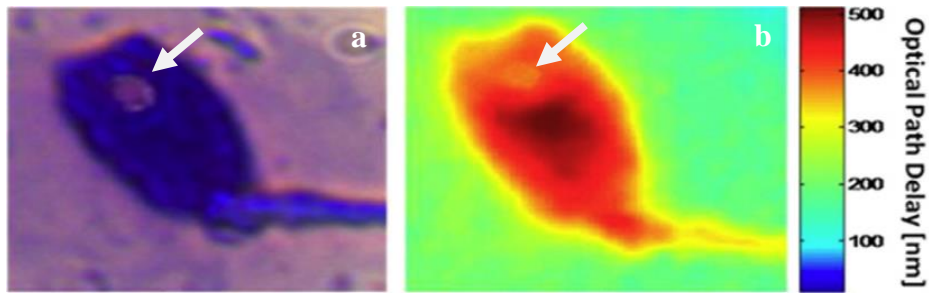
Figure 8 The comparison of sperm cell imaged with label-based BFM and QPM. (a) BFM image of sperm head stained with Quick Stain (Biological Industries) and **(b)** phase-contrast map of the same cell acquired by QPM. BFM image was performed using an inverted microscope (Axio Observer, Zeiss). The QPM system was comprised of portable interferometric module TAU. The sperm vacuole is marked with an arrow.

_____

The vacuole analysis in the sperm head was performed more in detail by Coppola and colleagues (Coppola *et al.,* 2014). They presented a quantitative comparison between a morphologically normal cell and a cell with a vacuole in the head region. The cell with the vacuole had distinct depression in the height profile along the major axis of the sperm head that might affect the volume of the sperm head (Figure 9). As one can see from the figure, vacuoles can be easily located on the phase map due to decreased refractive index, resulting in the drop of optical path delay.

QPM has been used to compare quantitative phase-contrast between normal sperm cells and sperm cells from the semen samples with multiple abnormalities such as oligoasthenoteratospermia (AOT) (Crha *et al.,* 2011). It has been detected that cells from the normal samples have significantly higher maximum phase shift rather than AOT samples. Interestingly, the architecture and integrity of the genetic material in the abnormal sperm head seem to affect the cell's quantitative value detected by QPM. This suggestion appears to be proved by the study of Barnea (2018), where the cells with different DNA fragmentation levels differ significantly regarding QPM quantitative parameters. It is found that a combination of the different criteria extracted from the phase maps of sperm cells can predict the fragmentation status of DNA. For example, cells from the most fragmented group are characterized by a large

nuclear area and small acrosomes. At the same time, the less fragmented group is characterized by the largest head area and the large acrosome dry mass (Barnea *et al.,* 2018).
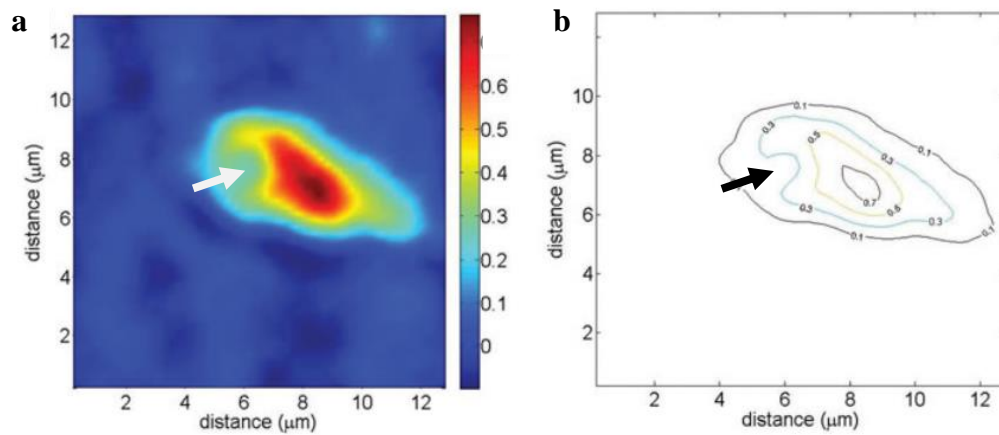
Figure 9 The vacuole detection in sperm head by QPM. (a) Phase-contrast map and **(b)** an isoline plot of a spermatozoon with a vacuole. The vacuole region is marked with an arrow.

_____

This figure was published in *Zygote*, 22(4), Coppola G., Di Caprio G., Wilding M., Ferraro P., Esposito G., Di Matteo L., Dale R., & Dale B., Digital holographic microscopy for the evaluation of human sperm structure, pp. 446-454, ***Copyright Cambridge University Press*** (2014).

Biophysical evaluation of sperm cells using QPM

QPM allows extracting the biophysical parameters such as biovolume and dry mass. For instance, the biovolume of live bovine sperm cells was analyzed using the combination of optical tweezer and QPM to enhance the precision of 3D reconstruction of quantitative phase maps. The optical tweezer provides an opportunity for optical trapping and rotating the flowing cell into a microfluidic channel with the subsequent recording of the interferograms for further mathematical processing (Figure 10). All acquired 2D holograms were combined to get 3D visualization of the analyzed cell (Merola *et al.,* 2013). Another analysis by Coppola (2013) revealed that the mean volume of a fixed human sperm cell is 8.03 ± 0.72 µm^3 based on quantitative phase shift information from QPM (Coppola *et al.,* 2013). Dry mass is another biophysical parameter being detected by QPM. Dry mass is a density of the cell's non-aqueous content, mainly proteins, carbohydrates and lipids. In Balberg's (2017) recent study, the dry mass of the sperm nucleus and acrosome region of unlabeled immobilized spermatozoa was quantitatively measured by QPM for the first time. The optical resolution of the system enables

the differentiation of the nuclear compartments of the sperm cell. Thus, the precise determination of acrosome and nucleus was done based on the BFM stained image of the same cells. The average dry mass was $5.96 \pm 1.15 \times 10^{-12}$ grams and $1.54 \pm 0.58 \times 10^{-12}$ grams for the nucleus and acrosomal region, respectively (Balberg *et al.*, 2017).
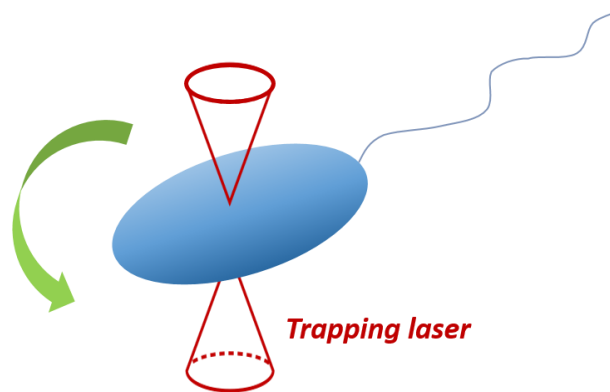
Figure 10 The optical trapping and rotating of the sperm cell into a microfluidic channel. The schematic representation of the interaction between the trapping laser (red) and moving sperm cell into the microfluidic chamber.

_____

Kinematic study of sperm cells by QPM

Besides morphological and biophysical analyses, QPM has been used to study the kinematics (motility) of sperm cells applying the 3D spatial motion over time. The first holographic image of moving bovine sperm cells in a microfluidic chamber was reported in 2010 by Di Caprio and colleagues. Later the same authors reported the automated detection and tracking of human spermatozoa using partial spatial coherent DHM (Di Caprio *et al.,* 2014). The phase maps of the moving cell were reconstructed using the holograms collected during the tracking. To provide the quantitative kinematic pattern and to describe the trajectory, several velocity parameters and their ratio were analyzed, such as curvilinear velocity (VCL), straight-line velocity (VSL), average path velocity (VAP). VCL relates to a total distance that sperm head swims for a certain observational time; the VSL refers to the distance between the first and the last points of the trajectory; the VAP is the distance that the cell has translocated in the average direction of movement in the study period. Retrieved quantitative motility parameters were compared between progressive and non-progressive motile sperm cells. In particular, the

morphologically abnormal cell had nonlinear motion detected with the system. Moreover, the group of sperm cells was tracked, detecting the anomalous behavior of non-progressive cells based on the quantitative kinematic value VSL (green line, Figure 11).
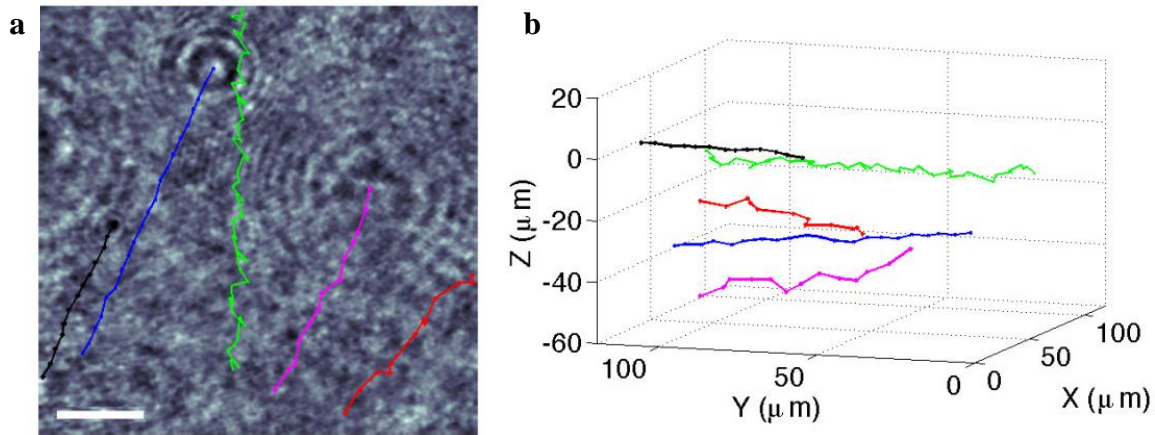
Figure 11 Multiple sperm cell tracking. **(a)** Transversal and **(b)** reconstructed three-dimensional path of sperm cell tracking. Data were acquired over 11 s. The scale bar is 20 µm.

_____

1.3.1.3 Artificial intelligence and QPM framework: application in ART

Artificial intelligence (AI) is a promising tool for automated image processing in medicine (Lee *et al.,* 2017; Shen *et al.,* 2017). In order to reach the specificity of the automated analysis and segmentation of the images, the form of AI called machine learning is thoroughly implemented. Many old machine learning algorithms exist, such as Support Vector Machine (SVM) and newer ones – Deep Neural Networks (DNNs). DNNs use the abundance of data points to train the model so that further outputs can be predicted based on the training data set. Usually, 70% of data is used for the training, while the other 30% is allocated as a test data set. The bigger the training data set, the better the predictive value of the algorithm. The current application of AI to reproductive urology is in its primary stage (Figure 12). However, it has already been shown that AI can learn and successfully identify sperm cells of high quality (Chu *et al.,* 2019). For instance, 371 of 415 sperm images acquired by clinical microscopes were

identified correctly using transfer learning with a deep convolutional network (Thirumalaraju *et al.,* 2018).
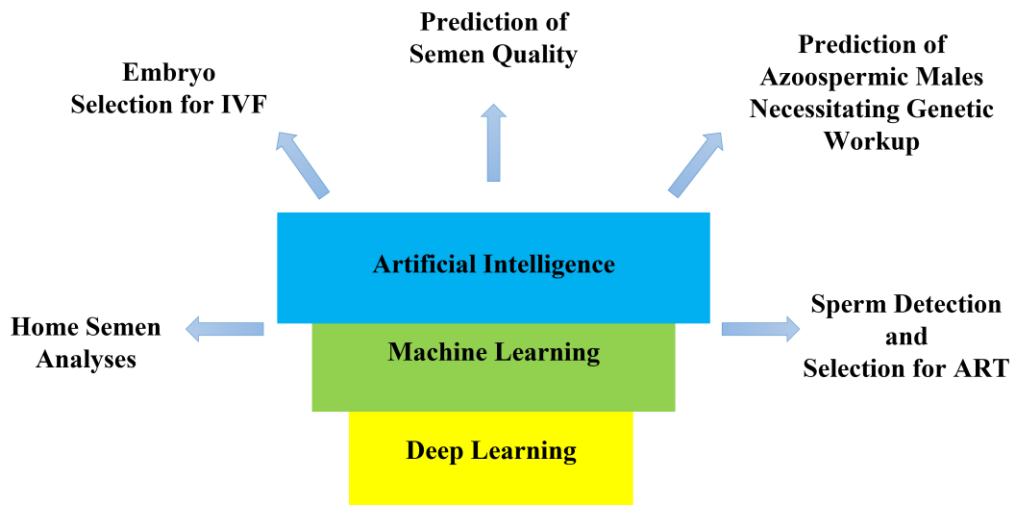
Figure 12 Current artificial intelligence application in reproductive medicine.

_____

This figure was adapted from *Current Urology Reports*, 20(9), Chu K. Y., Nassau D. E., Arora H., Lokeshwar S. D., Madhusoodanan V., & Ramasamy R., Artificial Intelligence in Reproductive Urology, Article 52, (2019).

AI can be applied to different imaging systems, including QPM. The merging of QPM with machine learning increases the chance of the automated classification of cells. The interferograms of sperm cells can be processed very fast on numerous spermatozoa using trained algorithms. For example, in the work of Mirsky (2017), the SVM classifier was designed for the automated classification of human spermatozoa's phase maps based on sperm cell morphology. The phase maps are used to extract morphology parameters of the cell to train the SVM algorithm to classify normal and abnormal sperm cells afterward (Mirsky *et al.,* 2017). Newer machine learning – DNNs combined with QPM have a more precise sensitivity to detect tiny changes in the sperm head, midpiece, and tail than SVM algorithms. Moreover, the system can suggest a new approach for the functional analysis of sperm cells by measuring the biophysical parameters. For instance, Kandel and colleagues (2020) presented a highly sensitive QPM and deep learning framework for the precise measurement of dry mass in the bovine spermatozoa compartments such as head, midpiece, and tail. Interestingly, the data revealed the predictive value of dry-mass ratios (head/midpiece, head/tail, midpiece/tail) for

zygote formation and blastocyst development (Kandel *et al.,* 2020) which might open a new perspective for the application of the QPM-AI framework in ART.

1.3.1.4 Clinical application of QPM

Despite the successful implementation of QPM for the study of sperm cells, there is a need for clinical trials of this technique to be implemented in the assisted reproductive technologies. Several issues postpone the clinical trials of QPM. Namely, the QPM requires a specially trained operator to interpret the results of the imaging. At the same time, a clinical system should be easy and fast due to the limited diagnostics or sperm selection time under the ICSI procedure. Additionally, the precision of the resulted interferogram is defined by the technical equipment, which might be expensive for routine use in the laboratory.

Currently, there is a close interdisciplinary collaboration between physicists, biologists and clinicians to improve the method and evaluate the clinical relevance of QPM. Thus, the QPM has been effectively implemented for the study of sperm biology (Mico *et al.,* 2008; Crha *et al.,* 2011; Coppola *et al.,* 2013; Di Caprio *et al.,* 2014; Haifler *et al.,* 2015; Eravuchira *et al.,* 2015; Balberg *et al.,* 2017; Mirsky *et al.,* 2017; Barnea *et al.,* 2018; Dardikman-Yoffe *et al.,* 2020; Kandel *et al.,* 2020). In order to bring the technique to broad usage, several interferogram devices have been developed so far (Girshovitz *et al.,* 2013; Lee *et al.,* 2014). For instance, the Israeli research group led by prof. Shaked has proposed a portable module for QPM of sperm cells called TAU interferometer, which can be attached to the existing microscopes for interferometric optical thickness measurements (Girshovitz *et al.,* 2013). However, the test-specificity and robustness of the system for the particular tasks should be done in the near term before the clinical trials and marketing of the QPM devices.

1.3.2 Mitochondrial DNA in sperm cells

The World Health Organization recommends performing the semen analysis uniformly according to established criteria (WHO 2010). Each semen parameter by itself has a limited prognostic value in defining sperm fertilizing potential and cannot be a reliable predictor individually for male fertility status (Barratt *et al.,* 2017). Moreover, men who have semen parameters below the reference limits are not necessarily infertile. For example, men with morphologically normal forms less than 4% had normal fertilization rates using conventional IVF (Mortimer & Mortimer 2020). For that reason, the search for new sperm factors and the

development of practical diagnostic assays in addition to the classical method should be encouraged for more extensive and robust semen analysis thoroughly reflecting the fertility status of the patient.

Sperm cell consists of various structures, the pathophysiology of which might reflect the male reproductive health. For instance, male infertility can be associated with adverse sperm mitochondrial functions (Figure 13). Mitochondria carry DNA in the form of a double-stranded circular nucleoprotein molecule called nucleoid (Anderson *et al.,* 1981). Most of the mitochondrial proteins are nuclear-encoded, while some of the genes are transcribed in mitochondria. After fertilization, paternal mitochondria and mitochondrial genome are eliminated by selective destruction through the ubiquitination in the early embryo in mammals (Sutovsky *et al.,* 1999), thereby enabling the uniparental inheritance of mitochondrial genes (Hutchison *et al.,* 1974). Moreover, paternal mitochondria and mtDNA are almost physically excluded before fertilization in mammals. Namely, a substantial portion of mitochondria is eliminated with cytoplasm in the form of residual bodies during spermiogenesis (De Luca & O'Farrell, 2012).

Point mutations and deletions in mtDNA are responsible for sperm cellular dysfunctions manifested in adverse semen parameters. Multiple deletions of mtDNA are associated with idiopathic astheno-, asthenoterato-, and oligoasthenoteratospermia (Colagar *et al.,* 2014; Gholinezhad *et al.,* 2019). In particular, low sperm motility has been associated with a missense mutation in the mitochondrial COIII gene (cytochrome c oxidase subunit III) (Baklouti-Gargouri *et al.,* 2014), large scale 7436-bp deletions in mtDNA (m.8637-m.8649/m.16073-m.16085) (Ambulkar *et al.,* 2016), single nucleotide polymorphism of mtDNA (ex. m.11696G>A) (Ji *et al.,* 2017), 4977-bp deletions (m.8470-m.8483/m.13447-m.13460) (Kao *et al.,* 1995), A3243G point mutation (m.3243A>G) (Spiropoulos *et al.,* 2002). To compensate for the adverse effect of mitochondrial DNA mutations and deletions, the change of sperm mtDNA copy numbers during spermatogenesis might abate a severe disease manifestation. This hypothesis might be supported by the significantly higher numbers of sperm mitochondrial DNA in abnormal semen samples in comparison to normal ejaculates of fertile donors. A few studies reported a negative correlation between mitochondrial DNA quantity and various semen parameters. For example, mitochondrial DNA copy numbers increase has been negatively associated with sperm motility (Tian *et al.,* 2014; Bonanno *et al.,* 2016; Faja *et al.,* 2019), total sperm count (Song *et al.,* 2008), sperm concentration (Amaral *et al.,* 2007; Tian *et al.,* 2014) and sperm morphology (Amaral *et al.,* 2007). These findings suggest the predictive value of mitochondrial DNA copy numbers and integrity for male reproductive status assessment.
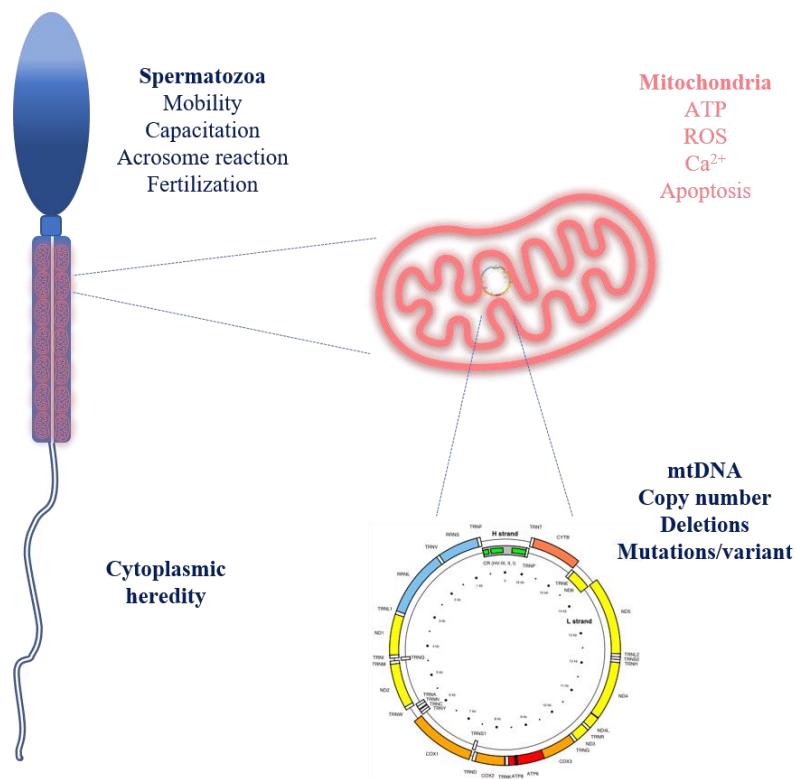
Figure 13 Overview of mitochondria functions in spermatozoa, and their multiple, potentially harmful consequences on reproductive function. Sperm mitochondria are not transmitted to descendants but involved in different sperm functions such as (1) producing energy in the form of adenosine triphosphate (ATP) required for cellular functions; (2) production of Reactive Oxygen Species (ROS), which are involved in sperm functioning, but can be detrimental beyond a certain level; (3) calcium regulation (Ca^{2+}), and (4) apoptosis. The defects in any of these functions can lead to sperm functioning abnormalities in mobility, capacitation, acrosome reaction, and as a consequence in fertilization. The circle represents the double-stranded sperm mitochondrial DNA (mtDNA) with genes marked in colors.

_____

This figure was adapted from *Human Reproduction Update*, 0(0), Boguenet M., Bouet P. E., Spiers A., Reynier P., & May-Panloup P., Mitochondria: their role in spermatozoa and in male infertility, pp. 1-23, (2021). Some elements of the figure were taken from Microsoft Office stock images and Wikipedia.org.

2 AIM AND OBJECTIVES

The overall aim of this PhD project was to investigate the potential of new sperm imaging techniques for biological and clinical application. In addition, we also wanted to explore whether mitochondrial DNA copy numbers are valuable for male fertility assessment.

Specific objectives of paper I

1) To set up imaging conditions for high-resolution imaging of living human sperm cells by SIM.
2) To specify the imaging protocol for multi-color imaging of sperm cells by SIM.
3) To characterize the ultrastructure of living human spermatozoa by SIM.

Specific objectives of paper II

1) To evaluate the effect of various concentrations of hydrogen peroxide (H_2O_2) on human sperm motility.
2) To analyze the optical thickness of the human sperm head upon gradual peroxidation by using holographic microscopy (QPM).
3) To classify the normal spermatozoa and cells upon oxidative stress by SVM classifier.

Specific objectives of paper III

1) To classify four different pathophysiological groups of human spermatozoa by applying deep learning and the QPM framework.
2) To compare DNN architectures with feature extraction-based machine learning models for the classification of sperm cells.

The specific objective of paper IV

- To summarize the evidence from literature regarding the association of mitochondrial DNA copy numbers and semen quality.

3 MATERIALS AND METHODS

3.1 Ethical approval

Ethics of conduct was strictly followed. The Regional Committee for Medical Research Ethics North Norway approved all study protocols (2014/932/REK Nord; date of approval: 28.11.2014).

The semen samples were collected from men who attended the IVF clinic of the Department of Obstetrics and Gynecology, University Hospital of North Norway, Tromsø. Informed consent was obtained from all participants.

3.2 Semen preparation

The samples were collected according to the WHO 2010 criteria after 3–5 days of abstinence. The Neubauer-improved counting chamber was used to count sperm cells number after liquefaction. All semen samples used in the experiments met the requirements of the WHO 2010 criteria to be considered as "normal".

The swim-up or gradient centrifugation methods were used to eliminate seminal plasma and isolate sperm cells with progressive motility and normal morphology. In the case of gradient centrifugation, one milliliter of semen was placed on each 1.5 ml of 90% and 45% gradient layers of SpermGrad (Vitrolife, Sweden) and centrifugated at 500×g for 15 min. A human Quinn's Sperm Washing Medium (Origio, Denmark) was used to wash the pellet twice at 300×g for 5 min. The cells after centrifugation were adjusted to the necessary concentration with Quinn's Advantage Fertilization Medium (Origio, Denmark) supplemented with 5 mg/ml human serum albumin (Sigma) for the following procedures.

As described in Paper I (Oppstad *et al.,* 2018), the semen samples were washed by swim-up method. Samples were centrifuged twice with 5 ml of Sperm Washing Medium (Sage) for 10 min at 700×g. After the supernatant disposal, 0.5 ml of swim-up medium was layered on top of the cells, and the tube was put into an incubator (5.0% CO_2, 37 °C). After 1 h of incubation, PR motile spermatozoa migrated to the swim-up medium. Then the supernatant was aspirated with a pipette, centrifuged, and the sediment was used for the following procedures.

3.3 Simulation of various pathophysiological cell conditions

To perform experiments with externally induced oxidative stress in Paper II (Dubey *et al.,* 2019), Quinn's Advantage Protein Plus Fertilization Medium (SAGE, Denmark) was used to dilute purified sperm cells to a concentration of 5.0×10^6 cells/ml. Further, sperm cells were put in a medium into 96-well cell culture plates (Corning, Germany) where different concentrations of H_2O_2 (10 µM, 40 µM, 70 µM, 100 µM) were added. For the control, the reference chamber was filled with the same concentration of semen without H_2O_2. The semen samples were incubated for 1 h at 37°C, 5–6% CO_2.

For automated classification of different pathophysiological groups of spermatozoa in Paper III (Butola *et al.,* 2020), purified semen samples were placed into 96-well cell culture plates (Corning, Germany) in a concentration of 2×10^4 cells per ml with 200 µM H_2O_2 (for oxidatively stressed samples) or 2% ethanol (for ethanol-affected samples), the reference chamber was filled with purified semen only. The samples were incubated for 1 h at 37 °C, 5% CO_2.

3.4 Cryopreservation and thawing

Cryopreservation and thawing of semen samples were performed following the Sperm Freezing Medium protocol (Origio, Denmark). Before the freezing, the Sperm Freezing Medium was placed for a minimum of 2 h at room temperature (RT). After semen purification, the semen sample and the Sperm Freezing Medium were mixed on a 1:1 (v/v) ratio. The medium was added onto the semen sample by dribs, and the solution was carefully mixed after each addition. The mixture was left at RT for a minimum of 10 min. Next, the diluted semen was loaded into cryo-tubes (Thermo Fisher Scientific Nunc, Germany). The tubes were placed in the gas phase of the liquid nitrogen for 30 min. Then the cryo-tubes were transferred into the liquid nitrogen and stored at -196ºC. During the thawing process, the cryo-tubes were put at RT for 5 min. Then samples were washed by centrifugation in Quinn's Sperm Washing Medium (Origio, Denmark). After washing, the supernatant was aspirated, and cells from the sediment were used for the following procedures.

3.5 Sperm motility assessment

The sperm cell's motility was graded as progressive (PR) and non-progressive (NP) following the WHO 2010 criteria after liquefaction at 30 min. A Neubauer-improved counting chamber was used for the motility evaluations under the inverted phase-contrast microscope

with a ×40 magnification objective. First, the grid section was scored for PR cells, next for NP spermatozoa in the same grid section in three different replicates for each sample.

3.6 Statistical analysis

Descriptive statistics such as mean, standard deviation (SD), and n (%) were used to summarize the semen analysis variables. Differences between means were tested using t-Test: Paired Two Sample for Means. A level of statistical significance was set at $p < 0.05$. Analyses and graphical visualization were performed in Microsoft Excel.

3.7 Immunofluorescent staining

Suspension of washed human sperm cells was fixed with 4% PFA (Paraformaldehyde, Sigma-Aldrich, Germany) for 10 min. PFA was discarded by centrifugation in 1×PBS (Phosphate-Buffered Saline, Sigma-Aldrich, Germany) for 10 min. Cells were pipetted onto the slides, fixed in 4% PFA in 1×PBS for 10 min in a humid chamber, and washed for 5 min in 1×PBS. Cell membranes were permeabilized with 0.5% Triton X-100 (Sigma-Aldrich, Germany) for 5 min and washed in 1×PBS for 5 min.

Table 2 Antibodies and labeling conditions for immunofluorescent staining of sperm cells.

Primary antibodies	Stock concentration	Dilution	Total volume: 200 μl
Rabbit anti-human TOM20	0.2 mg/ml	1:200	1 μl
Secondary antibodies			
Alexa Fluor 647-donkey anti-rabbit	2 mg/ml	1: 500	0.4 μl

For immunofluorescent staining, human sperm cells were treated with 1% blocking reagent (BSA, Bovine Serum Albumin, Sigma-Aldrich, Germany) in 1×PBS for 1 h. Then cells were incubated with primary antibodies for mitochondrial import receptor subunit TOM20 (Rabbit anti-human TOM20, Thermo Fisher Scientific, Germany) diluted in 1% BSA in 1×PBS for 1 h at RT. After incubation with primary antibodies, sperm cells were washed thrice in 1×PBS and then incubated with secondary antibodies (Alexa Fluor 647-donkey anti-rabbit, Thermo Fisher Scientific, Germany) diluted in 1% BSA in 1×PBS for 1 h at RT. Then cells were washed similarly, dehydrated and air-dried (Table 2).

3.8   Live-cell fluorescent labeling

For the live-cell imaging by SIM, CellMask Orange for cell membrane, MitoTracker Green for mitochondria, Hoechst 34580 for nuclear DNA, PicoGreen for nuclear and mitochondrial DNA, and SiR-tubulin for tubulin were used. All probes were purchased from Thermo Fisher Scientific (Germany), besides SiR-tubulin purchased from Spirochrome (Switzerland). Cells were incubated with probes at RT in Live Cell Imaging Solution (Molecular Probes, Germany) or in 1×PBS. Labeling conditions are summarized in Table 3. In the case of multi-color labeling, the dye with the longest staining time was added first, with sequential administration of other dyes. After incubation, cells were washed by centrifugation in 1×PBS for 10 min at 800×g. After centrifugation, the supernatant was discarded, and the samples resuspended in 1×PBS to a concentration found suitable for the imaging.

Table 3 Dyes and labeling conditions applied for SIM imaging of sperm cells.

Dye	Working concentration	Incubation time
CellMask Orange	5 µg/ml	10 min
MitoTracker Green	200 nM	20 min
Hoechst 34580	5 µg/ml	20 min
SiR-tubulin	1 µM	2 h
PicoGreen	100 nM	10 min

3.9   Structured Illumination Microscopy and image processing

Fluorescent imaging of living human sperm cells was done using Structured Illumination Microscopy. For the imaging process, the suspension of the cells was placed on slides (#1.5, Thermo Fisher Scientific, Germany) and covered with patches of 2% agarose (High-resolution, Sigma Aldrich, Germany) in 1×PBS for the immobilization of sperm cells. After placing the agarose patches, the samples were protected by a plastic lid against drying during imaging.

As described in Paper I (Oppstad *et al.,* 2018), a DeltaVision OMX V4 Blaze imaging system (GE Healthcare, Chicago, USA) equipped with a 60X 1.42NA oil-immersion objective (Olympus, Tokyo, Japan), three sCMOS cameras, and 405, 488, 568, and 642 nm lasers for

excitation were used for imaging. The optical resolution of the system depended on a color channel and was rated at 110-160 nm laterally and 340-380 nm axially. The reconstruction software was used to obtain super-resolution images. Deconvolution and 3D SIM image reconstruction were completed using the manufacturer-supplied SoftWoRx program (GE Healthcare, USA). Image registration (color alignment) was also performed in SoftWoRx using experimentally measured calibration values compensating for minor lateral and axial shifts, rotation, and magnification differences between cameras. Fiji/ImageJ software was applied for image processing (Schindelin *et al.*, 2012).

3.10 Quantitative Phase Microscopy

For quantitative phase imaging of human spermatozoa the partial spatial coherence gate QPM/DHM system (PSC-DHM) with He-Ne light source was applied. The diagram of the PSC-DHM system is shown in Figure 14. A polydimethylsiloxane chamber (PDMS) on a reflecting silicon (Si) chip was used for sperm imaging. Samples were fixed with 4% PFA for 30 min at RT and washed in 1×PBS for 5 min to immobilize the sperm cells. Finally, the PDMS chamber with fixed cells was filled with 50μL of 1×PBS, and the samples were covered by a 170 μm thickness cover glass (Thermo Fisher Scientific, Germany).

3.11 Data analysis

Sperm cells were classified into control and oxidatively stressed groups by extracting the phase maps from recorded off-axis holograms using a Matlab program (Paper II). A graphical user interface (GUI) was developed for the automated selection of sperm heads from the background of phase maps by putting a threshold value. The reconstructed and segmented phase maps of sperm heads were utilized to calculate the various morphological and texture parameters. These parameters were used for the binary classification of the specimen's state using the SVM algorithm. The samples were divided into two different sets of data, i.e., training and testing data. The algorithm was trained by 60% of the total samples, while 40% were used for the classification. Receiver Operative Characteristic (ROC) curves were used to describe and to compare the performance and accuracy of the classification.
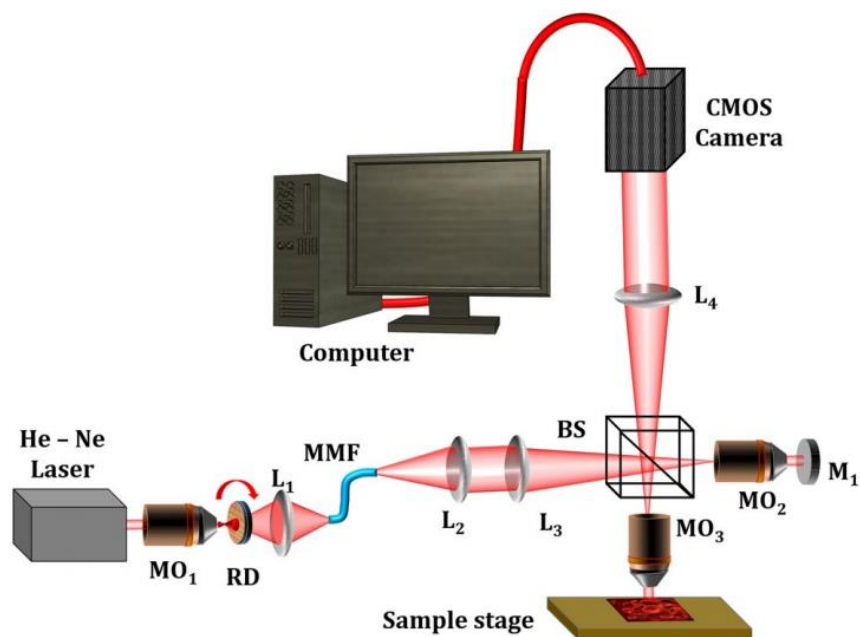
Figure 14 The diagram of the DHM setup with a pseudo thermal light source for acquiring the quantitative phase maps of a sperm sample. RD – rotating diffuser, L – lens, BS – beam splitter, MO – microscope objective, MMF – multiple multi-mode fiber bundle (Paper II).

Convolutional Neural Networks (CNNs) were used for the classification of sperm cells under four different conditions (control, cryopreserved, after oxidative stress, and ethanol exposure) (Paper III). CNNs is an advanced machine learning technique that automatically generates abstract convolutional features from the training dataset. All image processing was implemented in MATLAB 2019a on a 64-bit Windows OS, Intel Xeon CPU E5-1650 v4 at 3.6 GHz with 64 GB RAM and NVIDIA 2080 Ti GPU. For the classification of phase maps of normal and stress affected sperm cells seven DNNs were used. The classifier was trained by 70% of the total samples, and the rest of 30% was used for the testing.

3.12 Meta-analysis and systematic review

We performed a systematic review and meta-analysis to study the difference in mtDNAcn between the sperm cells of males with normal semen analysis and males with an abnormal semen analysis. The review protocol was developed following CRD's guidance in health care (Centre for Reviews and Dissemination). PRISMA guidelines were followed to report the results. The current review was registered in the international prospective register of systematic review (PROSPERO: CRD42019118841).

Cochrane methodology was used for electronic and hand searching in Embase Classic and Ovid MEDLINE databases on December 07, 2020. The search covered the period from 1946 to 2020. The controlled vocabulary of Medical Subject Headings (MeSH) terms "Male Infertility" and 17 additional keywords related to outcome or participants were used. Only the English language manuscripts providing the human study were included. Moreover, the studies that analyzed the semen following either the WHO 1999 or the WHO 2010 criteria were included in the meta-analysis. The Newcastle-Ottawa Scale (NOS) modified for non-interventional observational cross-sectional studies was applied to assess the study's quality.

The pooled estimates for the outcome were presented as Standardized Mean Difference (SMD) with 95% confidence intervals using the random-effects model and inverse variance method. Statistical significance was assumed when $p<0.05$. The authors were contacted when the studies presented the results in an inappropriate way for our data extraction, for example, in the form of correlation analysis.

4   SUMMARY OF RESULTS

Paper I: Live-cell imaging of human spermatozoa using Structured Illumination Microscopy (SIM).

Super-Resolution Imaging by SIM of living human sperm cells was done for the first time. Sample movement was effectively eliminated using agarose patches being placed on top of the sample. Various live-cell compatible biomarkers were used for single and multi-color super-resolution imaging (CellMask Orange for cell membrane; MitoTracker Green for mitochondria; Hoechst 34580 for DNA and SiR-tubulin for microtubulin). The contrast and resolution enhancement of SIM was prominent for all cell structures, especially for mitochondria-containing midpiece, where structures around 100 nm length-scale were resolved. The resolution doubling provided by SIM made it possible to resolve the centriole from the rest of the axoneme completely. The usage of photostable dyes with lowered illumination intensities and longer exposure times enabled multi-color super-resolution imaging of living human sperm cells. Optical aberrations were reduced due to the thickness of the sample, the sample placement directly on the coverslip and by optimizing the immersion oil.

Paper II: Partially spatially coherent digital holographic microscopy and machine learning for quantitative analysis of human spermatozoa under oxidative stress condition.

Quantitative Phase Microscopy made it possible to detect changes in the optical thickness of human sperm heads after exposure to oxidative stress. It was proved that the maximum phase value of sperm cells upon the different concentrations of H_2O_2 decreased gradually compared to the control. Moreover, the decrease in phase value of sperm heads upon gradual peroxidation correlated with a dose-dependent decrease in the clinically relevant parameter such as progressive motility. The head morphological changes after oxidative stress were measured by extracting numerical parameters from the phase maps. Further, normal and oxidatively stressed sperm cells were classified by a support vector machine based classifier (SVM). The SVM classifier was trained using the numerical parameters extracted from phase maps. Namely, 60% of the total samples were used as a training dataset, while the rest of 40% were used for testing. For the classification of sperm cells SVM model provided an accuracy of 89.93%.

Paper III: High spatially sensitive quantitative phase imaging assisted with deep neural network for classification of human spermatozoa under stressed condition.

In this study, a total of 10.163 interferograms (2.400 normal, 2.750 cryopreserved, 2.515 oxidatively stressed, and 2.498 ethanol-affected) of human spermatozoa were imaged using PSC-DHM system. The deep neural networks were trained by 70% of the reconstructed phase maps of spermatozoa and the remaining 30% were used to check the classification accuracy of the networks. It has been shown that different DNN architectures had a sufficient classification accuracy in separating the different groups of human spermatozoa. The DNN ResNet-101 presented the best accuracy with the result of 85.6%. In addition, the accuracy of DNN architectures was higher than the accuracy of old machine learning algorithms for the classification of sperm cells.

Paper IV: Sperm mitochondrial DNA copy numbers in normal and abnormal semen analysis: a systematic review and meta-analysis.

The systematic review and meta-analysis summarized the evidence from 10 published studies regarding the association of mtDNAcn and semen quality, emphasizing spermatozoa motility. Sperm mitochondrial DNA copy numbers were reported as a primary outcome. Significantly higher mtDNAcn have been shown in abnormal semen analysis in comparison to normal semen analysis. Moreover, a significant negative correlation between mitochondrial DNA copy numbers and semen parameters has been revealed in three studies excluded from the meta-analysis. The quality of evidence was assessed as good to very good in 60% of the studies.

5 GENERAL DISCUSSION

The development of precise and robust methods for semen analysis and spermatozoa selection is important for male fertility assessment and medically assisted reproduction. Specifically, the ART outcome is being rapidly improved since the active development and innovations in reproductive biology and medicine. Since the development of ICSI, hundreds of thousands of men became fathers, which was not even considered to be possible before. Nevertheless, children conceived with ICSI tend to have adverse perinatal outcomes than naturally conceived (Pinborg *et al.,* 2013). Moreover, it has been reported on a limited number of studies that the fertility of ICSI conceived men is affected, probably, due to inheritance of infertility factors from their fathers (Katagiri *et al.,* 2004; Palermo *et al.,* 2008; Belva *et al.,* 2016; Belva *et al.,* 2017; Rumbold *et al.,* 2019). For that reason, the accuracy and safety aspects of ART technologies are pivotal for research projects.

5.1 Morphological analysis of sperm cells at the nanoscale level

The development of methods for semen analysis and sperm cell selection is one of the key targets in ART. Along with other sperm factors, the characterization of sperm morphology is an important parameter to consider male fertility status when analyzing semen. The predictive value of sperm morphology for male fertility potential and ART outcome has been reported in a number of studies (Kruger *et al.,* 1986; Ombelet *et al.,* 1994; Li *et al.,* 2014; Kohn *et al.,* 2018; Liu *et al.,* 2021). It is well known that subfertile or infertile patients with a lower likelihood of contributing to pregnancy have a higher level of morphologically abnormal forms of spermatozoa (Palermo *et al.,* 1992; Guzick *et al.,* 2001). Nevertheless, in contrast to sperm motility, cell concentration and seminal fluid volume of ejaculate, spermatozoa morphology analysis seems to be a debated predictor of semen quality and fertilizing potential of the cells (Auger *et al.,* 2016; Danis and Samplaski, 2019). For example, current evidence suggests sperm cell morphology has a limited predictive value for pregnancy outcome in ART (Aziz *et al.,* 1996; Karabinus *et al.,* 1997; Li *et al.,* 2017; Zhou *et al.,* 2021) or in natural conception (Kovac *et al.,* 2017). The reasons for these rather contradictory results are still not entirely clear. We believe that the modern achievements in physics and biomedical optics might shed light on the predictive value of morphology for semen analysis and cell selection, which might be implemented in infertility treatment.

In our work, we use two types of super-resolved microscopies for the analysis of human sperm cell morphology: label-based Structured Illumination Microscopy **(Paper I)** and Quantitative Phase Microscopy, which does not rely on using any fluorescent markers **(Paper II)**. In the first paper, we succeeded in performing super-resolution imaging of living human sperm cells with an axial resolution of ~120 nm (Jost & Heintzmann, 2013). So far, multiple studies have been performed to characterize sperm cell biology using different fluorescent super-resolution techniques. For instance, the analysis of actin dynamics in live mouse sperm cells during the acrosomal reaction was done by the Total Internal Reflection Fluorescence (TIRF) method (Romarowski *et al.,* 2018); the actin-based cytoskeleton in the mouse sperm flagellum was described by using stochastic optical reconstruction microscopy (3D STORM) (Gervasi *et al.,* 2018); the precise localization of tetraspanin family protein CD151 in male germ cells was determined by SIM (Jankovikova *et al.,* 2020); the positioning of the flagellar ion channel Hv1, which is important for sperm rotation was done by 3D STORM (Miller *et al.,* 2018), and protein kinase A localization dynamics during capacitation in mouse sperm cells was analyzed by Stimulated Emission Depletion Microscopy (STED) (Stival *et al.,* 2018).

The high-resolution microscopy of living sperm cells is challenging to work with due to an extremely high sperm velocity of ~ 90 µm/s that creates aberrations and imaging inaccuracy, especially while taking the nanoscale images (Beauchamp *et al.,* 1984). For that reason, the above-mentioned studies performed experiments on immobile sperm cells, except the study of Romarowski (2018) with cell immobilization on concanavalin-A coated coverslips for the live cell imaging by TIRF (Romarowski *et al.,* 2018). We first attempted to image living human sperm cells using SIM applying sperm immobilization with agarose patches. As a result, we succeeded in acquiring SIM images at a high resolution and contrast of cell structures such as cell membrane, mitochondria, nucleus, centriole and tail tubulin. The most prominent resolution has been shown for the longitudinal section of the sperm midpiece, where structures around 100 nm length-scale were resolved, which suggested the helical organization of mitochondrial sheath. The resolution beyond the diffraction limit (~250 nm) makes it possible to count the number of full helical turns in the midpiece around the flagellum of living human spermatozoa, which is confirmed by transmission electron microscopy (Fujita *et al.,* 1970). Similarly, the periodical structure of mitochondria using SIM has been reported by Gervasi and colleagues on fixed mouse sperm cells (Gervasi *et al.,* 2018).

In our next study (**Paper II**), we applied QPM to analyze human sperm morphology quantitatively. We also compared the quantitative data of normal sperm cells to those sperm cells with externally induced oxidative stress conditions in order to distinguish the sperm cells

under pathophysiological conditions. QPM reconstructs the image based on the optical light delay associated with the biological sample. Thereby the information about the local thickness of the sample without any labeling becomes available. Moreover, due to interferometry, QPM provides nanoscale sensitivity of morphological changes in the sample (Park *et al.,* 2018). Using the advantages of the QPM technique, we found out that the thickness of the sperm heads decreases with the gradual increase of externally induced oxidative stress caused by hydrogen peroxide. The decrease in the optical thickness means flattening of the sperm head. These gradual head morphology changes might be associated with decondensation of genetic material due to DNA fragmentation upon oxidative stress. For example, it has been shown that *in vitro* human sperm incubation with H_2O_2 induces DNA fragmentation in a dose-dependent manner (Duru *et al.,* 2000). Interestingly, our result might be consistent with a previously reported study showing that the mean optical thickness of human sperm cells acquired with QPM declines from the most DNA fragmented group to the least fragmented (Barnea *et al.,* 2018). In addition, the decrease in the optical thickness of sperm heads upon peroxidation was found to be associated with clinically relevant motility parameters of the sperm cells. Namely, our results support the previous studies that concentrations of H_2O_2 above the physiological level produce a concentration-dependent effect on motion parameters probably due to lipid peroxidation, which can alter sperm fertilizing potential (De Lamirande and Gagnon 1992; Duru *et al.,* 2000; Kao *et al.,* 2008; Gibb *et al.,* 2020). Taken together and considering the sensitivity of the QPM method, the optical thickness of the cell might be a good marker of the pathophysiological condition, for example, oxidative stress and DNA fragmentation. Moreover, the characterization of optical thickness of sperm, measured by QPM, might be an important parameter to consider when selecting the individual sperm cell for ICSI during ART procedure.

5.2   Automated classification of sperm cells by QPM-AI framework

Considering the ability of QPM to detect the tiny changes in morphological features of sperm cells in a non-label manner, merging QPM with artificial intelligence might have a promising value for virtual image classification of the phase data. Moreover, the QPM-AI framework might minimize observer bias and inter-individual variability to provide more objective sperm analysis and cell selection (Eustache and Auger, 2001). In a broader context, the synergistic application of holographic microscopy and deep learning have been successfully employed, for example, to distinguish two types of macrophages cultured under gravity and microgravity (Li *et al.,* 2020), to convert QPM images of tissue sections into BFM images that

are equivalent to histological staining (Rivenson *et al.,* 2019), to classify individual *Bacillus* spores in diagnostic of pathogens (Jo *et al.,* 2017).

Until now, there is scant data looking at the sperm cell classification by DNNs in combination with QPM. However, the classification of QPM data of human spermatozoa was done using simple machine learning systems by extracting the numerical parameters from the phase maps (Mirsky *et al.,* 2017; Dubey *et al.,* 2019). Opposite to simple machine learning algorithms, in our study **(Paper III),** we applied deep learning without extracting any numerical parameters from the phase images. Put it another way, our QPM-AI framework utilizes information about the whole sperm cell and does not require segmentation of head parts as in the case of simple machine learning techniques **(Paper II)**.

To get various classes of sperm cells for the classification, we performed sperm cryopreservation, peroxidation and ethanol incubation. Morphology changes of spermatozoa upon cryopreservation have been reported in many studies (Hammadeh *et al.,* 1999; Donnelly *et al.,* 2001; O'Connell *et al.,* 2002; Ozkavukcu *et al.,* 2008; Boitrelle *et al.,* 2012; Raad *et al.,* 2018). At the same time, the effect of oxidative stress on sperm cell morphology can be assessed indirectly through the level of antioxidant defense and seminal ROS, which has been found to be associated with male infertility (Lenzi *et al.,* 1994, Vezina *et al.,* 1996; Said *et al.,* 2005; Colagar *et al.,* 2013; Eroglu *et al.,* 2014; El-Taieb *et al.,* 2015; Roychoudhury *et al.,* 2016; Majzoub *et al.,* 2018; Oumaima *et al.,* 2018). Similarly, multiple studies have been performed to characterize direct and indirect effects of ethanol on different parameters of semen quality, including sperm cell morphology (Donnelly *et al.,* 1999; Rahimipour *et al.,* 2013; Jensen *et al.,* 2014; Silva *et al.,* 2017).

In our study, the percentage of progressive and nonprogressive motility was chosen for cross-validation of stress agent's effect on spermatozoa. The progressive motility decreased significantly in all three stress groups. One explanation of the ethanol-affected decrease in spermatozoa motility is an alteration in membrane proteins structure (Donnelly *et al.,* 1999). At the same time, the peroxidation of unsaturated fatty acids in membrane lipids is a principal mechanism of peroxidation on spermatozoa motility. Consequently, the changed physical qualities of cell membrane result in disrupted tail motion (Gibb *et al.,* 2020). The functional changes of sperm cells after cryopreservation lead to motility and survival rate decrease (Kopeika *et al.,* 2015), ultrastructure and cell morphology changes (Woolley & Richardson 1978; Barthelemy *et al.,* 1990; Ozkavukcu *et al.,* 2008) and mitochondrial activity reduction (O'Connell *et al.,* 2002).

Seven deep neural networks were applied to classify the phase maps of four different groups of spermatozoa. The best sensitivity (85.5%), specificity (94.7%), and accuracy (85.6%) were provided by ResNet-101 network. Further, the accuracy of DNNs was compared with a total of 3 feature extraction-based machine learning classifiers, which were less specific and accurate in comparison to DNN architectures. However, the classification accuracy of the QPM-AI system might be improved by applying virtual staining of different sperm subcellular structures, which can improve the chemical specificity of the QPM technique (Jiang *et al.,* 2019; Rivenson *et al.,* 2019; Dardikman-Yoffe *et al.,* 2020). Another method for classification improvement is Phase Imaging with the Computational Specificity method (PICS) recently proposed by Gabriel Popescu and colleagues at the University of Illinois at Urbana Champaign (Kandel *et al.,* 2020b). PICS encompasses software based on deep-CNN (U-Net architecture). Kandel and colleagues (2020) applied PICS for the classification of the bovine sperm cells using an automated spatial light-interference microscopy system (SLIM) (Kandel *et al.,* 2020a). PICS provides the pixel labeling in the phase image with computational specificity to distinguish parts of the sperm cell such as head, midpiece and tail. As a result, the combination of nanoscale morphological information provided by interference microscopy and deep learning made it possible to measure dry mass of each component of the cell, which represented the predictive value for zygote cleavage and embryo blastocyst development (Kandel *et al.,* 2020a).

5.3 Mitochondrial DNA content in human sperm cells

Fluorescent microscopy is a commonly used method for mitochondrial DNA detection and visualization in different types of eukaryotic cells (Legros *et al.,* 2004; Ashley *et al.,* 2005; Kasashima *et al.,* 2014). However, the location of mtDNA in human sperm cells has not been imaged so far. In our paper **(Paper I)**, we present the imaging of different sperm parts, including mitochondria and nuclear DNA by using high-resolution microscopy (SIM). At the same time, the data about mtDNA imaging have been excluded from the article due to negative results. Namely, combining PicoGreen labeling for nuclear/mtDNA and Mitochondrial Import Receptor Subunit TOM20 labeling for mitochondria did not reveal the location of mtDNA in the midpiece of human sperm cells (Figure 15a). Similarly, the negative result was found upon living sperm cell imaging by using PicoGreen only (Figure 15b).
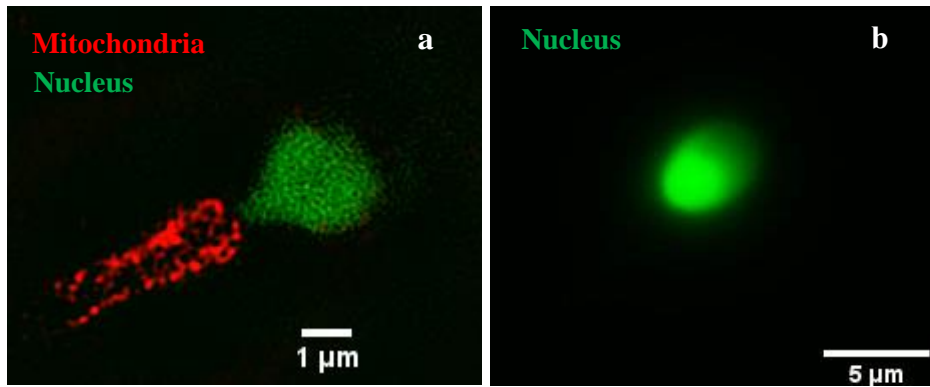
Figure 15 The sperm nucleus and mitochondria-containing midpiece. (a) Immunofluorescence on human sperm cells stained with antibodies against the Mitochondrial Import Receptor Subunit TOM20, clearly showing the localization of the sperm mitochondria (red). PicoGreen was used as a DNA counterstain for the sperm nucleus (green). **(b)** Stacks projection of average intensities of living sperm cell stained with PicoGreen. All images acquired by SIM.

The negative results might be explained by the overlapping of mtDNA signals with extensive fluorescence from nuclear DNA. Other reasons for the failure of mtDNA detection in spermatozoa is mtDNA degradation or insufficient quantity of these molecules for the detection by label-based microscopy. For that reason, mtDNA imaging failure in sperm cells led us to perform a meta-analysis and a systematic review about mtDNA copy numbers.

The aim of our systematic review and meta-analysis was to summarize the evidence from literature regarding the association of mitochondrial DNA content and semen quality with special attention on spermatozoa motility. It has been shown a significant difference in sperm mtDNAcn in abnormal human spermatozoa in comparison to normal sperm cells. Three studies presented a negative correlation between sperm mtDNAcn and (1) motility (Tian *et al.,* 2014, Bonano *et al.,* 2016, Faja *et al.,* 2019), (2) total count of spermatozoa (Song *et al.,* 2008), (3) sperm concentration per ml (Amaral *et al.,* 2007, Tian *et al.,* 2014) and (4) morphology (Amaral *et al.,* 2007) between patients with abnormal semen parameters and control groups. Moreover, the intrasample variation of mtDNAcn has been described in two studies by Díez-Sánchez (2003) and May-Panloup (2003), where cells with abnormal morphology and motility had higher mtDNAcn than sperm cells having normal characteristics (Díez-Sánchez *et al.,* 2003; May-Panloup *et al.,* 2003). Of note, our review revealed that mtDNAcn increased more significantly in the group of multiple abnormalities, namely, those who have more than two abnormal parameters (AOT patients). At the same time, mtDNA content per sperm from the

group with the only motility defect did not differ significantly from the sperm of the normal group.

The molecular mechanisms behind the negative association of mtDNAcn and semen analysis are still unknown. During spermiogenesis at the stage of elongated spermatids, mitochondria are eliminated with a large part of cytoplasm in the form of residual bodies (Figure 16). As a result, only 22-75 mitochondria are present in the mature mammalian spermatozoa (Otani *et al.,* 1988). Concomitantly, the number of mtDNA decreases during spermiogenesis through the downregulation of TFAM protein, which is known to be the regulator of transcription and replication processes (Larsson *et al.,* 1997; Larsson *et al.,* 1998; Rantanen and Larsson, 2000). Maintaining of mtDNAcn during spermiogenesis might have a compensatory significance in case of genetic abnormalities in mitochondrial DNA. For example, it was found that the increase of mtDNAcn could improve a severe disease manifestation resulted from mtDNA mutations in testis (Jiang *et al.,* 2017). In other words, the level of normal mtDNA without mutation will be higher, but the mtDNA mutation load remains the same.

Apart from male fertility assessment, mtDNA copy numbers might have a predictive value for early ART outcome. For instance, the association of sperm mtDNAcn with lower pregnancy probabilities has been demonstrated in the study of Rosati (2020). Moreover, it was found that the fertilization by sperm with high mitochondrial DNA content might lead to lower odds of embryo development to the blastocyst stage (Wu *et al.,* 2019). At the same time, Tiegs (2020) reported no correlation among sperm mitochondrial DNA quantity and fertilization, blastocyst development, and live birth rates from patients undergoing ICSI. However, the analysis confirmed the association between increased sperm mtDNAcn and decreased spermatozoa motility (Tiegs *et al.,* 2020).

The level of mtDNAcn may also indicate spermatogenic dysfunction. For example, mtDNAcn have been proposed as an indicator of spermatogenesis's efficiency based on the significant decrease of mtDNAcn after varicocelectomy (Gabriel *et al.,* 2012). Moreover, the mtDNAcn in human sperm have been associated with different environmental pollutants such as air pollutants (Zhang *et al.,* 2020), polycystic aromatic hydrocarbons (PAHs) (Ling *et al.,* 2017) and synthetic organic chemicals such as monocarboxy-isononyl phthalate (Huffman *et al.,* 2017). Interestingly, the study by Luo (2012) demonstrated increased mtDNAcn at high altitudes (5.300 m), i.e., at hypoxic conditions (Luo *et al.,* 2011). Given the impact of environmental factors and lifestyle on mtDNAcn, Wu (2019) suggested mtDNAcn as an

indicator of male fertility based on consecutive diagnoses rather than a single abnormal sample (Wu *et al.,* 2019).
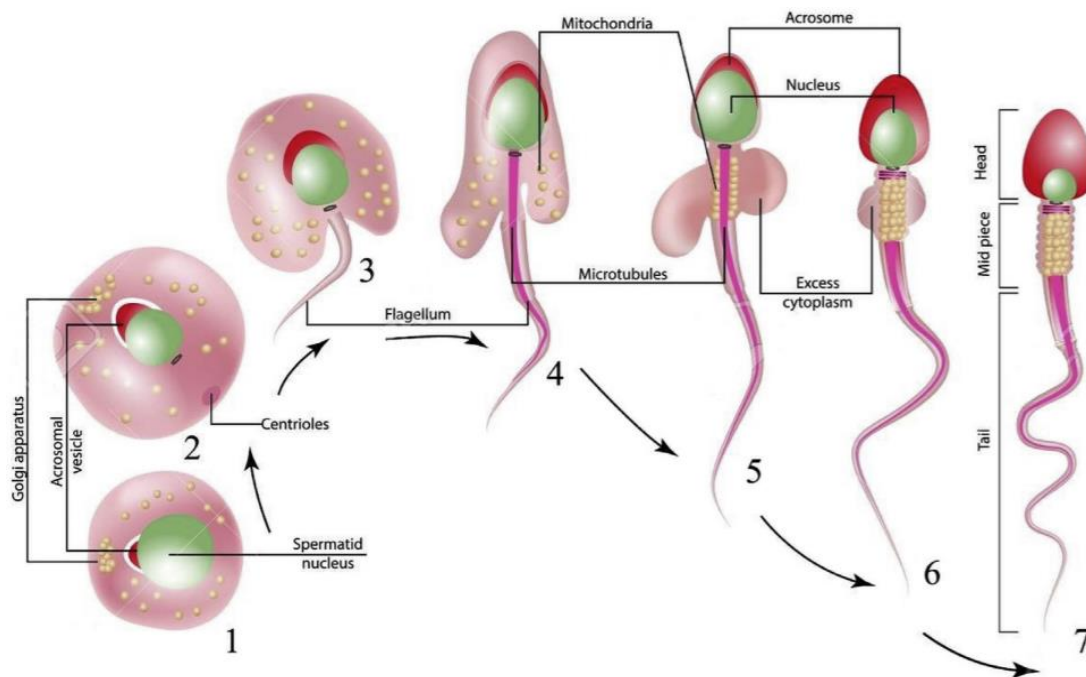
Figure 16 Morphologic changes during spermiogenesis. (1) The round spermatids start the formation of the acrosomal vesicle from the trans-Golgi stacks. **(2)** More advanced round spermatids develop the acrosome, cluster the Golgi apparatus and initiate nucleus condensation. **(3, 4)** The process of spermatid elongation. The proximal centriole participates in flagellum formation. Mitochondria are organized into longitudinal rows in the cytoplasmic lobes of the spermatids in preparation for loading onto the outer dense fibers. **(5, 6)** Elongated spermatid with well defined acrosome, hyper condensed nucleus, and excess cytoplasm containing residual mitochondria (not specified in the figure). **(7)** Fully mature spermatozoon released at spermiation, without a residual body.

_____

5.4   Limitations of the study

In **Paper I,** we provide a methodology for high-resolution imaging of human spermatozoa applying live-cell compatible fluorescent probes and subsequent cell immobilization with patches of agarose. A background signal has been detected for the

uppermost part of the imaging stacks contacting with the agarose patch. Despite this, the method revealed structural details of the cells. However, SIM of living spermatozoa cannot be applied directly to the clinical practice due to the usage of fluorescent probes and the expensive equipment.

For the analysis and classification of human sperm cells in **Papers II-III** we applied QPM assisted with AI. Despite the feasibility of the non-labeled nanoscopic imaging technique, a clinical trial is required to translate the innovation into life. However, there are some concerns to consider before clinical trial and application steps. One important aspect is the time required for imaging processing, which might be crucial for sperm analysis and selection upon manipulations in reproductive clinics. Moreover, a specially trained operator is required to interpret the results of the QPM imaging. Instead of this, the system should be user-friendly, provide fast and automated results. Additionally, the precision of the resulted interferogram is defined by the technical equipment, which might be expensive for routine use in the IVF laboratory.

For our systematic review and meta-analysis **(Paper IV)** on differences in mtDNAcn between the patients with normal and abnormal semen analyses, only five of 10 selected studies were included for quantitative synthesis. Moreover, some studies performed the semen analysis based on WHO 1999 criteria (May-Panloup *et al.,* 2003; Amaral et al., 2007), whereas others used the WHO 2010 criteria (Tian *et al.,* 2014; Bonanno *et al.,* 2016; Faja *et al.,* 2019). A subgroup analysis including different sperm abnormalities, i.e., astheno-, oligoastheno-, asthenoterato-, oligoasthenoteratospermia, etc., was not possible to conduct due to not all studies divided the abnormal semen analyses into subgroups. Some studies included groups of patients with only reduced sperm motility and normal sperm counts as the abnormal semen analysis for the study group.

5.5 Future perspectives

There are several translational points on the way to the clinical implementation of any innovation. The proof of principle and feasibility of non-invasive QPM has been demonstrated effectively for analyzing human spermatozoa. However, before initiating a clinical trial, researchers and clinicians have to establish the correlation between sperm cell morphology and fertilizing potential of the individual cell. Assessment of fertilizing potential of individual sperm cell might be performed by measuring different features, including mtDNAcn. The optimization of the QPM method has to be done to improve the system's specificity for the

sperm cells analysis. First, the development of holographic approaches to image motile spermatozoa is needed. Second, the implementation of virtual staining achieved by advanced deep learning analysis of unlabeled QPM data may provide detailed information about different cellular components, which appears to be one of the most promising tools in ART settings in the future.

Finally, uncovering the association between mtDNAcn and semen quality suggests future research, including detection of the underlying mechanisms behind mtDNA increase at abnormal semen analysis. Moreover, further works need to be done on the connection of sperm mtDNAcn and ART outcome.

6 CONCLUSIONS

Given the importance of characterizing the sperm cell morphology, which is a relevant parameter for semen analysis and spermatozoa selection, we employed the advantages of nano-optics to study and classify human sperm cells. First, we provided a methodology for live-cell imaging of human spermatozoa using Structured Illumination Microscopy, which has shown a significant resolution of spermatozoa features compatible with transmission electron microscopy imaging. This methodology is expected to be a promising tool for sperm cell research, especially in subcellular structures analysis. Secondly, we used the technical capability of holographic microscopy to detect the morphology changes of spermatozoa upon oxidative stress. The result of our study suggests the shift of optical properties of human sperm heads after exposure to oxidative stress. Moreover, QPM provided an opportunity to distinguish the normal sperm cells from those under pathophysiological conditions applying deep learning algorithms. This quantitative non-invasive imaging method may be of great significance for automated analysis of the semen and spermatozoa selection in ART.

Additionally, our systematic review and meta-analysis on published literature provided evidence that the increase of sperm mitochondrial DNA copy numbers is associated with abnormal semen quality. The mechanism by which mtDNAcn is increased in males with semen abnormalities is still unclear. However, considering the presence of a higher number of mitochondrial DNA in abnormal semen, the detection of mtDNAcn may be used for diagnostic purposes.

References

Adamopoulos, D. A., Pappa, A., Nicopoulou, S., Andreou, E., Karamertzanis, M., Michopoulos, J., Deligianni, V., & Simou, M. (1996). Seminal volume and total sperm number trends in men attending subfertility clinics in the Greater Athens area during the period 1977-1993. *Human Reproduction*, *11*(9), 1936-1941.

Adams, J. A., Galloway, T. S., Mondal, D., Esteves, S. C., & Mathews, F. (2014). Effect of mobile telephones on sperm quality: A systematic review and meta-analysis. *Environment International*, *70*, 106-112.

Afeiche, M., Williams, P. L., Mendiola, J., Gaskins, A. J., Jorgensen, N., Swan, S. H., & Chavarro, J. E. (2013). Dairy food intake in relation to semen quality and reproductive hormone levels among physically active young men. *Human Reproduction*, *28*(8), 2265-2275.

Agarwal, A., Baskaran, S., Parekh, N., Cho, C. L., Henkel, R., Vij, S., Arafa, M., Panner Selvam, M. K., & Shah, R. (2021). Male infertility. *Lancet*, *397*(10271), 319-333.

Agarwal, A., & Kumar Panner Selvam, M. (2018). Advanced Sperm Processing/Selection Techniques. In A. A. Zini, Ashok (Eds.), *A Clinician's Guide to Sperm DNA and Chromatin Damage,* (pp.529-543). Springer International Publishing.

Ainsworth, C., Nixon, B., & Aitken, R. J. (2005). Development of a novel electrophoretic system for the isolation of human spermatozoa. *Human Reproduction*, *20*(8), 2261-2270.

Aitken, J.R. (2020). Sperm selection for ART success. In J. R. Aitken, D. Mortimer, & G. Kovacs (Eds.), *Male and Sperm Factors that Maximize IVF Success* (pp.1-14). Cambridge University Press.

Ambulkar, P. S., Waghmare, J. E., Chaudhari, A. R., Wankhede, V. R., Tarnekar, A. M., Shende, M. R., & Pal, A. K. (2016). Large Scale 7436-bp Deletions in Human Sperm Mitochondrial DNA with Spermatozoa Dysfunction and Male Infertility. *Journal of Clinical and Diagnostic Research*, *10*(11), GC9-GC12.

Amaral, A., Ramalho-Santos, J., & St John, J. C. (2007). The expression of polymerase gamma and mitochondrial transcription factor A and the regulation of mitochondrial DNA content in mature human sperm. *Human reproduction*, *22*(6), 1585–1596.

Anderson, S., Bankier, A. T., Barrell, B. G., Debruijn, M. H. L., Coulson, A. R., Drouin, J., Eperon, I. C., Nierlich, D. P., Roe, B. A., Sanger, F., Schreier, P. H., Smith, A. J. H., Staden, R., & Young, I. G. (1981). Sequence and organization of the human mitochondrial genome. *Nature*, *290*(5806), 457-465.

Angelis, A. De, Ferrara, M. A., Coppola, G., Luca, A. C. De. (2018). Advanced Label-Free Optical Methods for Spermatozoa Quality Assessment and Selection. In R. Meccariello, R. Chianese (Eds.), *Spermatozoa-Facts and Perspectives*, (pp. 219-240). IntechOpen.

Ashley, N., Harris, D., & Poulton, J. (2005). Detection of mitochondrial DNA depletion in living human cells using PicoGreen staining. *Experimental Cell Research*, *303*(2), 432-446.

Auger, J., Jouannet, P., & Eustache, F. (2016). Another look at human sperm morphology. *Human Reproduction*, *31*(1), 10-23.

Auger, J., Kunstmann, J. M., Czyglik, F., & Jouannet, P. (1995). Decline in semen quality among fertile men in Paris during the past 20 years. *New England Journal of Medicine*, *332*(5), 281-285.

Avendano, C., Mata, A., Sanchez Sarmiento, C. A., & Doncel, G. F. (2012). Use of laptop computers connected to internet through Wi-Fi decreases human sperm motility and increases sperm DNA fragmentation. *Fertility and Sterility*, *97*(1), 39-U93.

Aziz, N., Buchan, I., Taylor, C., Kingsland, C. R., & LewisJones, I. (1996). The sperm deformity index: A reliable predictor of the outcome of oocyte fertilization in vitro. *Fertility and Sterility*, *66*(6), 1000-1008.

Baklouti-Gargouri, S., Ghorbel, M., Ben Mahmoud, A., Mkaouar-Rebai, E., Cherif, M., Chakroun, N., Sellami, A., Fakhfakh, F., & Ammar-Keskes, L. (2014). Identification of a novel m.9588G > a missense mutation in the mitochondrial COIII gene in asthenozoospermic Tunisian infertile men. *Journal of Assisted Reproduction and Genetics*, *31*(5), 595–600.

Balberg, M., Levi, M., Kalinowski, K., Barnea, I., Mirsky, S. K., & Shaked, N. T. (2017). Localized measurements of physical parameters within human sperm cells obtained with wide-field interferometry. *Journal of Biophotonics*, *10*(10), 1305-1314.

Barnea, I., Karako, L., Mirsky, S. K., Levi, M., Balberg, M., & Shaked, N. T. (2018). Stain-free interferometric phase microscopy correlation with DNA fragmentation stain in human spermatozoa. *Journal of biophotonics*, *11*(11), e201800137.

Barratt, C. L. R., Bjorndahl, L., De Jonge, C. J., Lamb, D. J., Osorio Martini, F., McLachlan, R., Oates, R. D., van der Poel, S., St John, B., Sigman, M., Sokol, R., & Tournaye, H. (2017). The diagnosis of male infertility: an analysis of the evidence to support the development of global WHO guidance-challenges and future research opportunities. *Human Reproduction Update*, *23*(6), 660-680.

Barthelemy, C., Royere, D., Hammamah, S., Lebos, C., Tharanne, M. J., & Lansac, J. (1990). Ultrustructural changes in membranes and acrosomes of human sperm during cryopreservation. *Archives of Andrology*, *25*(1), 29-40.

Bartoov, B., Berkovitz, A., Eltes, F., Kogosowski, A., Menezo, Y., & Barak, Y. (2002). Real-time fine morphology of motile human sperm cells is associated with IVF-ICSI outcome. *Journal of Andrology*, *23*(1), 1-8.

Basnet, P., Hansen, S. A., Olaussen, I. K., Hentemann, M. A., & Acharya, G. (2016). Changes in the semen quality among 5739 men seeking infertility treatment in Northern Norway over past 20 years (1993–2012). *Journal of Reproductive Biotechnology and Fertility*, *5*, 1-7.

Bay, B., Lyngso, J., Hohwu, L., & Kesmodel, U. S. (2019). Childhood growth of singletons conceived following in vitro fertilisation or intracytoplasmic sperm injection: a systematic review and meta-analysis. *Bjog-an International Journal of Obstetrics and Gynaecology*, *126*(2), 158-166.

Beauchamp, P. J., Galle, P. C., & Blasco, L. (1984). Human sperm velocity and postinsemination cervical mucus test in the evaluation of the inferile couple. *Archives of Andrology*, *13*(2-3), 107-112.

Beck-Fruchter, R., Shalev, E., & Weiss, A. (2016). Clinical benefit using sperm hyaluronic acid binding technique in ICSI cycles: a systematic review and meta-analysis. *Reproductive Biomedicine Online*, *32*(3), 286-298.

Belva, F., Bonduelle, M., Roelants, M., Michielsen, D., Van Steirteghem, A., Verheyen, G., & Tournaye, H. (2016). Semen quality of young adult ICSI offspring: the first results. *Human Reproduction*, *31*(12), 2811-2820.

Belva, F., Roelants, M., De Schepper, J., Van Steirteghem, A., Tournaye, H., & Bonduelle, M. (2017). Reproductive hormones of ICSI-conceived young adult men: the first results. *Human Reproduction*, *32*(2), 439-446.

Berkovitz, A., Eltes, F., Ellenbogen, A., Peer, S., Feldberg, D., & Bartoov, B. (2006a). Does the presence of nuclear vacuoles in human sperm selected for ICSI affect pregnancy outcome? *Human Reproduction*, *21*(7), 1787-1790.

Berkovitz, A., Eltes, F., Lederman, H., Peer, S., Ellenbogen, A., Feldberg, B., & Bartoov, B. (2006b). How to improve IVF-ICSI outcome by sperm selection. *Reproductive Biomedicine Online*, *12*(5), 634-638.

Berntsen, S., Söderström-Anttila, V., Wennerholm, U. B., Laivuori, H., Loft, A., Oldereid, N. B., Romundstad, L. B., Bergh, C., & Pinborg, A. (2019). The health of children conceived by ART: 'the chicken or the egg?'. *Human Reproductin Update*, *25*(2), 137-158.

Birkhead, T. R., Montgomerie, R. (2009). Sperm, human fertility and society. In T. R. Birkhead, D. J. Hosken, S. Pitnick (Eds.), *Three centuries of sperm research* (pp. 1-42). Academic Press.

Bloom, M. S., Whitcomb, B. W., Chen, Z., Ye, A., Kannan, K., & Louis, G. M. B. (2015). Associations between urinary phthalate concentrations and semen quality parameters in a general population. *Human Reproduction*, *30*(11), 2645-2657.

Boguenet, M., Bouet, P. E., Spiers, A., Reynier, P., & May-Panloup, P. (2021). Mitochondria: their role in spermatozoa and in male infertility. *Human Reproduction Update, 0*(0), 1-23.

Boitrelle, F., Albert, M., Theillac, C., Ferfouri, F., Bergere, M., Vialard, F., Wainer, R., Bailly, M., & Selva, J. (2012). Cryopreservation of Human Spermatozoa Decreases the Number of Motile Normal Spermatozoa, Induces Nuclear Vacuolization and Chromatin Decondensation. *Journal of Andrology*, *33*(6), 1371-1378.

Bonanno, O., Romeo, G., Asero, P., Pezzino, F. M., Castiglione, R., Burrello, N., Sidoti, G., Frajese, G. V., Vicari, E., & D'Agata, R. (2016). Sperm of patients with severe asthenozoospermia show biochemical, molecular and genomic alterations. *Reproduction*, *152*(6), 695–704.

Boulet, S. L., Mehta, A., Kissin, D. M., Warner, L., Kawwass, J. F., & Jamieson, D. J. (2015). Trends in Use of and Reproductive Outcomes Associated With Intracytoplasmic Sperm Injection. *Jama-Journal of the American Medical Association*, *313*(3), 255-263.

Bunge, R. G., & Sherman, J. K. (1953). Fertilizing capacity of frozen human spermatozoa. *Nature*, *172*(4382), 767-768.

Calhaz-Jorge, C., De Geyter, C., Kupka, M. S., de Mouzon, J., Erb, K., Mocanu, E., Motrenko, T., Scaravelli, G., Wyns, C., & Goossens, V. (2017). Assisted reproductive technology in Europe, 2013: results generated from European registers by ESHRE. The European IVF-monitoring Consortium (EIM) for the European Society of Human Reproduction and Embryology (ESHRE). *Human Reproduction*, *32*(10), 1957-1973.

Carlsen, E., Giwercman, A., Keiding, N., & Skakkebaek, N. E. (1992). Evidence for decreasing quality of semen during past 50 years. *BMJ (Clinical research ed.)*, *305*(6854), 609–613.

Catford, S. R., McLachlan, R. I., O'Bryan, M. K., & Halliday, J. L. (2017). Long-term follow-up of intra-cytoplasmic sperm injection-conceived offspring compared with in vitro fertilization-conceived offspring: a systematic review of health outcomes beyond the neonatal period. *Andrology*, *5*(4), 610-621.

Catford, S. R., McLachlan, R. I., O'Bryan, M. K., & Halliday, J. L. (2018). Long-term follow-up of ICSI-conceived offspring compared with spontaneously conceived offspring: a systematic review of health outcomes beyond the neonatal period. *Andrology*, *6*(5), 635-653.

Chang, V., Heutte, L., Petitjean, C., Hartel, S., & Hitschfeld, N. (2017). Automatic classification of human sperm head morphology. *Computers in Biology and Medicine*, *84*, 205-216.

Chiu, Y.-H., Gaskins, A. J., Williams, P. L., Mendiola, J., Jorgensen, N., Levine, H., Hauser, R., Swan, S. H., &

Chavarro, J. E. (2016). Intake of Fruits and Vegetables with Low-to-Moderate Pesticide Residues Is Positively Associated with Semen-Quality Parameters among Young Healthy Men. *Journal of Nutrition*, *146*(5), 1084-1092.

Chu, K. Y., Nassau, D. E., Arora, H., Lokeshwar, S. D., Madhusoodanan, V., & Ramasamy, R. (2019). Artificial Intelligence in Reproductive Urology. *Current Urology Reports*, *20*(9), Article 52.

Colagar, A. H., & Karimi, F. (2014). Large scale deletions of the mitochondrial DNA in astheno, asthenoterato and oligoasthenoterato-spermic men. *Mitochondrial DNA*, *25*(4), 321-328.

Colagar, A. H., Karimi, F., & Jorsaraei, S. G. A. (2013). Correlation of Sperm Parameters With Semen Lipid Peroxidation and Total Antioxidants Levels in Astheno- and Oligoasheno-Teratospermic Men. *Iranian Red Crescent Medical Journal*, *15*(9), 780-785.

Cooper, T. G., Noonan, E., von Eckardstein, S., Auger, J., Baker, H. W. G., Behre, H. M., Haugen, T. B., Kruger, T., Wang, C., Mbizvo, M. T., & Vogelsong, K. M. (2010). World Health Organization reference values for human semen characteristics. *Human Reproduction Update*, *16*(3), 231-245.

Coppola, G., Di Caprio, G., Wilding, M., Ferraro, P., Esposito, G., Di Matteo, L., Dale, R., & Dale, B. (2013). Digital holographic microscopy for the evaluation of human sperm structure. *Zygote*, *22*(4), 446-454.

Crha, I., Zakova, J., Huser, M., Ventruba, P., Lousova, E., & Pohanka, M. (2011). Digital holographic microscopy in human sperm imaging. *Journal of Assisted Reproduction and Genetics*, *28*(8), 725–729.

Curchoe, C. L., & Bormann, C. L. (2019). Artificial intelligence and machine learning for human reproduction and embryology presented at ASRM and ESHRE 2018. *Journal of Assisted Reproduction and Genetics*, *36*(4), 591-600.

Dallinga, J. W., Moonen, E. J. C., Dumoulin, J. C. M., Evers, J. L. H., Geraedts, J. P. M., & Kleinjans, J. C. S. (2002). Decreased human semen quality and organochlorine compounds in blood. *Human Reproduction*, *17*(8), 1973-1979.

Danis, R. B., & Samplaski, M. K. (2019). Sperm Morphology: History, Challenges, and Impact on Natural and Assisted Fertility. *Current Urology Reports*, *20*(8), Article 43.

Dardikman-Yoffe, G., Mirsky, S. K., Barnea, I., & Shaked, N. T. (2020). High-resolution 4-D acquisition of freely swimming human sperm cells without staining. *Science Advances*, *6*(15), Article eaay7619.

Davies, M. J., Moore, V. M., Willson, K. J., Van Essen, P., Priest, K., Scott, H., Haan, E. A., & Chan, A. (2012). Reproductive Technologies and the Risk of Birth Defects. *New England Journal of Medicine*, *366*(19), 1803-1813.

Davies, M. J. (2020). Perinatal outcomes from IVF and ICSI. In R. J. Aitken, D. Mortimer , & G. Kovacs (Eds.), *Male and Sperm Factors that Maximize IVF Success* (pp. 141-153). Cambridge University Press.

De Lamirande, E., & Gagnon, C. (1992). Reactive oxygen species and human spermatozoa. 1. Effects on the motility of intact spermatozoa and on sperm axonemes. *Journal of Andrology*, *13*(5), 368-378.

De Luca, S. Z., & O'Farrell, P. H. (2012). Barriers to Male Transmission of Mitochondrial DNA in Sperm Development. *Developmental Cell*, *22*(3), 660-668.

Di Caprio, M. Gioffrè, N. Saffioti, S. Grilli, P. Ferraro, R. Puglisi, D. Balduzzi, A. Galli, and G. Coppola. (2010). Quantitative label-free animal sperm imaging by means of digital holographic microscopy. *IEEE Journal of Quantum Electronics,* 16(4), 833–840.

Di Caprio, G., El Mallahi, A., Ferraro, P., Dale, R., Coppola, G., Dale, B., Coppola, G., & Dubois, F. (2014). 4D tracking of clinical seminal samples for quantitative characterization of motility parameters. *Biomedical Optics Express*, *5*(3), 690–700.

Díez-Sánchez, C., Ruiz-Pesini, E., Lapeña, A. C., Montoya, J., Pérez-Martos, A., Enríquez, J. A., & López-Pérez, M. J. (2003). Mitochondrial DNA content of human spermatozoa. *Biology of Reproduction*, *68*(1), 180–185.

Donnelly, E. T., Steele, E. K., McClure, N., & Lewis, S. E. M. (2001). Assessment of DNA integrity and morphology of ejaculated spermatozoa from fertile and infertile men before and after cryopreservation. *Human Reproduction*, *16*(6), 1191-1199.

Donnelly, G. P., McClure, N., Kennedy, M. S., & Lewis, S. E. M. (1999). Direct effect of alcohol on the motility and morphology of human spermatozoa. *Andrologia*, *31*(1), 43-47.

Dubey, V., Popova, D., Ahmad, A., Acharya, G., Basnet, P., Mehta, D. S. I., & Ahluwalia, B. S. I. (2019). Partially spatially coherent digital holographic microscopy and machine learning for quantitative analysis of human spermatozoa under oxidative stress condition. *Scientific Reports*, *9*, Article 3564.

Duru, N. K., Morshedi, M., & Oehninger, S. (2000). Effects of hydrogen peroxide on DNA and plasma membrane integrity of human spermatozoa. *Fertility and Sterility*, *74*(6), 1200-1207.

Dyer, S., Chambers, G. M., de Mouzon, J., Nygren, K. G., Zegers-Hochschild, F., Mansour, R., Ishihara, O., Banker, M., & Adamson, G. D. (2016). International Committee for Monitoring Assisted Reproductive Technologies world report: Assisted Reproductive Technology 2008, 2009 and 2010. *Human Reproduction*, *31*(7), 1588-1609.

El-Taieb, M. A., Ali, M. A., & Nada, E. A. (2015). Oxidative stress and acrosomal morphology: A cause of

infertility in patients with normal semen parameters. *Middle East Fertility Society Journal*, *20*(2), 79-85.

Eravuchira, P. J., Mirsky, S. K., Barnea, I., Levi, M., Balberg, M., & Shaked, N. T. (2018). Individual sperm selection by microfluidics integrated with interferometric phase microscopy. *Methods*, *136*, 152-159.

Erberelli, R. F., Salgado, R. M., Mendes Pereira, D. H., & Wolff, P. (2017). Hyaluronan-binding system for sperm selection enhances pregnancy rates in ICSI cycles associated with male factor infertility. *Jornal Brasileiro De Reproducao Assistida*, *21*(1), 2-6.

Eroglu, M., Sahin, S., Durukan, B., Ozakpinar, O. B., Erdinc, N., Turkgeldi, L., Sofuoglu, K., & Karateke, A. (2014). Blood Serum and Seminal Plasma Selenium, Total Antioxidant Capacity and Coenzyme Q10 Levels in Relation to Semen Parameters in Men with Idiopathic Infertility. *Biological Trace Element Research*, *159*(1-3), 46-51.

Eustache, F., & Auger, J. (2003). Inter-individual variability in the morphological assessment of human sperm: effect of the level of experience and the use of standard methods. *Human Reproduction*, *18*(5), 1018-1022.

Faja, F., Carlini, T., Coltrinari, G., Finocchi, F., Nespoli, M., Pallotti, F., Lenzi, A., Lombardo, F., & Paoli, D. (2019). Human sperm motility: a molecular study of mitochondrial DNA, mitochondrial transcription factor A gene and DNA fragmentation. *Molecular Biology Reports*, *46*(4), 4113–4121.

Ferlin, A. (2020). Prevention of Male Infertility: From Childhood to Adulthood. In J. R. Aitken, D. Mortimer, & G. Kovacs (Eds.), *Male and Sperm Factors that Maximize IVF Success* (pp. 211-228). Cambridge University Press.

Ferlin, A., Raicu, F., Gatta, V., Zuccarello, D., Palka, G., & Foresta, C. (2007). Male infertility: role of genetic background. *Reproductive Biomedicine Online*, *14*(6), 734-745.

Fleming, S. D., Ilad, R. S., Griffin, A. M. G., Wu, Y., Ong, K. J., Smith, H. C., & Aitken, R. J. (2008). Prospective controlled trial of an electrophoretic method of sperm preparation for assisted reproduction: comparison with density gradient centrifugation. *Human Reproduction*, *23*(12), 2646-2651.

Fujita, T., Miyoshi, M., & Tokunaga, J. (1970). Scanning and transmission electron microscopy of human ejaculate spermatozoa with special reference to their abnormal forms. *Zeitschrift fur Zellforschung und Mikroskopische Anatomie*, *105*(4), 483–497.

Gabriel, M. S., Chan, S. W., Alhathal, N., Chen, J. Z., & Zini, A. (2012). Influence of microsurgical varicocelectomy on human sperm mitochondrial DNA copy number: a pilot study. *Journal of Assisted Reproduction and Genetics*, *29*(8), 759-764.

Gangrade, B. K. (2013). Cryopreservation of testicular and epididymal sperm: techniques and clinical outcomes of assisted conception. *Clinics*, *68*, 131-140.

Geoffroy-Siraudin, C., Loundou, A. D., Romain, F., Achard, V., Courbiere, B., Perrard, M.-H., Durand, P., & Guichaoua, M.-R. (2012). Decline of semen quality among 10 932 males consulting for couple infertility over a 20-year period in Marseille, France. *Asian Journal of Andrology*, *14*(4), 584-590.

Gervasi, M. G., Xu, X. R., Carbajal-Gonzalez, B., Buffone, M. G., Visconti, P. E., & Krapf, D. (2018). The actin cytoskeleton of the mouse sperm flagellum is organized in a helical structure. *Journal of Cell Science*, *131*(11), Article jcs215897.

Gholinezhad, M., Yousefnia-pasha, Y., Colagar, A. H., Mohammadoo-Khorasani, M., & Bidmeshkipour, A. (2019). Comparison of large-scale deletions of the sperm mitochondrial DNA in normozoospermic and asthenoteratozoospermic men. *Journal of Cellular Biochemistry*, *120*(2), 1958-1968.

Gibb, Z., Griffin, R. A., Aitken, R. J., & De Iuliis, G. N. (2020). Functions and effects of reactive oxygen species in male fertility. *Animal Reproduction Science*, *220*, Article 106456.

Gil, M., Sar-Shalom, V., Melendez Sivira, Y., Carreras, R., & Angel Checa, M. (2013). Sperm selection using magnetic activated cell sorting (MACS) in assisted reproduction: a systematic review and meta-analysis. *Journal of Assisted Reproduction and Genetics*, *30*(4), 479-485.

Gimenes, F., Souza, R. P., Bento, J. C., Teixeira, J. J. V., Maria-Engler, S. S., Bonini, M. G., & Consolaro, M. E. L. (2014). Male infertility: a public health issue caused by sexually transmitted pathogens. *Nature Reviews Urology*, *11*(12), 672-687.

Girshovitz, P., & Shaked, N. T. (2013). Compact and portable low-coherence interferometer with off-axis geometry for quantitative phase microscopy and nanoscopy. *Optics Express*, *21*(5), 5701-5714.

Gook, D. A., & Edgar, D. H. (2007). Human oocyte cryopreservation. *Human reproduction update*, *13*(6), 591–605.

Gordon, J. W., Grunfeld, L., Garrisi, G. J., Talansky, B. E., Richards, C., & Laufer, N. (1988). Fertilization of human oocytes by sperm from infertile males after zona pellucida drilling. *Fertility and Sterility*, *50*(1), 68-73.

Guzick, D. S., Overstreet, J. W., Factor-Litvak, P., Brazil, C. K., Nakajima, S. T., Coutifaris, C., Carson, S. A., Cisneros, P., Steinkampf, M. P., Hill, J. A., Xu, D., Vogel, D. L., & Natl Cooperative Reprod Med, N. (2001). Sperm morphology, motility, and concentration in fertile and infertile men. *New England Journal of Medicine*, *345*(19), 1388-1393.

Haifler, M., Girshovitz, P., Band, G., Dardikman, G., Madjar, I., & Shaked, N. T. (2015). Interferometric phase microscopy for label-free morphological evaluation of sperm cells. *Fertility and Sterility*, *104*(1), 43-47.

Hammadeh, M. E., Askari, A. S., Georg, T., Rosenbaum, P., & Schmidt, W. (1999). Effect of freeze-thawing procedure on chromatin stability, morphological alteration and membrane integrity of human spermatozoa in fertile and subfertile men. *International Journal of Andrology*, *22*(3), 155-162.

Hauser, R., Meeker, J. D., Duty, S., Silva, M. J., & Calafat, A. M. (2006). Altered semen quality in relation to urinary concentrations of phthalate monoester and oxidative metabolites. *Epidemiology*, *17*(6), 682-691.

Hu, C., & Popescu, G. (2019). Quantitative Phase Imaging: Principles and Applications. In V. Astratov (Ed.), *Label-Free Super-Resolution Microscopy* (pp.1-18). Springer International Publishing.

Huffman, A. M., Wu, H. T., Rosati, A., Rahil, T., Sites, C. K., Whitcomb, B. W., & Pilsner, J. R. (2018). Associations of urinary phthalate metabolites and lipid peroxidation with sperm mitochondrial DNA copy number and deletions. *Environmental Research*, *163*, 10-15.

Huszar, G., Jakab, A., Sakkas, D., Ozenci, C. C., Cayli, S., Delpiano, E., & Ozkavukcu, S. (2007). Fertility testing and ICSI sperm selection by hyaluronic acid binding: clinical and genetic aspects. *Reproductive Biomedicine Online*, *14*(5), 650-663.

Hutchison C.A., Newbold, J. E., Potter, S. S., & Edgell, M. H. (1974). Maternal inheritance of mammalian mitochondrial DNA. *Nature*, *251*(5475), 536-538.

Irvine, S., Cawood, E., Richardson, D., MacDonald, E., & Aitken, J. (1996). Evidence of deteriorating semen quality in the United Kingdom: Birth cohort study in 577 men in Scotland over 11 years. *Bmj-British Medical Journal*, *312*(7029), 467-471.

Itoh, N., Kayama, F., Tatsuki, T. J., & Tsukamoto, T. (2001). Have sperm counts deteriorated over the past 20 years in healthy, young Japanese men? Results from the Sapporo area. *Journal of Andrology*, *22*(1), 40-44.

Jang, T. H., Park, S. C., Yang, J. H., Kim, J. Y., Seok, J. H., Park, U. S., Choi, C. W., Lee, S. R., & Han, J. (2017). Cryopreservation and its clinical applications. *Integrative Medicine Research*, *6*(1), 12-18.

Jankovicova, J., Frolikova, M., Palenikova, V., Valaskova, E., Cerny, J., Secova, P., Bartokova, M., Horovska, L., Manaskova-Postlerova, P., Antalikova, J., & Komrskova, K. (2020). Expression and distribution of CD151 as a partner of alpha6 integrin in male germ cells. *Scientific Reports*, *10*(1), Article 4374.

Jensen, T. K., Gottschau, M., Madsen, J. O. B., Andersson, A. M., Lassen, T. H., Skakkebaek, N. E., Swan, S. H., Priskorn, L., Juul, A., & Jorgensen, N. (2014). Habitual alcohol consumption associated with reduced semen quality and changes in reproductive hormones; a cross-sectional study among 1221 young Danish men. *Bmj Open*, *4*(9), Article e005462.

Jensen, T. K., Heitmann, B. L., Jensen, M. B., Halldorsson, T. I., Andersson, A.-M., Skakkebaek, N. E., Joensen, U. N., Lauritsen, M. P., Christiansen, P., Dalgard, C., Lassen, T. H., & Jorgensen, N. (2013). High dietary intake of saturated fat is associated with reduced semen quality among 701 young Danish men from the general population. *American Journal of Clinical Nutrition*, *97*(2), 411-418.

Ji, J., Xu, M. F., Huang, Z. Y., Li, L., Zheng, H. X., Yang, S. P., Li, S. L., Jin, L., Ling, X. F., Xia, Y. K., Lu, C. C., & Wang, X. R. (2017). Mitochondrial DNA sequencing and large-scale genotyping identifies MT-ND4 gene mutation m.11696G>A associated with idiopathic oligoasthenospermia. *Oncotarget*, *8*(32), 52975-52982.

Jiang, M., Kauppila, T. E. S., Motori, E., Li, X. P., Atanassov, I., Folz-Donahue, K., Bonekamp, N. A., Albarran-Gutierrez, S., Stewart, J. B., & Larsson, N. G. R. (2017). Increased Total mtDNA Copy Number Cures Male Infertility Despite Unaltered mtDNA Mutation Load. *Cell Metabolism*, *26*(2), 429-436.e4.

Jiang, H., Kwon, J. W., Lee, S., Jo, Y. J., Namgoong, S., Yao, X. R., Yuan, B., Zhang, J. B., Park, Y. K., & Kim, N. H. (2019). Reconstruction of bovine spermatozoa substances distribution and morphological differences between Holstein and Korean native cattle using three-dimensional refractive index tomography. *Scientific reports*, *9*(1), 8774.

Jo, Y., Park, S., Jung, J., Yoon, J., Joo, H., Kim, M. H., Kang, S. J., Choi, M. C., Lee, S. Y., & Park, Y. (2017). Holographic deep learning for rapid optical screening of anthrax spores. *Science Advances*, *3*(8), Article e1700606.

Jost, A., & Heintzmann, R. (2013). Superresolution Multidimensional Imaging with Structured Illumination Microscopy. *Annual Review of Materials Research, 43*, 261-282.

Kai, C. M., Main, K. M., Andersen, A. N., Loft, A., Skakkebaek, N. E., & Juul, A. (2007). Reduced serum testosterone levels in infant boys conceived by intracytoplasmic sperm injection. *Journal of Clinical Endocrinology & Metabolism*, *92*(7), 2598-2603.

Kallen, B., Finnstrom, O., Nygren, K. G., & Olausson, P. O. (2005). In vitro fertilization (IVF) in Sweden: Risk for congenital malformations after different IVF methods. *Birth Defects Research Part a-Clinical and Molecular Teratology*, *73*(3), 162-169.

Kamischke, A., Gromoll, J., Simoni, M., Behre, H. M., & Nieschlag, E. (1999). Transmission of a Y chromosomal deletion involving the deleted in azoospermia (DAZ) and chromodomain (CDY1) genes from father to

son through intracytoplasmic sperm injection. *Human Reproduction*, *14*(9), 2320-2322.

Kandel, M. E., He, Y. C. R., Lee, Y. J., Chen, T. H. Y., Sullivan, K. M., Aydin, O., Saif, M. T. A., Kong, H., Sobh, N., & Popescu, G. (2020). Phase imaging with computational specificity (PICS) for measuring dry mass changes in sub-cellular compartments. *Nature Communications*, *11*(1), Article 6256.

Kandel, M. E., Rubessa, M., He, Y. R., Schreiber, S., Meyers, S., Naves, L. M., Sermersheim, M. K., Sell, G. S., Szewczyk, M. J., Sobh, N., Wheeler, M. B., & Popescu, G. (2020). Reproductive outcomes predicted by phase imaging with computational specificity of spermatozoon ultrastructure. *Proceedings of the National Academy of Sciences of the United States of America*, *117*(31), 18302-18309.

Kao, S. H., Chao, H. T., Chen, H. W., Hwang, T. I. S., Liao, T. L., & Wei, Y. H. (2008). Increase of oxidative stress in human sperm with lower motility. *Fertility and Sterility*, *89*(5), 1183-1190.

Kao, S. H., Chao, H. T., & Wei, Y. H. (1995). Mitochondrial deoxyribonucleic acid 4977-bp deletion is associated with diminished fertility and motility of human sperm. *Biology of Reproduction*, *52*(4), 729-736.

Karabinus, D. S., & Gelety, T. J. (1997). The impact of sperm morphology evaluated by strict criteria on intrauterine insemination success. *Fertility and Sterility*, *67*(3), 536-541.

Kasashima, K., Nagao, Y., & Endo, H. (2014). Dynamic regulation of mitochondrial genome maintenance in germ cells. *Reproductive Medicine and Biology*, *13*(1), 11-20.

Katagiri, Y., Neri, Q. V., Takeuchi, T., Schlegel, P. N., Megid, W. A., Kent-First, M., Rosenwaks, Z., & Palermo, G. D. (2004). Y chromosome assessment and its implications for the development of ICSI children. *Reproductive Biomedicine Online*, *8*(3), 307-318.

Kemper, B., Carl, D., Schnekenburger, J., Bredebusch, I., Schaefer, M., Domschke, W., & von Bally, G. (2006). Investigation of living pancreas tumor cells by digital holographic microscopy. *Journal of Biomedical Optics*, *11*(3), Article 034005.

Kohn, T. P., Kohn, J. R., & Ramasamy, R. (2018). Effect of Sperm Morphology on Pregnancy Success via Intrauterine Insemination: A Systematic Review and Meta-Analysis. *Journal of Urology*, *199*(3), 812-821.

Kopeika, J., Thornhill, A., & Khalaf, Y. (2015). The effect of cryopreservation on the genome of gametes and embryos: principles of cryobiology and critical appraisal of the evidence. *Human Reproduction Update*, *21*(2), 209-227.

Kovac, J. R., Smith, R. P., Cajipe, M., Lamb, D. J., & Lipshultz, L. I. (2017). Men with a complete absence of normal sperm morphology exhibit high rates of success without assisted reproduction. *Asian Journal of Andrology*, *19*(1), 39-42.

Kovacs, G. T. (2020). The History of Utilization of IVF for Male Factor Subfertility. In R. J. Aitken , D. Mortimer, & G. Kovacs (Eds.), *Male and Sperm Factors that Maximize IVF Success* (pp. 121-129). Cambridge University Press.

Kruger, T. F., Menkveld, R., Stander, F. S. H., Lombard, C. J., Vandermerwe, J. P., Vanzyl, J. A., & Smith, K. (1986). Sperm morphological features as a prognostic factor in vitro fertilization.. *Fertility and Sterility*, *46*(6), 1118-1122.

Larsson, N. G., Oldfors, A., Garman, J. D., Barsh, G. S., & Clayton, D. A. (1997). Down-regulation of mitochondrial transcription factor A during spermatogenesis in humans. *Human Molecular Genetics*, *6*(2), 185-191.

Larsson, N. G., Wang, J. M., Wilhelmsson, H., Oldfors, A., Rustin, P., Lewandoski, M., Barsh, G. S., & Clayton, D. A. (1998). Mitochondrial transcription factor A is necessary for mtDNA maintenance and embryogenesis in mice. *Nature Genetics*, *18*(3), 231-236.

Lawsking, A., Trounson, A., Sathananthan, H., & Kola, I. (1987). Fertilization of human oocytes by microinjection of a single spermatozoon under the zona pellucida. *Fertility and Sterility*, *48*(4), 637-642.

Lee, J.-G., Jun, S., Cho, Y.-W., Lee, H., Kim, G. B., Seo, J. B., & Kim, N. (2017). Deep Learning in Medical Imaging: General Overview. *Korean Journal of Radiology*, *18*(4), 570-584.

Lee, K., & Park, Y. (2014). Quantitative phase imaging unit. *Optics Letters*, *39*(12), 3630-3633.

Legros, F., Malka, F., Frachon, P., Lombes, A., & Rojo, M. (2004). Organization and dynamics of human mitochondrial DNA. *Journal of Cell Science*, *117*(13), 2653-2662.

Lenzi, A., Picardo, M., Gandini, L., Lombardo, F., Terminali, O., Passi, S., & Dondero, F. (1994). Glutathione treatment of dyspermia – effect on the lipoperoxidation process. *Human Reproduction*, *9*(11), 2044-2050.

Levine, H., Jorgensen, N., Martino-Andrade, A., Mendiola, J., Weksler-Derri, D., Mindlis, I., Pinotti, R., & Swan, S. H. (2017). Temporal trends in sperm count: a systematic review and meta-regression analysis. *Human Reproduction Update*, *23*(6), 646-659.

Li, B., Ma, Y. F., Huang, J. L., Xiao, X. F., Li, L., Liu, C., Shi, Y. Q., Wang, D., & Wang, X. H. (2014). Probing the Effect of Human Normal Sperm Morphology Rate on Cycle Outcomes and Assisted Reproductive Methods Selection. *Plos One*, *9*(11), Article e113392.

Li, M. Z., Wang, H., Li, W., & Shi, J. Z. (2017). Effect of normal sperm morphology rate (NSMR) on clinical outcomes for rescue-ICSI(R-ICSI) patients. *Gynecological Endocrinology*, *33*(6), 458-461.

Li, Y., Di, J. L., Wang, K. Q., Wang, S. F., & Zhao, J. L. (2020). Classification of cell morphology with quantitative phase microscopy and machine learning. *Optics Express*, *28*(16), 23916-23927.

Li, Y., Lin, H., Li, Y. F., & Cao, J. (2011). Association between socio-psycho-behavioral factors and male semen quality: systematic review and meta-analyses. *Fertility and Sterility*, *95*(1), 116-123.

Ling, X., Zhang, G. W., Sun, L., Wang, Z., Zou, P., Gao, J. F., Peng, K. G., Chen, Q., Yang, H., Zhou, N. Y., Cui, Z. H., Zhou, Z. Y., Liu, J. Y., Cao, J., & Ao, L. (2017). Polycyclic aromatic hydrocarbons exposure decreased sperm mitochondrial DNA copy number: A cross-sectional study (MARHCS) in Chongqing, China. *Environmental Pollution*, *220*, 680-687.

Liu, C. Y., Tu, C. F., Wang, L. B., Wu, H., Houston, B. J., Mastrorosa, F. K., Zhang, W., Shen, Y., Wang, J. X., Tian, S. X., Meng, L. L., Cong, J. S., Yang, S. M., Jiang, Y. W., Tang, S. Y., Zeng, Y. Y., Lv, M. R., Lin, G., Li, J. S., Saiyin, H., He, X. J., Jin, L., Toure, A., Ray, P. F., Veltman, J. A., Shi, Q. H., O'Bryan, M. K., Cao, Y. X., Tan, Y. Q., & Zhang, F. (2021). Deleterious variants in X-linked CFAP47 induce asthenoteratozoospermia and primary male infertility. *American Journal of Human Genetics*, *108*(2), 309-323.

Liu, J., Dai, Y., Li, Y., Yuan, E., Wang, Q., Wang, X., & Guan, Y. (2020). A longitudinal study of semen quality among Chinese sperm donor candidates during the past 11 years. *Scientific Reports*, *10*(1), 10771.

Liu, K., Li, Y., Zhang, G., Liu, J., Cao, J., Ao, L., & Zhang, S. (2014). Association between mobile phone use and semen quality: a systemic review and meta-analysis. *Andrology*, *2*(4), 491-501.

Luo, Y. J., Liao, W. G., Chen, Y., Cui, J. H., Liu, F. Y., Jiang, C. H., Gao, W. X., & Gao, Y. Q. (2011). Altitude can alter the mtDNA copy number and nDNA integrity in sperm. *Journal of Assisted Reproduction and Genetics*, *28*(10), 951-956.

Majumdar, G., & Majumdar, A. (2013). A prospective randomized study to evaluate the effect of hyaluronic acid sperm selection on the intracytoplasmic sperm injection outcome of patients with unexplained infertility having normal semen parameters. *Journal of Assisted Reproduction and Genetics*, *30*(11), 1471-1475.

Majzoub, A., Arafa, M., Mahdi, M., Agarwal, A., Al Said, S., Al-Emadi, I., El Ansari, W., Alattar, A., Al Rumaihi, K., & Elbardisi, H. (2018). Oxidation-reduction potential and sperm DNA fragmentation, and their associations with sperm morphological anomalies amongst fertile and infertile men. *Arab Journal of Urology*, *16*(1), 87-95.

Malter, H. E., & Cohen, J. (1989). Partial zona dissection of the human oocyte – a nontraumatic method using micromanipulation to assist zona pellucida penetration. *Fertility and Sterility*, *51*(1), 139-148.

Mangoli, E., & Khalili, M. A. (2020). The Beneficial Role of Intra Cytoplasmic Morphologically Selected Sperm Injection (IMSI) in Assisted Reproduction. *Journal of Reproduction & Infertility*, *21*(1), 3-10.

Marino, J. L., Moore, V. M., Willson, K. J., Rumbold, A., Whitrow, M. J., Giles, L. C., & Davies, M. J. (2014). Perinatal Outcomes by Mode of Assisted Conception and Sub-Fertility in an Australian Data Linkage Cohort. *Plos One*, *9*(1), Article e80398.

Marquet, P., Depeursinge, C., & Magistretti, P. J. (2014). Review of quantitative phase-digital holographic microscopy: promising novel imaging technique to resolve neuronal network activity and identify cellular biomarkers of psychiatric disorders. *Neurophotonics*, *1*(2), Article 20901.

Martenies, S. E., & Perry, M. J. (2013). Environmental and occupational pesticide exposure and human sperm parameters: A systematic review. *Toxicology*, *307*, 66-73.

Martikainen, H., Tiitinen, A., Tomás, C., Tapanainen, J., Orava, M., Tuomivaara, L., Vilska, S., Hydén-Granskog, C., Hovatta, O., & Finnish ET Study Group (2001). One versus two embryo transfer after IVF and ICSI: a randomized study. *Human reproduction*, *16*(9), 1900–1903.

May-Panloup, P., Chrétien, M. F., Savagner, F., Vasseur, C., Jean, M., Malthièry, Y., & Reynier, P. (2003). Increased sperm mitochondrial DNA content in male infertility. *Human reproduction*, *18*(3), 550–556.

McDowell, S., Kroon, B., Ford, E., Hook, Y., Glujovsky, D., & Yazdani, A. (2014). Advanced sperm selection techniques for assisted reproduction. *Cochrane Database of Systematic Reviews,* (10), Article Cd010461.

Merola, F., Miccio, L., Memmolo, P., Di Caprio, G., Galli, A., Puglisi, R., Balduzzi, D., Coppola, G., Netti, P., & Ferraro, P. (2013). Digital holography as a method for 3D imaging and estimating the biovolume of motile cells. *Lab on a Chip*, *13*(23), 4512-4516.

Mico, V., Zalevsky, Z., Ferreira, C., & Garcia, J. (2008). Superresolution digital holographic microscopy for three-dimensional samples. *Optics Express*, *16*(23), 19260-19270.

Miller, M. R., Kenny, S. J., Mannowetz, N., Mansell, S. A., Wojcik, M., Mendoza, S., Zucker, R. S., Xu, K., & Lishko, P. V. (2018). Asymmetrically Positioned Flagellar Control Units Regulate Human Sperm Rotation. *Cell Reports*, *24*(10), 2606-2613.

Mir, M., Wang, Z., Shen, Z., Bednarz, M., Bashir, R., Golding, I., Prasanth, S. G., & Popescu, G. (2011). Optical measurement of cycle-dependent cell growth. *Proceedings of the National Academy of Sciences of the United States of America*, *108*(32), 13124-13129.

Mirsky, S.K., Barnea, I., Shaked, N.T. (2016). Label-free Quantitative Imaging of Sperm for In Vitro Fertilization using Interferometric Phase Microscopy. *Journal of fertilization: In Vitro – IVF – Worldwide,*

Reproductive Medicine, Genetic and Stem Cell Biology, 4(3), 1000190.

Mirsky, S. K., Barnea, I., Levi, M., Greenspan, H., & Shaked, N. T. (2017). Automated analysis of individual sperm cells using stain-free interferometric phase microscopy and machine learning. *Cytometry. Part A : the Journal of the International Society for Analytical Cytology*, *91*(9), 893–900.

Mortimer, D., & Mortimer, S. T. (2013). Density gradient separation of sperm for artificial insemination. *Methods in molecular biology*, *927*, 217-226.

Mortimer , D., & Mortimer, S. T. (2020). The Case Against Intracytoplasmic Sperm Injection for All. In J. R. M. Aitken, David Kovacs, Gabor (Eds.), *Male and Sperm Factors that Maximize IVF Success* (pp. 130-140). Cambridge University Press.

Nordkap, L., Jensen, T. K., Hansen, A. M., Lassen, T. H., Bang, A. K., Joensen, U. N., Jensen, M. B., Skakkebaek, N. E., & Jorgensen, N. (2016). Psychological stress and testicular function: a cross-sectional study of 1,215 Danish men. *Fertility and Sterility*, *105*(1), 174-87.e872.

Nordkap, L., Joensen, U. N., Jensen, M. B., & Jorgensen, N. (2012). Regional differences and temporal trends in male reproductive health disorders: Semen quality may be a sensitive marker of environmental exposures. *Molecular and Cellular Endocrinology*, *355*(2), 221-230.

O'Connell, M., McClure, N., & Lewis, S. E. M. (2002). The effects of cryopreservation on sperm morphology, motility and mitochondrial function. *Human Reproduction*, *17*(3), 704-709.

Oehninger, S., Kruger T.F. (2021). Sperm morphology and its disorders in the context of infertility. *Fertility and Sterility Reviews, 2(1),* 75-92.

Ombelet, W., Fourie, F. L., Vandeput, H., Bosmans, E., Cox, A., Janssen, M., & Kruger, T. (1994). Teratozoospermia and In Vitro Fertilization – a randomized prospective study. *Human Reproduction*, *9*(8), 1479-1484.

Onofre, J., Baert, Y., Faes, K., & Goossens, E. (2016). Cryopreservation of testicular tissue or testicular cell suspensions: a pivotal step in fertility preservation. *Human Reproduction Update*, *22*(6), 744-761.

Otani, H., Tanaka, O., Kasai, K., & Yoshioka, T. (1988). Development of mitochondrial helical sheath in the middle piece of the mouse spermatid tail: regular dispositions and synchronized changes. *The Anatomical record*, *222*(1), 26–33.

Oumaima, A., Tesnim, A., Zohra, H., Amira, S., Ines, Z., Sana, C., Intissar, G., Lobna, E., Ali, J., & Meriem, M. (2018). Investigation on the origin of sperm morphological defects: oxidative attacks, chromatin immaturity, and DNA fragmentation. *Environmental Science and Pollution Research*, *25*(14), 13775-13786.

Ozkavukcu, S., Erdemli, E., Isik, A., Oztuna, D., & Karahuseyinoglu, S. (2008). Effects of cryopreservation on sperm parameters and ultrastructural morphology of human spermatozoa. *Journal of Assisted Reproduction and Genetics*, *25*(8), 403-411.

Pacey, A. A. (2009). Sperm, human fertility and society. In T. R. Birkhead, D. J. Hosken, S. Pitnick (Eds.), *Sperm biology: an evolutionary perspective* (pp. 565-597). Academic Press.

Palermo, G., Joris, H., Devroey, P., & Vansteirteghem, A. C. (1992). Pregnancies after intracytoplasmic injection of single spermatozoon into an oocyte. *Lancet*, *340*(8810), 17-18.

Palermo, G. D., Neri, Q. V., Takeuchi, T., Squires, J., Moy, F., & Rosenwaks, Z. (2008). Genetic and epigenetic characteristics of ICSI children. *Reproductive Biomedicine Online*, *17*(6), 820-833.

Park, Y., Depeursinge, C., & Popescu, G. (2018). Quantitative phase imaging in biomedicine. *Nature Photonics*, *12*(10), 578-589.

Parmegiani, L., Cognigni, G. E., Bernardi, S., Troilo, E., Ciampaglia, W., & Filicori, M. (2010). "Physiologic ICSI": Hyaluronic acid (HA) favors selection of spermatozoa without DNA fragmentation and with normal nucleus, resulting in improvement of embryo quality. *Fertility and Sterility*, *93*(2), 598-604.

Penzias, A., Azziz, R., Bendikson, K., Falcone, T., Hansen, K., Hill, M., Hurd, W., Jindal, S., Kalra, S., Mersereau, J., Racowsky, C., Rebar, R., Reindollar, R., Steiner, A., Stovall, D., Tanrikut, C., Practice Comm Amer Soc Reprod, M., & Practice Comm Soc Assisted, R. (2020). Intracytoplasmic sperm injection (ICSI) for non-male factor indications: a committee opinion. *Fertility and Sterility*, *114*(2), 239-245.

Pinborg, A., Wennerholm, U. B., Romundstad, L. B., Loft, A., Aittomaki, K., Söderström-Anttila, V., Nygren, K. G., Hazekamp, J., & Bergh, C. (2013). Why do singletons conceived after assisted reproduction technology have adverse perinatal outcome? Systematic review and meta-analysis. *Human Reproduction Update*, *19*(2), 87-104.

Pitnick, A. A. (2009). Sperm morphological diversity. In T. R. Birkhead, D. J. Hosken, S. Pitnick (Eds.), *Sperm biology: an evolutionary perspective* (pp. 69-149). Academic Press.

Raad, G., Lteif, L., Lahoud, R., Azoury, J., Tanios, J., & Hazzouri, M. (2018). Cryopreservation media differentially affect sperm motility, morphology and DNA integrity. *Andrology*, *6*(6), 836-845.

Rahimipour, M., Talebi, A. R., Anvari, M., Sarcheshmeh, A. A., & Omidi, M. (2013). Effects of different doses of ethanol on sperm parameters, chromatin structure and apoptosis in adult mice. *European Journal of Obstetrics & Gynecology and Reproductive Biology*, *170*(2), 423-428.

Rantanen, A., & Larsson, N. G. (2000). Regulation of mitochondrial DNA copy number during spermatogenesis. *Human Reproduction (Oxford, England)*, *15*(Suppl 2), 86-91.

Rivenson, Y., Liu, T., Wei, Z., Zhang, Y., de Haan, K., & Ozcan, A. (2019). PhaseStain: the digital staining of label-free quantitative phase microscopy images using deep learning. *Light, Science & Applications*, *8*(23).

Romarowski, A., Velasco Félix, Á. G., Torres Rodríguez, P., Gervasi, M. G., Xu, X., Luque, G. M., Contreras-Jiménez, G., Sánchez-Cárdenas, C., Ramírez-Gómez, H. V., Krapf, D., Visconti, P. E., Krapf, D., Guerrero, A., Darszon, A., & Buffone, M. G. (2018). Super-resolution imaging of live sperm reveals dynamic changes of the actin cytoskeleton during acrosomal exocytosis. *Journal of Cell Science*, *131*(21), jcs218958.

Rolland, M., Le Moal, J., Wagner, V., Royere, D., & De Mouzon, J. (2013). Decline in semen concentration and morphology in a sample of 26 609 men close to general population between 1989 and 2005 in France. *Human Reproduction*, *28*(2), 462-470.

Rosati, A. J., Whitcomb, B. W., Brandon, N., Louis, G. M. B., Mumford, S. L., Schisterman, E. F., & Pilsner, J. R. (2020). Sperm mitochondrial DNA biomarkers and couple fecundity. *Human Reproduction*, *35*(11), 2619-2625.

Rousset-Jablonski, C., Chevillon, F., Dhedin, N., & Poirot, C. (2016). Fertility preservation in adolescents and young adults with cancer. *Bulletin Du Cancer*, *103*(12), 1019-1034.

Roychoudhury, S., Sharma, R., Sikka, S., & Agarwal, A. (2016). Diagnostic application of total antioxidant capacity in seminal plasma to assess oxidative stress in male factor infertility. *Journal of Assisted Reproduction and Genetics*, *33*(5), 627-635.

Rumbold, A. R., Moore, V. M., Whitrow, M. J., Oswald, T. K., Moran, L. J., Fernandez, R. C., Barnhart, K. T., & Davies, M. J. (2017). The impact of specific fertility treatments on cognitive development in childhood and adolescence: a systematic review. *Human Reproduction*, *32*(7), 1489-1507.

Rumbold, A. R., Sevoyan, A., Oswald, T. K., Fernandez, R. C., Davies, M. J., & Moore, V. M. (2019). Impact of male factor infertility on offspring health and development. *Fertility and Sterility*, *111*(6), 1047-1053.

Said, T. M., Grunewald, S., Paasch, U., Glander, H. J., Baumann, T., Kriegel, C., Li, L., & Agarwal, A. (2005). Advantage of combining magnetic cell separation with sperm preparation techniques. *Reproductive Biomedicine Online*, *10*(6), 740-746.

Said, T. M., & Land, J. A. (2011). Effects of advanced selection methods on sperm quality and ART outcome: a systematic review. *Human Reproduction Update*, *17*(6), 719-733.

Sakkas, D. (2013). Novel technologies for selecting the best sperm for in vitro fertilization and intracytoplasmic sperm injection. *Fertility and Sterility*, *99*(4), 1023-1029.

Sandin, S., Nygren, K. G., Iliadou, A., Hultman, C. M., & Reichenberg, A. (2013). Autism and Mental Retardation Among Offspring Born After In Vitro Fertilization. *Jama-Journal of the American Medical Association*, *310*(1), 75-84.

Sanger, W. G., Olson, J. H., & Sherman, J. K. (1992). Semen cryobanking for men with cancer – criteria change. *Fertility and Sterility*, *58*(5), 1024-1027.

Sermondade, N., Faure, C., Fezeu, L., Shayeb, A. G., Bonde, J. P., Jensen, T. K., Van Wely, M., Cao, J., Martini, A. C., Eskandar, M., Chavarro, J. E., Koloszar, S., Twigt, J. M., Ramlau-Hansen, C. H., Borges, E., Lotti, F., Steegers-Theunissen, R. P. M., Zorn, B., Polotsky, A. J., La Vignera, S., Eskenazi, B., Tremellen, K., Magnusdottir, E. V., Fejes, I., Hercberg, S., Levy, R., & Czernichow, S. (2013). BMI in relation to sperm count: an updated systematic review and collaborative meta-analysis. *Human Reproduction Update*, *19*(3), 221-231.

Shaked, N. T., Satterwhite, L. L., Telen, M. J., Truskey, G. A., & Wax, A. (2011). Quantitative microscopy and nanoscopy of sickle red blood cells performed by wide field digital interferometry. *Journal of Biomedical Optics*, *16*(3), Article 030506.

Sharma, R., Harlev, A., Agarwal, A., & Esteves, S. C. (2016). Cigarette smoking and semen quality: a new meta-analysis examining the effect of the 2010 world health organization laboratory methods for the examination of human semen. *Human Reproduction*, *31*, 154-154.

Sharpe, R. M. (2010). Environmental/lifestyle effects on spermatogenesis. *Philosophical Transactions of the Royal Society B-Biological Sciences*, *365*(1546), 1697-1712.

Sharpe, R. M., & Skakkebaek, N. E. (1993). Are estrogens involved in falling sperm counts and disorders of the male reproductive tract. *Lancet*, *341*(8857), 1392-1395.

Shen, D., Wu, G., & Suk, H.-I. (2017). Deep Learning in Medical Image Analysis. *Annual Review of Biomedical Engineering, 19*, 221-248.

Schindelin, J., Arganda-Carreras, I., Frise, E., Kaynig, V., Longair, M., Pietzsch, T., Preibisch, S., Rueden, C., Saalfeld, S., Schmid, B., Tinevez, J.Y., White, D.J., Hartenstein, V., Eliceiri, K., Tomancak, P., Cardona, A. (2012) Fiji: an open-source platform for biological-image analysis. *Nature Methods*, 9(7), 676–682.

Silva, J. V., Cruz, D., Gomes, M., Correia, B. R., Freitas, M. J., Sousa, L., Silva, V., & Fardilha, M. (2017). Study

on the short-term effects of increased alcohol and cigarette consumption in healthy young men's seminal quality. *Scientific Reports*, *7*, Article 45457.

Skakkebaek, N. E., Rajpert-De Meyts, E., Louis, G. M. B., Toppari, J., Andersson, A.-M., Eisenberg, M. L., Jensen, T. K., Jorgensen, N., Swan, S. H., Sapra, K. J., Ziebe, S., Priskorn, L., & Juul, A. (2016). Male reproductive disorders and fertility trends: influences of envoronment and genetic susceptibility. *Physiological Reviews*, *96*(1), 55-97.

Skakkebaek, N. E., Rajpert-De Meyts, E., & Main, K. M. (2001). Testicular dysgenesis syndrome: an increasingly common developmental disorder with environmental aspects. *Human Reproduction*, *16*(5), 972-978.

Song, G. J., & Lewis, V. (2008). Mitochondrial DNA integrity and copy number in sperm from infertile men. *Fertility and sterility*, *90*(6), 2238-2244.

Spiropoulos, J., Turnbull, D. M., & Chinnery, P. F. (2002). Can mitochondrial DNA mutations cause sperm dysfunction? *Molecular Human Reproduction*, *8*(8), 719-721.

Stival, C., Ritagliati, C., Xu, X. R., Gervasi, M. G., Luque, G. M., Graf, C. B., De la Vega-Beltran, J. L., Torres, N., Darszon, A., Krapf, D., Buffone, M. G., & Visconti, P. E. (2018). Disruption of protein kinase A localization induces acrosomal exocytosis in capacitated mouse sperm. *Journal of Biological Chemistry*, *293*(24), 9435-9447.

Sung, Y., Choi, W., Lue, N., Dasari, R. R., & Yaqoob, Z. (2012). Stain-Free Quantification of Chromosomes in Live Cells Using Regularized Tomographic Phase Microscopy. *Plos One*, *7*(11), Article e49502.

Sutovsky, P., Moreno, R. D., Ramalho-Santos, J., Dominko, T., Simerly, C., & Schatten, G. (1999). Ubiquitin tag for sperm mitochondria. *Nature*, *402*(6760), 371–372.

Svalander, P., Wikland, M., Jakobsson, A. H., & Forsberg, A. S. (1994). Subzonal Insemination (SUZI) or in vitro fertilization (IVF) in microdroplets for the treatment of male factor infertility. *Journal of Assisted Reproduction and Genetics*, *11*(3), 149-155.

Swan, S. H., Elkin, E. P., & Fenster, L. (2000). The question of declining sperm density revisited: An analysis of 101 studies published 1934-1996. *Environmental Health Perspectives*, *108*(10), 961-966.

Szell, A. Z., Bierbaum, R. C., Hazelrigg, W. B., & Chetkowski, R. J. (2013). Live births from frozen human semen stored for 40 years. *Journal of Assisted Reproduction and Genetics, 30*(6), 743-744.

Teixeira, D. M., Barbosa, M. A. P., Ferriani, R. A., Navarro, P. A., Raine-Fenning, N., Nastri, C. O., & Martins, W. P. (2013). Regular (ICSI) versus ultra-high magnification (IMSI) sperm selection for assisted reproduction. *Cochrane Database of Systematic Reviews,* (7), Article Cd010167.

Temple-Smith, P. D., Southwick, G. J., Yates, C. A., Trounson, A. O., & de Kretser, D. M. (1985). Human pregnancy by in vitro fertilization (IVF) using sperm aspirated from the epididymis. *Journal of In Vitro Fertilization and Embryo Transfer, 2*(3), 119-122.

Thirumalaraju P., Borman C.L., Kanakasabapathy M., Doshi F., Souter I., Dimitriadis I., Shafiee H. (2018) Automated sperm morphology testing using artificial intelligence. *Fertility and Sterility, 110*(4):e432

Tian, M., Bao, H., Martin, F. L., Zhang, J., Liu, L., Huang, Q., & Shen, H. (2014). Association of DNA methylation and mitochondrial DNA copy number with human semen quality. *Biology of Reproduction, 91*(4), 101.

Tiegs, A. W., Tao, X., Landis, J., Zhan, Y., Franasiak, J. M., Seli, E., Wells, D., Fragouli, E., & Scott, R. T., Jr (2020). Sperm Mitochondrial DNA Copy Number Is Not a Predictor of Intracytoplasmic Sperm Injection (ICSI) Cycle Outcomes. *Reproductive Sciences, 27*(6), 1350-1356.

Vanderzwalmen, P., Hiemer, A., Rubner, P., Bach, M., Neyer, A., Stecher, A., Uher, P., Zintz, M., Lejeune, B., Vanderzwalmen, S., Cassuto, G., & Zech, N. H. (2008). Blastocyst development after sperm selection at high magnification is associated with size and number of nuclear vacuoles. *Reproductive Biomedicine Online, 17*(5), 617-627.

Vezina, D., Mauffette, F., Roberts, K. D., & Bleau, G. (1996). Selenium-vitamin E supplementation in infertile men - Effects on semen parameters and micronutrient levels and distribution. *Biological Trace Element Research, 53*(1-3), 65-83.

Virtanen, H. E., Jorgensen, N., & Toppari, J. (2017). Semen quality in the 21st century. *Nature Reviews Urology, 14*(2), 120-130.

Woolley, D. M., & Richardson, D. W. (1978). Ultrastructural injury to human spermatozoa after freezing and thawing. *Journal of Reproduction and Fertility*, 53(2), 389-394.

World Health Organization (2010). WHO Laboratory Manual for the Examination and Processing of Human Semen. *Geneva: World Health Organization*.

Wu, H. T., Huffman, A. M., Whitcomb, B. W., Josyula, S., Labrie, S., Tougias, E., Rahil, T., Sites, C. K., & Pilsner, J. R. (2019). Sperm mitochondrial DNA measures and semen parameters among men undergoing fertility treatment. *Reproductive Biomedicine Online, 38*(1), 66-75.

Wu, H., Whitcomb, B. W., Huffman, A., Brandon, N., Labrie, S., Tougias, E., Lynch, K., Rahil, T., Sites, C. K., & Pilsner, J. R. (2019). Associations of sperm mitochondrial DNA copy number and deletion rate with fertilization and embryo development in a clinical setting. *Human reproduction, 34*(1), 163-170.

Younglai, E. V., Collins, J. A., & Foster, W. G. (1998). Canadian semen quality: an analysis of sperm density

among eleven academic fertility centers. *Fertility and Sterility, 70*(1), 76-80.

Zhang, G., Jiang, F., Chen, Q., Yang, H., Zhou, N., Sun, L., Zou, P., Yang, W., Cao, J., Zhou, Z., & Ao, L. (2020). Associations of ambient air pollutant exposure with seminal plasma MDA, sperm mtDNA copy number, and mtDNA integrity. *Environment International*, *136,* Article 105483.

Zhou, W.-J., Huang, C., Jiang, S.-H., Ji, X.-R., Gong, F., Fan, L.-Q., & Zhu, W.-B. (2021). Influence of sperm morphology on pregnancy outcome and offspring in in vitro fertilization and intracytoplasmic sperm injection: a matched case-control study. *Asian journal of andrology*. 10.4103/aja.aja_91_20. Advance online publication.

Appendix: Papers I-IV

Paper I

Live-cell imaging of human spermatozoa using structured illumination microscopy

Ida S. Opstad, Daria A. Popova, Ganesh Acharya, Purusotam Basnet, Balpreet S. Ahluwalia

Live-cell imaging of human spermatozoa using structured illumination microscopy

IDA S. OPSTAD,[1,5] **DARIA A. POPOVA,**[2,5] **GANESH ACHARYA,**[2,3] **PURUSOTAM BASNET,**[2,4] **AND BALPREET S. AHLUWALIA**[1,*]

[1]*Department of Physics and Technology, UiT The Arctic University of Norway, 9037 Tromsø, Norway*
[2]*Women's Health and Perinatology Research Group, Department of Clinical Medicine, UiT The Arctic University of Norway, Tromsø, Norway*
[3]*Department of Clinical Science, Intervention & Tech. Karolinska Institutet, Stockholm, Sweden*
[4]*IVF Unit, Department of Obstetrics & Gynecology, University Hospital North Norway, Tromsø, Norway*
[5]*Both authors contributed equally to this work*
[*]*balpreet.singh.ahluwalia@uit.no*

Abstract: Structural details of spermatozoa are interesting from the perspectives of fundamental biology and growing reproductive health problems. Studies of nanostructural details of these extremely motile cells have been limited to fixed cells, largely using electron microscopy. Here we provide the protocols for and demonstrate live-cell multi-color super-resolution imaging of human spermatozoa using structured illumination microscopy (SIM). By using patches of agarose for immobilization, we achieved four-channel 3D SIM imaging of the plasma membrane, nucleus, mitochondria and microtubulin in the same living sperm cells. We expect that high-resolution imaging of living spermatozoa will be implemented for research on fundamental cellular mechanisms together with morphological aberrations involved in male infertility for a future improved cell selection process in in vitro fertilization treatments.

1. Introduction

Research on subcellular organization of human reproductive cells and preimplantation embryos is becoming increasing popular as it is considered to be important to tackle growing reproductive health problems. Along with female infertility, male factor infertility is a significant issue which may result from different causes, such as anatomical anomalies, hormonal imbalances, infections or genetic abnormalities. However, the etiology of male infertility remains undiagnosed in about one third of the cases [1,2]. Nowadays, male reproductive health assessment is primarily based on sperm quality, and morphology is one of the main characteristics evaluated in clinical practice. Changes in the ultrastructure and general morphology of sperm cells serves as an indicator of the influence of different physical (e.g. freezing in reproductive technologies) [3,4], chemical (occupational exposure to toxic substances) or environmental factors on semen reflecting male reproductive health during life [5,6].

Until recently, numerous studies have been performed to study the ultrastructure of sperm cells using transmission electron microscopy (TEM) to obtain high resolution images [3,7–9]. Compared to TEM, optical microscopy often enables the analysis of living cells, resulting in the elimination of artifacts specific to cell fixation, such as changed protein conformation with associated loss of staining specificity [10,11]. Though a valuable tool, the diffraction limit renders conventional light microscopy unable to resolve details finer than about 250 nm laterally and 500 nm axially using a high-end microscope. Optical nanoscopy (or super-resolution optical microscopy) encompass an array of techniques for overcoming the resolution limit of conventional microscopy, opening avenues for studying biological samples

in much greater detail than previously possible without the extensive sample preparation required for electron microscopy [12].

Structured illumination microscopy (SIM) is a live-cell compatible super-resolution technique that achieves greatly enhanced contrast along with a factor of two resolution enhancement in all three spatial dimensions as compared to the diffraction limit [13]. For biological structures just below the conventional resolution limit, SIM can thus be applied as a tool for valuable additional structural information in living cells. In the case of sperm cells, structural analysis using multi-color SIM offers opportunities for a more precise description of disease specific defects responsible for infertility, like morphological aberrations associated with teratozoospermia [14] or asthenozoospermia [15,16]. In addition to a better description of morphology, we expect that live-cell studies of sperm cells at super-resolution and enhanced contrast will contribute to a gain in knowledge about fundamental cellular mechanisms that might be implemented for an improved reproductive cell selection process in future in vitro fertilization (IVF) treatments.

The biggest hurdle for live-cell high-resolution imaging of sperm cells has been the extreme motility associated with their progressive swimming ($\sim$66 µm/s [17]), in addition to their free-floating nature as suspension cells. Until now, to the best of our knowledge, all super-resolution imaging of human spermatozoa has been limited to fixed cells. Other challenges associated with multi-color super-resolution microscopy of any cell type are labeling, label induced toxicity and phototoxicity. Here we provide a methodology for overcoming above-mentioned hurdles and demonstrate up to four-channel 3D SIM imaging of different sub-cellular structures in living human spermatozoa. We also provide labeling protocols and discuss associated challenges and opportunities.

2. Materials and methods

2.1 Sample preparation

Semen preparation

The Regional Committee for Medical and Health Research Ethics of Norway (REK-Nord) approved the project. Experiments were performed using semen of donors from the IVF clinic of the University Hospital of North Norway, Tromsø, Norway. All participants signed a written informed consent. Semen samples were collected according to the guidelines of the World Health Organization (WHO) with an abstinence period of 3–5 days.

After liquefaction, semen samples were examined using light microscopy and Neubauer-improved counting chambers. In the experiments, all samples contained no less than 60 million cells per milliliter and had progressive motility >50%. The swim up method was used to wash the samples. The semen samples were diluted with 5 mL of sperm washing medium (Sage) and centrifuged for 10 min at 700 x g. Supernatant was removed and the pellet was washed again. After removing the supernatant, 0.5 mL of swim up medium was layered and the tube was put into an incubator (5.0% CO_2, 37°C). During 60 min of incubation, highly motile spermatozoa migrated to the above layered medium. After incubation, the supernatant was aspirated with pipette, centrifuged and the sediment was used for the following procedures.

Labeling, immobilization and imaging conditions

Labeling and imaging were done at room temperature ($\sim$23°C) in PBS or Live Cell Imaging Solution (Molecular Probes) as summarized in Table 1. For multi-color experiments, the label requiring the longest incubation time was added to the cells first, and then sequentially the rest of the probes, so that at the end of the incubation time, the cells had been subjected to approximately the concentrations and labeling times as listed in Table 1. After incubation with the labels, the samples were diluted in PBS ($\sim$1:15) and spun down using 800 x g for 10 min. The supernatant was removed and the samples resuspended in PBS to a concentration

found suitable for the respective sample and experiment. Drops of about 8 µL were placed on coverslips (#1.5 washed in 100% ethanol and placed in sample holders for live-cell microscopy) and covered with refrigerated patches of ~2% agarose (High-resolution, Sigma-Aldrich) in PBS. When the cells after a couple of minutes had become fully immobilized, the samples were covered with a plastic lid to prevent further drying during imaging. SiR-tubulin was purchased from Spirochrome (Cytoskeleton kit), while all other probes were purchased from Thermo Fisher Scientific.

Table 1. Labeling conditions applied for SIM imaging

Label	Concentration	Incubation time
CellMask Orange	1:1000	10 min
MitoTracker Green	200 nM	20 min
Hoechst 34580	5 µg/mL	20 min
SiR-tubulin	1 µM	2 h

2.2 Microscope

Images were acquired using a DeltaVision OMX V4 Blaze imaging system (GE Healthcare) equipped with a 60X 1.42NA oil-immersion objective (Olympus), three sCMOS cameras, and 405, 488, 568, and 642 nm lasers for excitation. The vendor specified optical resolution of the system (3D SIM) is 110-160 nm laterally, and 340-380 nm axially, depending on color channel. To surpass the diffraction limit, this SIM set-up uses sinusoidal illumination patterns and acquires 120 images per 1 µm z-stack thickness (3 illumination angles times 5 phase shifts times 8 planes/µm thickness) per color channel. Super-resolution 3D images are then obtained via image processing using the reconstruction software described below.

2.3 Image processing

Deconvolution and 3D SIM image reconstruction were completed using the manufacturer-supplied SoftWoRx program (GE Healthcare). Image registration (color alignment) was also performed in SoftWoRx using experimentally-measured calibration values compensating for minor lateral and axial shifts, rotation, and magnification differences between cameras. Further image processing was done using Fiji/ImageJ [18]

3. Results and discussion

3.1 Single-color imaging and immobilization

Immobilization using patches of agarose made high-resolution imaging of living spermatozoa possible. Figure 1 shows fluorescence microscopy images of living spermatozoa acquired using deconvolution microscopy (upper panel) and SIM (lower panel) for various live-cell compatible probes (CellMask Orange, panels (a) and (e); MitoTracker Green, panels (b) and (f); Hoechst 34580, panels (c) and (g); SiR-tubulin, panels (d) and (h)). The contrast and resolution enhancement for SIM compared to conventional deconvolution microscopy is apparent for all structures, but most prominent for the mitochondria-containing mid-piece, panels (a), (b), (e) and (f), where structures around 100 nm length-scale are prominent. For the nucleus, only minor contrast enhancement is visible, while for microtubulin (panels (d) and (h)) the resolution doubling provided by SIM makes it evident that the centriole (indicated by arrows) is completely separated from the rest of the axoneme.

Imaging from below through the coverslip (and not through the agarose) resulted in images not significantly affected by the agarose with absorbed leftover dye. Imaging a few planes below the agarose enabled us to acquire high quality SIM images of *most of* the living sperm cells, although not for the uppermost part (0.2 - 0.3 µm) of the cells, which was stuck in the agarose. To illustrate, the sample plane in Fig. 2(a) is unusable because of the signal from the agarose (with absorbed leftover dye), while for the neighboring sample planes shown in Fig. 2(b) and 2(c), the agarose is now above and not in the image plane, enabling us

to observe the cell at high resolution and contrast. In the particular cell depicted, an abnormally `puffed up' membrane morphology is revealed, clearly different from the tightly wrapped membrane in e.g. Fig. 1(e).

Though immobilization for live-cell microscopy using patches of agarose (often combined with cell growth medium) is widely applied in microbiology (e.g. discussed in [19]), this technique is not extensively used in the 'eukaryotic cell community'. We expect this immobilization technique applied here successfully for SIM of spermatozoa to be also directly applicable to other types of suspension cells that are challenging to image live otherwise. The addition of an agarose patch on top of the sample is suitable for imaging set-ups where both illumination and detection are conducted through the coverslip (and not through the agarose), as is often the case in fluorescence microscopy.
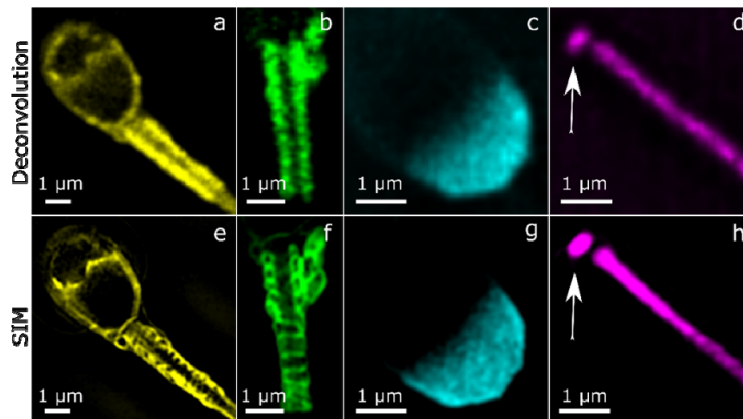

Fig. 1. Comparison of deconvolution microscopy (upper panels) and SIM (lower panels) images of living human spermatozoa for different probes. (a), (e) Plasma membrane labeled using CellMask Orange; (b), (f) Mitochondria labeled using MitoTracker Green; (c), (g) Nucleus labeled using Hoechst 34580; (d), (h) Microtubulin labeled using SiR-tubulin. The contrast and resolution enhancement are apparent for all probes, but most significant for the region containing mitochondria (panels (a), (b), (e) and (f)), but also for the centriole, indicated by arrows in panels (d) and (h). The images are single z-sections.
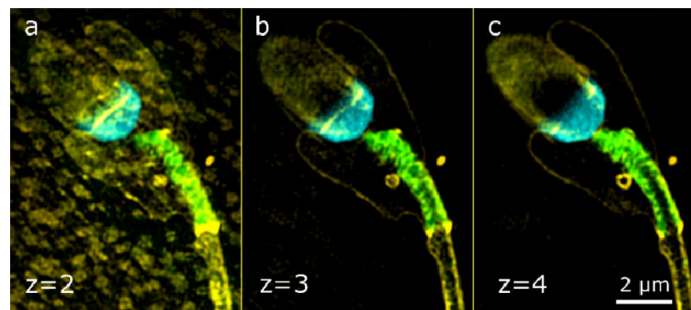

Fig. 2. Comparison of background signal in z-planes 2 (a), 3 (b) and 4 (c) counted from the agarose patch (top) used for immobilization. The distance between the z-slices is 125 nm. The agarose patch (with absorbed leftover dye) only causes significant background signal in the uppermost planes. The cells were labeled using CellMask Orange, MitoTracker Green and Hoechst 34580 and imaged live using SIM.
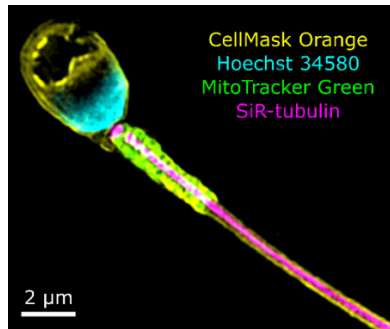
Fig. 3. Four-channel SIM image of living human spermatozoa labeled using CellMask Orange (yellow), MitoTracker Green (green), Hoechst 34580 (turquoise) and SiR-tubulin (magenta). The image is a 1 µm maximum intensity projected z-stack.

3.2 Multi-color SIM imaging

Figure 3 shows a four-channel SIM image of living human spermatozoa labeled using CellMask Orange, MitoTracker Green, Hoechst and SiR-tubulin. CellMask (yellow) labels the plasma membrane and outlines the entire cell, MitoTracker (green) labels mitochondria in the mid-piece clutching around the axoneme labeled using SiR-tubulin (magenta). Hoechst (cyan) labels DNA and is here visible only in the lower part of the head. For multi-color experiments, similar concentrations and labeling times were applicable as described for the single-probe experiments, though the labels were added sequentially to fit their individually optimized labeling time (with a single washing step in the end), resulting in slightly varying concentrations compared to the single-color experiments. Multi-color super-resolution imaging of living sperm cells unlocks exciting new possibilities regarding detailed analysis of subcellular structures for various cellular conditions, that can be employed to e.g. better understand diseases and the effect of different treatments in the field of reproductive medicine.

Four-channel SIM imaging of living cells is in general challenging for four reasons in particular: sample movement, photobleaching, phototoxicity, and depth-induced spherical aberrations. Sample movement was effectively eliminated using agarose patches. Photobleaching was countered using high labeling concentrations of bright photostable dyes with lowered illumination intensities and instead longer exposure times (20-30 ms) to ensure sufficient modulation contrast of the illumination pattern. Phototoxicity was not found problematic for these experiments as only single time-points were considered, although the four-channel imaging time for a 1.5 µm z-stack was around 20 s. Spherical aberrations were mitigated in these samples, through optimization of the immersion oil refractive index in use (1.516 was found appropriate for the four-channel imaging experiments), the tenuity of the samples (~0.5 – 3 µm thickness) and the sample placement directly on the coverslip. For thicker samples, spherical aberrations often cause SIM reconstruction artifacts, as the sample-induced aberrations can only be optimally corrected for one channel at a time.

4. Conclusions and summary

We provide a methodology for live-cell imaging of human spermatozoa using SIM, which is also applicable for a wide variety of other types of suspension cells and for imaging techniques where both illumination and detection are conducted through the coverslip. Labeling with fluorescent probes compatible with live-cell imaging, and subsequent immobilization using patches of agarose, enabled up to four-channel SIM imaging that revealed an unprecedented level of structural details of living sperm cells. This methodology shows great promise for shedding new light on sub-cellular structures and cellular mechanisms of the male reproductive cell in both healthy and diseased subjects, as live-cell imaging at super-resolution enables a much more precise description of e.g. morphological

aberrations responsible for infertility. As compared to electron microscopy, the proposed methodology not only enables live-cell experiments, but also eliminates fixation steps and fixation related artefacts. This enables reduced sample preparation time and allows for multi-channel colocalization experiments by means of standard labeling protocols. In addition to a better description of morphology, we expect that live-cell studies of sperm cells at high resolution and contrast will contribute to an increased knowledge of fundamental cellular mechanisms that might be implemented for an improved reproductive cell selection process in IVF treatments in the future.

Funding

Acknowledgments

Disclosures

The authors declare that there are no conflicts of interest related to this article.

References

1. G. Cavallini, "Male idiopathic oligoasthenoteratozoospermia," Asian J. Androl. **8**(2), 143–157 (2006).
2. N. Kumar and A. K. Singh, "Trends of male factor infertility, an important cause of infertility: A review of literature," J. Hum. Reprod. Sci. **8**(4), 191–196 (2015).
3. S. Ozkavukcu, E. Erdemli, A. Isik, D. Oztuna, and S. Karahuseyinoglu, "Effects of cryopreservation on sperm parameters and ultrastructural morphology of human spermatozoa," J. Assist. Reprod. Genet. **25**(8), 403–411 (2008).
4. C. Barthelemy, D. Royere, S. Hammahah, C. Lebos, M. J. Tharanne, and J. Lansac, "Ultrastructural changes in membranes and acrosome of human sperm during cryopreservation," Arch. Androl. **25**(1), 29–40 (1990).
5. N. Naha, R. B. Bhar, A. Mukherjee, and A. R. Chowdhury, "Structural alteration of spermatozoa in the persons employed in lead acid battery factory," Indian J. Physiol. Pharmacol. **49**(2), 153–162 (2005).
6. W. Asghar, H. Shafiee, V. Velasco, V. R. Sah, S. Guo, R. El Assal, F. Inci, A. Rajagopalan, M. Jahangir, R. M. Anchan, G. L. Mutter, M. Ozkan, C. S. Ozkan, and U. Demirci, "Toxicology Study of Single-walled Carbon Nanotubes and Reduced Graphene Oxide in Human Sperm," Sci. Rep. **6**(1), 30270 (2016).
7. D. Lacy, A. J. Pettitt, J. M. Pettitt, and B. S. Martin, "Application of scanning electron microscopy to semen analysis of the sub-fertile man utilising data obtained by transmission electron microscopy as an aid to interpretation," Micron (1969) **5**(2), 135–173 (1974).
8. B. Baccetti, S. Capitani, G. Collodel, G. Di Cairano, L. Gambera, E. Moretti, and P. Piomboni, "Genetic sperm defects and consanguinity," Hum. Reprod. **16**(7), 1365–1371 (2001).
9. E. H. Chemes and Y. V. Rawe, "Sperm pathology: a step beyond descriptive morphology. Origin, characterization and fertility potential of abnormal sperm phenotypes in infertile men," Hum. Reprod. Update **9**(5), 405–428 (2003).
10. A. J. Hobro and N. I. Smith, "An evaluation of fixation methods: Spatial and compositional cellular changes observed by Raman imaging," Vib. Spectrosc. **91**, 31–45 (2017).
11. J. Kiernan, *Formaldehyde, Formalin, Paraformaldehyde And Glutaraldehyde: What They Are And What They Do* (2000).
12. C. G. Galbraith and J. A. Galbraith, "Super-resolution microscopy at a glance," J. Cell Sci. **124**(10), 1607–1611 (2011).
13. R. Heintzmann and T. Huser, "Super-Resolution Structured Illumination Microscopy," Chem. Rev. **117**(23), 13890–13908 (2017).
14. E. Moretti, and G. Collodel, *Electron Microscopy in the Study of Human Sperm Pathologies* (2012).
15. V. Y. Rawe, G. D. Galaverna, A. A. Acosta, S. B. Olmedo, and H. E. Chemes, "Incidence of tail structure distortions associated with dysplasia of the fibrous sheath in human spermatozoa," Hum. Reprod. **16**(5), 879–886 (2001).
16. F. Pelliccione, A. Micillo, G. Cordeschi, A. D'Angeli, S. Necozione, L. Gandini, A. Lenzi, F. Francavilla, and S. Francavilla, "Altered ultrastructure of mitochondrial membranes is strongly associated with unexplained asthenozoospermia," Fertil. Steril. **95**(2), 641–646 (2011).

17. W. V. Holt, F. Shenfield, T. Leonard, T. D. Hartman, R. D. North, and H. D. Moore, "The value of sperm swimming speed measurements in assessing the fertility of human frozen semen," Hum. Reprod. **4**(3), 292–297 (1989).

18. J. Schindelin, I. Arganda-Carreras, E. Frise, V. Kaynig, M. Longair, T. Pietzsch, S. Preibisch, C. Rueden, S. Saalfeld, B. Schmid, J.-Y. Tinevez, D. J. White, V. Hartenstein, K. Eliceiri, P. Tomancak, and A. Cardona, "Fiji: an open-source platform for biological-image analysis," Nat. Methods **9**(7), 676–682 (2012).

19. G. Joyce, B. D. Robertson, and K. J. Williams, "A modified agar pad method for mycobacterial live-cell imaging," BMC Res. Notes **4**(1), 73 (2011).

Paper II

Partially spatially coherent digital holographic microscopy and machine learning for quantitative analysis of human spermatozoa under oxidative stress condition

Vishesh Dubey, Daria Popova, Azeem Ahmad, Ganesh Acharya, Purusotam Basnet, Dalip Singh Mehta1, Balpreet Singh Ahluwalia

SCIENTIFIC REPORTS

OPEN

Partially spatially coherent digital holographic microscopy and machine learning for quantitative analysis of human spermatozoa under oxidative stress condition

Vishesh Dubey [1,2], Daria Popova[3], Azeem Ahmad[1,2], Ganesh Acharya[3,4], Purusotam Basnet[3], Dalip Singh Mehta[1] & Balpreet Singh Ahluwalia[2]

Semen quality assessed by sperm count and sperm cell characteristics such as morphology and motility, is considered to be the main determinant of men's reproductive health. Therefore, sperm cell selection is vital in assisted reproductive technology (ART) used for the treatment of infertility. Conventional bright field optical microscopy is widely utilized for the imaging and selection of sperm cells based on the qualitative analysis by experienced clinicians. In this study, we report the development of a highly sensitive quantitative phase microscopy (QPM) using partially spatially coherent light source, which is a label-free, non-invasive and high-resolution technique to quantify various biophysical parameters. The partial spatial coherence nature of light source provides a significant improvement in spatial phase sensitivity and hence reconstruction of the phase of the entire sperm cell is demonstrated, which was otherwise not possible using highly spatially coherent light source. High sensitivity of the system enables quantitative phase imaging of the specimens having very low refractive index contrast with respect to the medium like tail of the sperm cells. Further, it also benefits with accurate quantification of 3D-morphological parameters of sperm cells which might be helpful in the infertility treatment. The quantitative analysis of more than 2500 sperm cells under hydrogen peroxide (H_2O_2) induced oxidative stress condition is demonstrated. It is further correlated with motility of sperm cell to study the effect of oxidative stress on healthy sperm cells. The results exhibit a decrease in the maximum phase values of the sperm head as well as decrease in the sperm cell's motility with increasing oxidative stress, i.e., H_2O_2 concentration. Various morphological and texture parameters were extracted from the phase maps and subsequently support vector machine (SVM) based machine learning algorithm is employed for the classification of the control and the stressed sperms cells. The algorithm achieves an area under the receiver operator characteristic (ROC) curve of 89.93% based on the all morphological and texture parameters with a sensitivity of 91.18%. The proposed approach can be implemented for live sperm cells selection in ART procedure for the treatment of infertility.

Infertility affects approximately 15% of couple worldwide[1]. Male factor infertility affects approximately 7% of the general male population, and poor semen quality is considered to be one of the main factors[2]. Along with inherited genetic problems, meiotic abnormalities causing miscarriages and inflammation, sperm abnormalities can be due to oxidative stress activated during the process of *in-vitro* fertilization (IVF) itself[3]. Standard sperm manipulations, such as wash from seminal plasma, cryopreservation and centrifugation, may impair antioxidant defence and increase the production of reactive oxygen species (ROS)[4,5]. Low level of ROS modulates signalling

[1]Applied Optics and Biophotonics Laboratory, Department of Physics, Indian Institute of Technology Delhi, Delhi, India. [2]Department of Physics and Technology, UiT The Arctic Univ. of Norway, Tromsø, Norway. [3]Department of Clinical Medicine, UiT The Arctic Univ. of Norway, Tromsø, Norway. [4]Department of Clinical Science, Intervention and Technology Karolinska Univ. Hospital, Karolinska, Sweden. Vishesh Dubey and Daria Popova contributed equally. Correspondence and requests for materials should be addressed to B.S.A. (email: balpreet.singh.ahluwalia@uit.no)

pathways required for human sperm activation, whereas high level impairs sperm function, leading to infertility. Specifically, oxidative stress is known to affect the integrity of the sperm genome, result in lipid peroxidation, loss in membrane fluidity, and decrease in sperm motility[6,7].

Adverse effects of oxidative stress might not be explored with light microscopy. For that reason, sperm cells with impaired fertilizing potential can be picked by embryologists for intracytoplasmic sperm injection (ICSI). At the same time, routine oxidative stress screening is not performed in IVF laboratories because of high cost and complexity of standard tests[8]. Moreover, implementation of rapid diagnostics could replace long and cumbersome multi-step analytic procedures that require complex experimental equipment.

The human sperm cells are relatively transparent in nature and have almost similar optical properties as surroundings leading to low refractive index (RI) contrast. Therefore, it is difficult to obtain a good contrast image by using bright field microscope. Several optical techniques have been developed for the contrast enhancement of sample images[9–11], however, they do not provide any quantitative information of the specimen[12,13]. When the light passes through the specimen, the optical path delay (OPD) is generated in light field due to the RI difference between the cell and the surrounding medium. The OPD is measured using quantitative phase microscopy (QPM) techniques, which are based on the principle of interferometry. It can be further utilized to measure several optical properties of specimen. The QPM techniques have been employed for the visualization and the evaluation of specimens that are particularly useful in cell biology[12–14]. The key advantage of these techniques is that they provide high resolution 3-D quantitative information of the specimen without any labelling.

In this study, we have investigated the effects of externally induced oxidative stress by treating healthy sperm cells with hydrogen peroxide (H_2O_2) using spatially low coherent QPM and further the findings are correlated with clinically relevant motility parameter of the sperm cells. A number of studies have been implemented for the quantitative assessment of normal and immotile sperm cells utilizing QPM[15–19], however the effect of oxidative stress on the morphology and motility of the sperm cells is not done previously. In addition, existing QPM either utilized a narrowband (i.e., lasers) or broadband (i.e., light emitting diodes and halogen lamp) light sources for phase imaging of sperm cells[17–20]. The use of highly temporal and spatial coherent light sources, like lasers, degrades the interferogram's quality due to speckle and spurious fringe formation, which eventually reduces the spatial sensitivity of the system[21–23]. This makes difficult to perform quantitative phase imaging (QPI) of the tail of sperm cells as it offers minute OPD[18,19]. The phase sensitivity can be improved by utilizing broadband light sources like white light, light emitting diodes and super-luminescent diodes[24–26]. However, such light sources require chromatic aberration corrected optics and dispersion compensation mechanism. In addition, single shot phase recovery over the whole camera field of view (FOV) is not possible due to low fringe density with low temporal coherent light sources[25]. Thus, a monochromatic extended (i.e., pseudo-thermal) light source can be implemented in QPM technique, which carries advantages of both narrow-band and broad-band light sources. Several methods have been proposed to synthesize pseudo-thermal light sources using rotating diffuser and vibrating multiple mode fiber bundle (MMFB), previously[22,23].

A monochromatic laser beam is passed through a rotating diffuse to synthesize a pseudo-thermal light source which carries high temporal coherence (helps to obtain high fringe density over whole camera FOV) and low spatial coherence (generate speckle and spurious fringe free interfergrams) properties. Such light source is employed with Linnik-type interference microscopy system to record off-axis holograms of sperm cells. The phase maps of sperm cells are then recovered with improved spatial phase sensitivity of the order of 20 ± 1.5 mrad. It is exhibited that phase map of the tail of sperm cell is nicely recovered with pseudo-thermal light source, which is otherwise not possible in laser based phase imaging. Most of the QPM techniques are, therefore, implemented only on dried sperm cells to recover phase map of the tail of sperm cells, previously[17,19]. Further, diagnosis of both the head and the tail of sperm cells are important for the procedures of artificial reproductive technologies. According to the WHO criteria, healthy tail having principle piece should be uniform along its length, be thinner than the midpiece, with a length of about 45 μm and without any sharp angle[27]. Thus, quantitative assessment of sperm tail can help to choose a healthy sperm in the clinical practice. QPM may also provide a better visualization to detect the abnormalities like defects of head neck attachment, primary ciliary dyskinesia (PCD), or dysplasia of fibrosis sheath (DFS).

It was observed that the optical thickness of the sperm's head decreases as a function of increase in the H_2O_2 concentration. Several morphological and texture parameters were extracted from the phase maps to measure the changes during oxidative stress. A support vector machine (SVM) based classifier is developed for the classification of normal and stressed sperm cells. The morphological and texture parameters extracted from phase maps were used to train the algorithm for better classification. For the training of the classifier, 60% of total samples were used and rest 40% were used as test specimen. We have achieved an accuracy of 89.93% for the classification of control and test sperm cells with SVM model. The observations support the hypothesis that changes caused by the oxidative stress could result in the decrease of maximum phase value of the sperm cell as compared to the normal one. The findings of QPM were correlated with a dose-dependent decrease in progressive motility of the sperm cells. The decrease in sperm motility with an increase in the H_2O_2 concentration was observed as compared to the controlled samples.

Methods and Materials

Principle of DHM. DHM is based on the principle of interferometry, in which a full or partially coherent light is divided into two beams, one as reference and other illuminates the specimen called object wave. Further, the scattered wave from object and reference waves interfere to generate the hologram and the 2D intensity distribution can be expressed as:

$$h(x, y) = a(x, y) + b(x, y)cos\left[2\pi i(f_x x + f_y y) + \Delta\phi(x, y)\right]$$

(1)

where a(x, y) and b(x, y) represent the background (DC) and the modulation terms, respectively, $\Delta\phi(x, y)$ is the phase difference between the object and reference fields, f_x and f_y are the spatial frequencies of the interference pattern along x and y directions, respectively.

For the convenience, the above intensity pattern of hologram can be rewritten in the following form

$$h(x, y) = a(x, y) + c(x, y)exp[2\pi i(f_x x + f_y y)] + c^*(x, y)exp[-2\pi i(f_x x + f_y y)]$$

where

$$c(x, y) = b(x, y)exp(i\phi(x, y))$$

The hologram reconstruction allows the retrieval of the complex object field. To retrieve the phase information, Fourier transform of the hologram is taken and one of the twin image peaks is filtered with numeric band pass filter in the frequency domain. Further, inverse Fourier transform is performed to reconstruct the hologram (h_{filt}) as a 2D array of complex numbers. The phase profile of the specimen is then simply measured as:

$$\Delta\phi = arctan\left(\frac{imag(h_{filt})}{real(h_{filt})}\right)$$

(2)

The phase $\Delta\phi$ depends on the thickness of the specimen and the RI difference of the specimen and the media containing the object itself. This phase variation having information of the morphology of specimen under investigation thus holography provides a 3D topographic profile of the specimen. The phase is related to the optical path difference (OPD) by the relation[12]:

$$\phi(x, y) = \frac{2\pi}{\lambda} \times 2h(x, y) * \{n_s(x, y) - n_0(x, y)\}$$

(3)

where λ is the wavelength of incident light, h is the geometrical thickness of the specimen; n_s and n_o are the refractive indices of the specimen and surrounding medium, respectively and there is an extra factor of 2 appears because the reflection configuration is utilized to record the hologram.

Morphological and Statistical Analysis. The analysis of recovered phase is very important for the image based computer-aided diagnosis (CAD), which provides excellent accuracy in early stage disease detection[28,29]. Machine learning is a subfield of computer science having a range of applications in biomedical imaging, which uses the extracted morphological and texture features of the image to make predictions[28,29]. For the classification of sperm cells under control and oxidative stress conditions, the phase map of the head of sperm cells are utilized for the calculation of the various texture parameters, which were further utilized in SVM algorithm.

Once the phase maps of the sperm cells were extracted from the hologram, the head of the sperm cell isolated to extract the phase map based morphological and texture features. The optical thickness (OT) is related to the phase of the specimen by the relation $OT = \phi(x, y) * \lambda/4\pi$ (for reflection geometry), where λ is the wavelength of the light. The measured OT is utilized to measure the volume of sperm head and can be calculated by integrating OT over projected area as[30,31]

$$V = \iint OT(x, y)dxdy$$

(4)

where dx and dy are the calibrated pixel width along x and y directions, respectively.

The area element dS of the cell surface is calculated by Monge parameterization defined as[30,32]

$$dS = dxdy\sqrt{1 + G_x^2 + G_y^2}$$

(5)

where G_x and G_y are the gradients along the x and y directions, respectively. Further, the surface area 'S' is defined as the sum of all the area elements and the projected area[32]. Next, sphericity 'Ψ' of the sperm head was determined, whose values lie between 0 and 1 (for laminar disk and perfect sphere, respectively). It is defined as the ratio between the surface area (S) of a cell with the volume of the same cell and calculated as[30,31,33]

$$\Psi = \frac{4.84_* V^{2/3}}{S}$$

(6)

Semen preparation. Semen samples were obtained from men who attended the IVF clinic for the investigation and/treatment of infertility. The Regional Committee for Medical and Health Research Ethics of Norway (REK_nord) approved the project. An informed consent was obtained from all participants.

The semen sample was collected according to the guidelines of the World Health Organization with an abstinence period of 3–5 days. After collection, the sample was allowed to liquefy for 30–40 min. Sperm counts were evaluated using the Neubauer-improved counting chambers. All ejaculates used in the experiments had an original sperm concentration more than 60 million of cells per milliliter, progressive motility more than 50% and with normal morphology >14% following strict criteria. The sperm fraction with high motility was isolated by density gradient centrifugation method (Vitrolife, Sweeden). One milliliter of semen was carefully placed on the gradient layers (90% and 45% layers) and centrifuged at 500 g for 20 min. The pellet from the centrifuge tube was washed
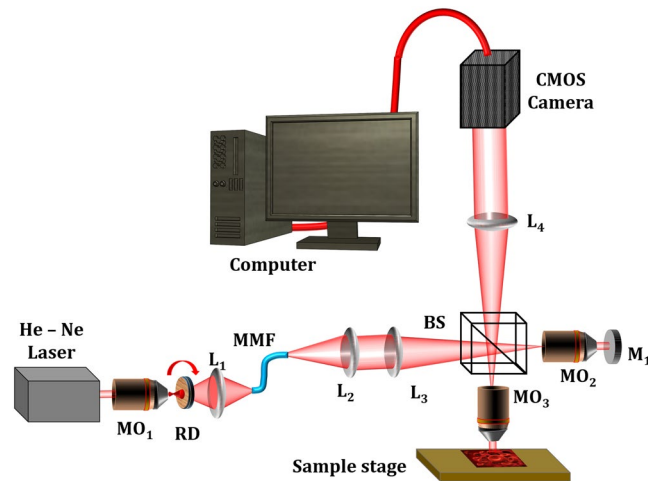
Figure 1. Schematic diagram of the DHM setup with pseudo thermal light source for the acquiring the quantitative phase maps of sperm sample. (RD- rotating diffuser, L- lens, BS- Beam splitter, MO-microscope objective, MMFB- multiple multi-mode fiber bundle).

twice with human Quinn's sperm washing medium (SM; Origio, Denmark) at $300\,g$ for 10 min. The supernatant was discarded, and the pellet was re-suspended in QA fert-medium supplemented with 5 mg/ml HSA and was used for following procedures.

To perform oxidative stress experiment, sperm sample was diluted to a concentration of 5.0×10^6 cells/ml using culture medium. Further, 96 well tissue culture plates were filled with sperm in medium (Quinn's Advantage Protein plus Fertilization medium, SAGE, Denmark) with different concentrations of H_2O_2 ($10\,\mu M$, $40\,\mu M$, $70\,\mu M$, $100\,\mu M$) and the reference chamber was filled with the same concentration of semen without H_2O_2. The samples were incubated for 1 hour at 37 °C, 5–6% CO_2. After incubation motility of each sperm sample was graded in two clusters: progressive motility (PR) and non-progressive motility (NP), which were reported as in percentages.

For QPM, the cells of each concentration were placed in a PDMS chamber on reflecting silicon (Si) chip after 1 hour of incubation. To immobilize the sperm cells, samples were fixed with 4% PFA for 30 min at RT and washed in phosphate-buffered saline (PBS) for 5 min. Finally, $50\,\mu L$ of PBS were added in the PDMS chamber with fixed cells and the samples were covered by cover glass.

Experimental Details. The schematic of the partial spatial coherence gated QPM/DHM system based on Linnik interferometer is shown in Fig. 1. To reduce the phase noise of the system, the spatial coherence of the laser light source is reduced and the resulting light beam illuminates the specimen. It is demonstrated that when a coherent light incident on a rotating diffuser (RD) and the diffused light is coupled into the multiple multi-mode fiber bundle (MMFB) then its output acts as a pseudo thermal light source having partial spatial and highly temporal coherence properties. The detailed study of the speckle reduction can be found elsewhere[21–23].

A highly coherent laser light (He-Ne @632.8 nm) beam is expanded using microscope objective MO_1 and passed through a RD. The beam spot size of 4.5 mm is made onto the diffuser plane to match the diameter of MMFB. The scattered photons are collected by lens L_1 (focal length $f_1 = 50$ mm) and pumped into the MMFB. The light from MMFB output is first collimated and then focused at the back-focal plane of the MO_3 by utilizing the lenses L_2 ($f_2 = 75$ mm), L_3 ($f_3 = 150$ mm) and beam splitter (BS). Thus the samples are illuminated by a nearly collimated beam for their accurate phase imaging. In the reference arm an optically flat mirror (of the order of $\lambda/10$) is used. The reflected light from the reference mirror and the specimen are re-combined at BS to form interference pattern. The interferograms are then projected on the CMOS image sensor (Hamamatsu ORCA-Flash4.0 LT, C11440-42U) using tube lens L_4 ($f_4 = 200$ mm). The camera exposure time is kept 50 ms.

Comparison of coherent laser and pseudo-thermal light source based phase imaging. In the proposed geometry, a pseudo thermal light source is used to reduce the spatial phase noise of the system which further enhances the measurement accuracy of the system. First, we have compared the spatial phase sensitivity of the system by imaging the sperm cell with fully coherent and partially coherent (pseudo-thermal) light sources. Figure 2 shows interferogram, reconstructed phase map of a sperm cell and the spatial phase noise of the system for fully and partially spatially coherence light sources. The spatial phase sensitivity of the system is enhanced when the test specimen is illuminated by the partially spatially coherent light source. Figure 2(a,d) show the interferograms of the sperm cell utilizing direct laser and synthesized pseudo-thermal light sources, respectively. Highly coherent nature of light source leads to speckle and non-uniform illumination of the specimen as shown in Fig. 2(a), while pseudo-thermal light source provides a speckle free uniform illumination (Fig. 2(d)). The object is clearly visible in Fig. 2(d) with illumination of pseudo-thermal light source which is otherwise not visible with direct laser source (Fig. 2(a)). Figure 2(b,e) show their corresponding reconstructed phase maps of the interferograms depicted in Figs 2(a) and 2(d). It can be observed from the phase images that the finer features of the sperm cells i.e. neck and tail is not resolved in phase map of hologram recorded by the direct laser, while whole sperm cell is clearly reconstructed in case of pseudo-thermal light source. In case of direct laser, the generation of speckle
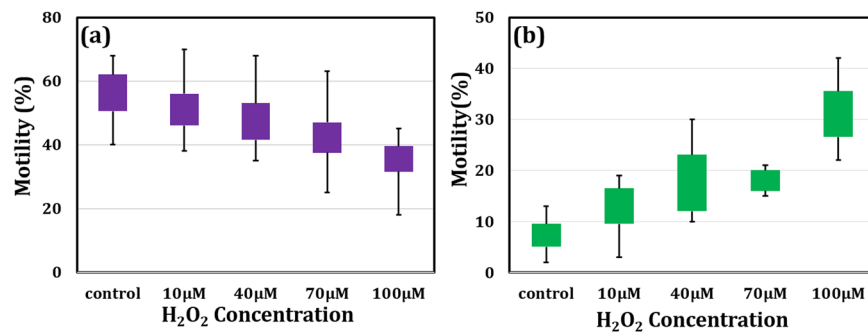
Figure 2. Measurement of the spatial phase sensitivity of QPM for direct laser and pseudo-thermal light sources. (**a,d**) are the interferograms obtained with healthy sperm cell as a test specimen, (**b,e**) reconstructed phase map of the sperm cell corresponding to (**a,d**), respectively and (**c,f**) spatial phase noise of the experimental setup for laser and pseudo-thermal light sources, respectively. Note that the scale of the color bars used in (**c,f**) having different values.
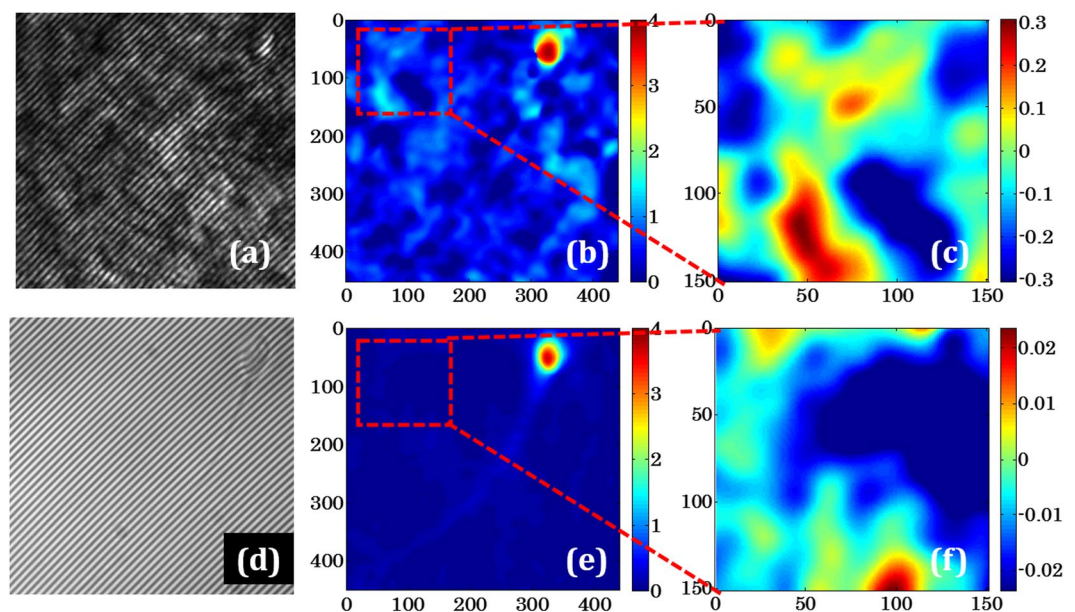

Figure 3. Effects of the H_2O_2 on the motility of sperm cells (**a**) changes in the percentage of progressive motility and (**b**) non-progressive motility of sperm cells after H_2O_2 treatment at different concentrations comparing to control (mean $\pm$ SE, $p < 0.05$ vs. control).

and non-uniform illumination reduces the over-all spatial phase sensitivity of the system which results in poor resolution. The spatial phase sensitivity of the system for both kind of light sources were measured and compared. High spatial phase sensitivity is essential where minute phase variations in the target are needed to be quantified. Here, we utilized pseudo-thermal light source to enhance the spatial phase sensitivity of the phase microscopy system. The difference in phase values of the controlled and the 10 μM sperm cells is only 8%, which would be difficult to differentiate with direct laser based QPM technique due to high spatial phase noise. Figure 2(c,f) show the spatial phase noise of the system for the direct laser and pseudo-thermal light sources, respectively, where the color bars having different scale values. By measuring the standard deviation of the phase distribution, one can estimate the spatial phase sensitivity of the system. In our case, the phase sensitivity is observed to be 300 ± 11.9 mrad and 20 ± 1.5 mrad for direct laser and pseudo-thermal light source, respectively.

Results and Discussion

Sperm cell motility after treatment with different concentrations of H_2O_2.
Significant differences in the motility parameters were detected when comparing the control sample with exposed samples with various H_2O_2 concentrations. The effect of different concentrations of H_2O_2 on progressive and non-progressive motility of spermatozoa are shown in Fig. 3(a,b) respectively (n = 7; seven ejaculates from different donors). Four different concentrations of H_2O_2 were tested (10 μM, 40 μM, 70 μM, 100 μM) for the oxidative stress study on sperm cells. Sperm samples were incubated for 1 hour at 37 °C in the absence (control) or presence (test) of H_2O_2.
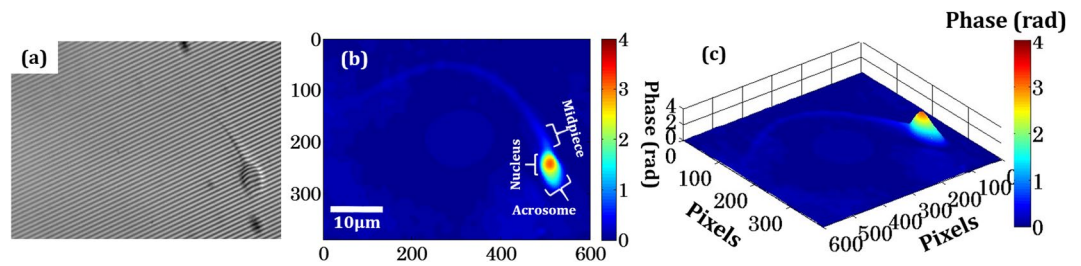
Figure 4. Digital holographic process and reconstructed phase maps of sperm cell (**a**) Typical hologram of the sperm cell recorded from partially coherent DHM setup, (**b**) reconstructed phase map of sperm cell with it's basic structure and (**c**) pseudo 3D phase map of the sperm cell. (color bar is showing the phase in radian, blue for zero and deep red for maximum phase).
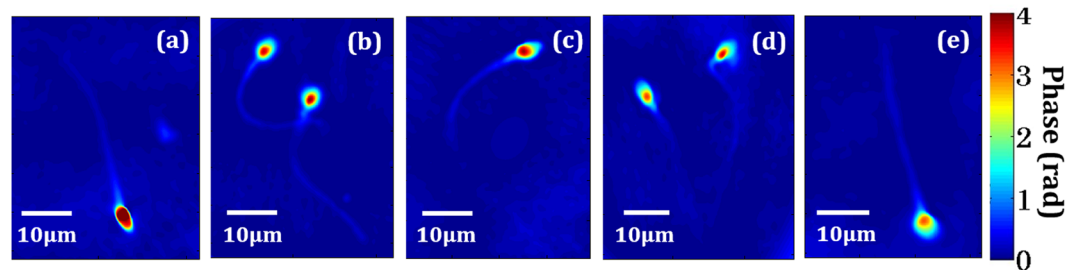

Figure 5. Pseudo-color plot of reconstructed phase maps of (**a**) normal sperm cells, and at different concentrations of (**b**) $10 \mu M$, (**c**) $40 \mu M$, (**d**) $70 \mu M$ and (**e**) $100 \mu M$ of concentration of H_2O_2, respectively (color bar shows the phase in radian, blue for zero and deep red for maximum phase).

Evaluation of cell motility was performed by experienced biologist according to WHO 2010 criteria[27]. The motility of progressive class was graded as moving actively, linearly or in a large circle, regardless of speed. Non-progressive motility was estimated as nonlinear movement with flagellar force hardly displacing the head, or with only flagellar or head trembling. At least 100 cells per each H_2O_2 concentration were analyzed. For the estimation of motility of sperm cells, the cells were kept in 96 well tissue culture plates and observed under the inverted microscope with 40X magnification objective lens. H_2O_2 produces a concentration-dependent decrease in progressive motility of sperm cells (ANOVA: $p < 0.05$). The concentration at $100 \mu M$ of H_2O_2 had the most significant effect on the decrease in numbers of progressive motile cells in comparison with other doses (Fig. 3(a), ($10 \mu M$: 51 ± 10.7; $40 \mu M$: 48 ± 10.9; $70 \mu M$: 42 ± 11.9; 100: μM 34 ± 8.8; versus control: $59 \pm 10.8\%$, paired t-test, $p < 0.05$). At the same time H_2O_2 affects most on the non-progressive motility at the concentrations of $70 \mu M$ and $100 \mu M$ as compared with control ($70 \mu M$: 19 ± 3.9; $100 \mu M$: 29 ± 7.4; versus control: $6 \pm 6.6\%$, paired t-test, $p < 0.05$). Both doses $10 \mu M$ and $40 \mu M$ of H_2O_2 did not influence to the non-progressive motility ($10 \mu M$: 14 ± 4.8; $40 \mu M$: 16 ± 5.4; versus control: $6 \pm 6.6\%$, paired t-test, $p > 0.05$, (Fig. 3(b)). Effects on non-progressive motility were statistically significant at H_2O_2 concentration of $70 \mu M$ and $100 \mu M$ ($p < 0.05$ when compared with controls).

The effect of oxidative stress on sperm motility has been demonstrated in number of studies[34–36]. H_2O_2 is externally supplemented agent to induce oxidative stress on sperm cells. Our results support the previous studies that the extent of motility decrease depends on the concentration of H_2O_2. The underlying mechanism of H_2O_2 influence to sperm motility is described previously[37,38]. Membrane lipids of sperm cells contain unsaturated fatty acids which are vulnerable to peroxidation. Sperm incubation with H_2O_2 triggers lipid peroxidation cascade results in membrane loss of flexibility and plasticity which determines disrupted tail motion[3,34,39]. Moreover, motility may be decreased because of restriction of energy production by damaged mitochondria after oxidation[40,41].

Quantitative phase imaging of sperm cells. The quantitative morphological analysis of the sperm cells provides a better understanding of the behaviour of sperm cells under control and oxidative stress conditions. Figure 4 shows the recorded hologram and pseudo colour unwrapped phase map of sperm cell. Figure 4(a) shows a typical low spatial coherence hologram of the sperm cell and 2D view of the recovered phase map is shown in Fig. 4(b). The basic structure of the sperm cell composed of the head, mid piece, tail and end piece, the head is partially covered with nucleus and acrosome. Figure 4(c) shows the pseudo 3D phase map of the same sperm cell where maximum optical path delay is generated by the head of the sperm cell having value approximately 4 rad.

The low spatial coherence QPM/DHM is further used for the evaluation of the effects of oxidative stress on the morphology of the human sperm cells. Figure 5 shows the recovered phase maps of sperm cells treated with different concentration of H_2O_2. Figure 5(a–e) show the reconstructed 3D phase maps for the control, $10 \mu M$, $40 \mu M$, $70 \mu M$ and $100 \mu M$ concentration of H_2O_2, respectively. It is observed from the phase images that with increasing concentration of H_2O_2, the maximum value of the phase of sperm head decreases which indicates that there is a change in the morphology of the sperm head. For the study of morphological changes in the sperm head during
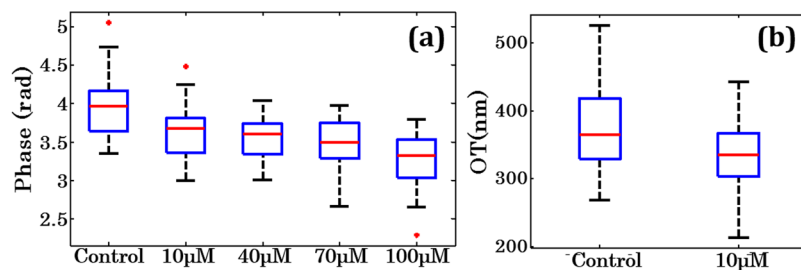
Figure 6. Whisker box plot for (**a**) maximum phase of the sperm head for control, $10\,\mu M$, $40\,\mu M$, $70\,\mu M$ and $100\,\mu M$ concentration of H_2O_2, respectively, and (**b**) optical thickness (OT) of the control vs. $10\,\mu M$ concentration of H_2O_2. The central red lines indicate the median, and bottom and top sides of blue box indicate the 25th and 75th percentiles, respectively. The black lines extended vertically from blue boxes specify extreme data points without outliers, and '+' symbols in red color are plotted for outliers.
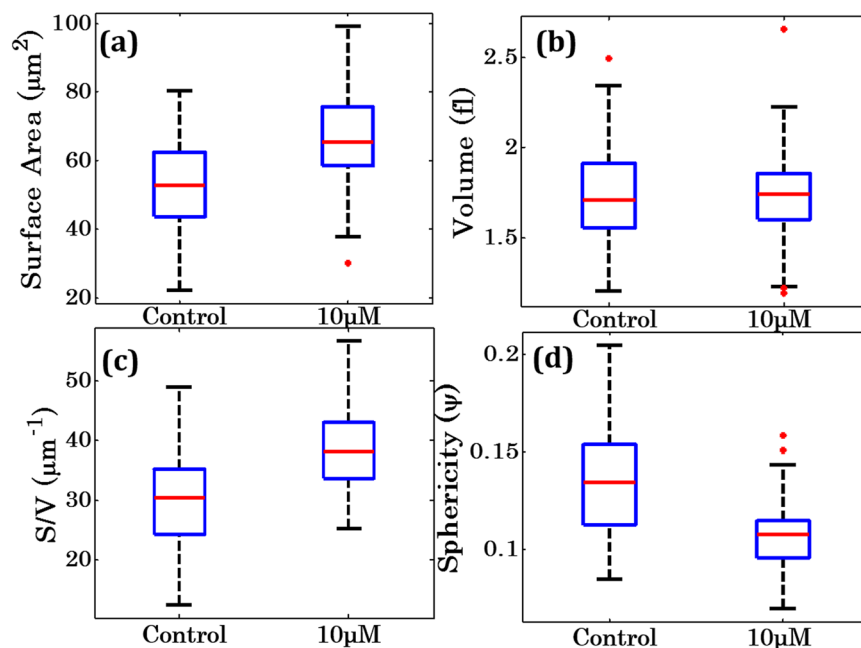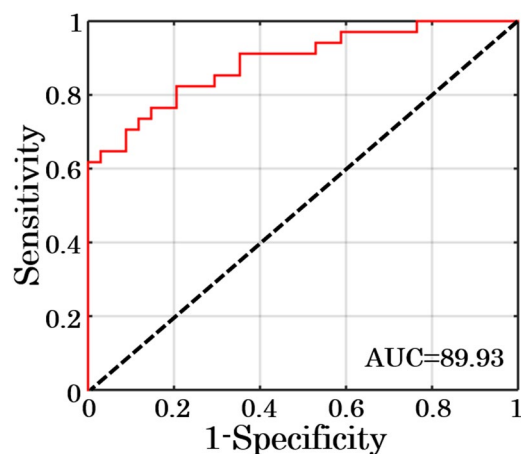

Figure 7. Morphological parameters of sperm head as expressed with the whisker box plots of (**a–d**) surface area, volume, surface area to volume ratio (S/V), and sphericity under normal (control) and oxidative stress conditions.

oxidative stress, several morphological parameters have been extracted from the phase maps. In total, more than 2500 sperm cells were analysed to measure the optical and morphological parameters. Figure 6(a) shows the whisker box plots of maximum phase of the sperm head at different concentrations of H_2O_2. Figure 6(b) shows the whisker box plot for the optical thickness of the sperm head for control and $10\,\mu M$ concentration of the H_2O_2. The optical thickness decreases after oxidative stress which further changes the morphology of the sperm cells. The structure of sperm suggest that the nucleus is tallest part sperm followed by acrosome and mid-piece which allows observer to distinguish nucleus from acrosome[17,18]. The reconstructed phase map show a clearly detectable edge of cell boundary and maximum phase in the nucleus region. The identification and quantification of the optical thickness of nucleus may provide the deformation of nucleus during oxidative stress as shown in Fig. 5. The acrosome having significant low OT due to lesser thickness as compared to nucleus. Hence, the quantification of the change in the OT of nucleus during deformation can be a good marker for the quantification of oxidative stress. Here, we have chosen control and $10\,\mu M$ concentration of the H_2O_2 only for the comparative study because there is almost linear decrease in the maximum phase with increasing concentration of the H_2O_2 (Fig. 6a).

Characterization of morphological and texture parameters during oxidative stress. In order to determine the effects of oxidative stress on the morphology of the sperm cell head, the morphology of head is quantified from the phase maps using calculations describes in materials and method section. Surface area (S), volume (V), surface to volume ratio (S/V) and sphericity (Ψ) parameters were analysed for classification of control and $10\,\mu M$ concentration of the H_2O_2. Figure 7(a–d) show the whisker box plots of these parameters for sperm head under control and oxidative stress conditions. The results show that the surface area increases in

Texture Parameter	Definition	Median value of the parameter for	
		Control samples	10 µM concentration
Mean (µ)	$\frac{1}{N}\sum_{i=1}^{N}\phi_i$	1.245	1.102
Variance (σ^2)	$\frac{1}{N}\sum_{i=1}^{N}(\phi_i - \mu)^2$	0.965	0.857
Kurtosis	$\frac{1}{N}\sum_{i=1}^{N}\left[\frac{(\phi_i - \mu)}{\sigma}\right]^4 - 3$	2.197	2.469
Skewness	$\frac{1}{N}\sum_{i=1}^{N}\left[\frac{(\phi_i - \mu)}{\sigma}\right]^3$	0.669	0.772
Entropy	$-\sum_{i=1}^{N}p(x_i)log_2 p(\phi_i)$	5.056	5.448
Energy	$\sum_{i=1}^{N-1}\sum_{j=1}^{N-1}(p_{ij})^2$	0.399	0.34

Table 1. Texture parameters of sperm cell head for normal (control) and externally induced oxidative stress (10 µM H_2O_2 concentration) conditions.

Figure 8. ROC curve for testing dataset of sperm head for control and 10 µM/ml H_2O_2 concentration treated sperm cells using eleven different morphological and texture parameters.

sperm cell head after the externally induced oxidative stress (Fig. 7a), while the volume is approximately constant during this process as can be seen in Fig. 7(b). There is an increase in the surface to volume ratio while sphericity decreases after oxidative stress. The increase in the S and S/V with decrease in ψ indicates that the flattening of the cells under stress assuming constant RI of the sperm head during whole process (Fig. 7(c,d)).

For the statistical analysis, selection and extraction of texture features are also important for the classification of any disease. Here, we have extracted various texture features from the phase maps of the sperm heads such as: mean, variance, entropy, kurtosis, skewness and energy. All the parameters were extracted by choosing a region of interest (ROI) of the sperm cells and listed in Table 1. There is a decrease in the mean value of the phase distribution over entire sperm head reflects the flattening of the sperm head i.e. decrease in the optical thickness of the sperm head after introducing 10 µM of H_2O_2 concentration. The decrease in the variance shows the less spread of data points around its mean value, while there is an increase in entropy predicts the increase in the randomness of phase distribution over entire sperm head. The increase in kurtosis and skewness show the more flatness and asymmetricity in phase distribution of sperm head. The decrease in the energy value shows the increase of heterogeneity in phase distribution of sperm cell head.

Once all the morphological and texture parameters were extracted from the phase maps of sperm cells, a support vector machine (SVM) classifier has been developed for the classification of the control and oxidative stress induced sperm cells[28,29,42]. Eleven parameters: OT, S, V, S/V, ψ, mean, variance, entropy, kurtosis, skewness and energy were utilized as input predictor variables and the genuine state of the sperm as a response variable i.e. 0 for control and 1 for 10 µM H_2O_2 concentration treated sperm cells. Sensitivity, specificity and area under receiver operating characteristic (ROC) curve were calculated to check the accuracy of the model. Total data points are divided into two sets, 60% for the training of the model and 40% for the testing purpose. Figure 8 shows the ROC curve for the testing data points with a specificity and sensitivity of 88.61% and 91.18%, respectively with an accuracy of 89.93% for the classification of control and test sperm cells.

Conclusion

In present study, the capability of DHM using low spatial coherence light source alongwith SVM classifier exploited to measure change in morphology of sperm head after oxidative stress. It is exhibited that pseudo-thermal light source based phase imaging provides reconstruction of the biological structure having minute optical thickness (i.e., tail of the sperm cells), which is otherwise not possible under coherent illumination.

It is known that fertilization capability of sperm cell is impaired under biological oxidative stress. The oxidative stress was induced using H_2O_2 treatment. Concentrations of H_2O_2 exceeding physiological threshold trigger the changes in semen leading to sperm cell dysfunction[7,35,38]. The evidence from previous studies suggests decrease of sperm cell motility due to membrane translocations of phospholipids[3,43]. In addition to membrane peroxidation, H_2O_2 initiates concentration-dependent increase of DNA fragmentation because of DNA strand breaks[3,36,44,45]. Using conventional microscopy, sperm cells with this type of anomalies might be amongst selected cells for intra-cytoplasmic sperm cell injection (ICSI) procedure leading to treatment failure. Therefore, it is of great significance to develop noninvasive methods for sperm cells selection. DHM appears to be one of the most promising noninvasive technique for the quantification of optical parameters of sperm cells[13,15,17].

We found that H_2O_2 induces oxidative stress to the sperm cells which leads to the sperm cell dysfunction by decreasing its motility. The result of our study suggests the association between gradual progressive motility loss (Fig. 3) and the shift of optical properties of the sperm head (Figs 6, 7) after exposure to various concentrations of H_2O_2. The head morphology changes resulting from peroxidation might be due to de-condensation of genetic material because of DNA fragmentation. Quantitative evaluation of the phase shift by DHM provides an opportunity to use SVM to obtain new information on the exact structure and better distinguish sperm cells that are normal from those under oxidative stress (Fig. 8). Development of such machine learning algorithms could play an important role in automatic classification of the healthy and stressed sperm cells. The origin of decrease in the maximum phase of sperm head could be due to various reasons such as: deformation in nucleus, structural organization of sperm DNA, condensation of chromatin etc[19]. The morphometric values obtained in our study can provide the volumetric estimation for the quantitative comparison between control and H_2O_2 treated sperm cells. The correlation of decrease in the phase and deformation in the nucleus can be quantify by multimodal imaging in future where the boundary can be located by fluorescence imaging and QPM can provide the changes in the maximum phase of nucleus. QPM may have capability to quantify the changes due to fragmentation in DNA after introducing oxidative stress in human sperm which can be the motivation for this kind of analysis on the fertilization capacitance of sperm cell[46,47].

One of the obstacles in IVF treatments is to recognize the sperm cells morphology by observing them under optical microscope whether it is under oxidative stress or not. However, by utilizing low spatial coherence DHM together with machine learning algorithms might provide better sperm selection during ICSI procedure. Moreover, as mentioned above, "hand-picked" spermatozoon for ICSI procedure might contain fragmented DNA, which can be detected indirectly by measuring sperm optical features using noninvasive, label-free QPM/DHM technique. We believe that our approach with DHM and machine learning based algorithm for sperm analysis at the cellular level has a strong potential for improving IVF procedures and their outcomes.

References

1. Agarwal, A., Mulgund, A., Hamada, A. & Chyatte, M. R. A unique view on male infertility around the globe. *Reproductive Biology and Endocrinology* **13**, 37 (2015).
2. Forti, G. & Krausz, C. Evaluation and treatment of the infertile couple. *The Journal of Clinical Endocrinology & Metabolism* **83**, 4177–4188 (1998).
3. John Aitken, R., Clarkson, J. S. & Fishel, S. Generation of reactive oxygen species, lipid peroxidation, and human sperm function. *Biology of reproduction* **41**, 183–197 (1989).
4. Iwasaki, A. & Gagnon, C. Formation of reactive oxygen species in spermatozoa of infertile patients. *Fertility and sterility* **57**, 409–416 (1992).
5. Shekarriz, M., Thomas, A. & Agarwal, A. Incidence and level of seminal reactive oxygen species in normal men. *Urology* **45**, 103–107 (1995).
6. Hughes, C. M., Lewis, S. E., McKelvey-Martin, V. J. & Thompson, W. A comparison of baseline and induced DNA damage in human spermatozoa from fertile and infertile men, using a modified comet assay. *MHR: Basic science of reproductive medicine* **2**, 613–619 (1996).
7. Twigg, J., Fulton, N., Gomez, E., Irvine, D. S. & Aitken, R. J. Analysis of the impact of intracellular reactive oxygen species generation on the structural and functional integrity of human spermatozoa: lipid peroxidation, DNA fragmentation and effectiveness of antioxidants. *Human reproduction (Oxford, England)* **13**, 1429–1436 (1998).
8. Ochsendorf, F. Infections in the male genital tract and reactive oxygen species. *Human Reproduction Update* **5**, 399–420 (1999).
9. Pluta, M. & Maksymilian, P. Advanced light microscopy. Vol. 1 (Elsevier Amsterdam, 1988).
10. Burch, C. & Stock, J. Phase-contrast microscopy. *Journal of Scientific Instruments* **19**, 71 (1942).
11. Lang, W. Nomarski differential interference-contrast microscopy. (Carl Zeiss, 1982).
12. Lee, K. *et al.* Quantitative phase imaging techniques for the study of cell pathophysiology: from principles to applications. *Sensors* **13**, 4170–4191 (2013).
13. Kim, M. K. Principles and techniques of digital holographic microscopy. *SPIE reviews* **1**, 018005 (2010).
14. Mir, M., Bhaduri, B., Wang, R., Zhu, R. & Popescu, G. Quantitative phase imaging. *Progress in optics* **57**, 133–217 (2012).
15. Coppola, G. *et al.* Digital holographic microscopy for the evaluation of human sperm structure. *Zygote* **22**, 446–454 (2014).
16. Crha, I. *et al.* Digital holographic microscopy in human sperm imaging. *Journal of assisted reproduction and genetics* **28**, 725 (2011).
17. Haifler, M. *et al.* Interferometric phase microscopy for label-free morphological evaluation of sperm cells. *Fertility and sterility* **104**, 43–47. e42 (2015).
18. Mirsky, S., Barnea, I. & Shaked, N. Label-Free quantitative imaging of sperm for *in vitro* fertilization using interferometric phase microscopy. *J Fertil In Vitro-IVF-Worldwide Reprod Med Genet Stem Cell Biol* **190** (2016).
19. Di Caprio, G. *et al.* Holographic imaging of unlabelled sperm cells for semen analysis: a review. *Journal of biophotonics* **8**, 779–789 (2015).
20. Dubey, V. *et al.* Multi-modal chip-based fluorescence and quantitative phase microscopy for studying inflammation in macrophages. *Optics express* **26**, 19864–19876, https://doi.org/10.1364/oe.26.019864 (2018).
21. Ahmad, A., Dubey, V., Singh, G., Singh, V. & Mehta, D. S. Quantitative phase imaging of biological cells using spatially low and temporally high coherent light source. *Optics letters* **41**, 1554–1557 (2016).
22. Ahmad, A., Srivastava, V., Dubey, V. & Mehta, D. Ultra-short longitudinal spatial coherence length of laser light with the combined effect of spatial, angular, and temporal diversity. *Applied Physics Letters* **106**, 093701 (2015).
23. Goodman, J. W. Speckle phenomena in optics: theory and applications. (Roberts and Company Publishers, 2007).
24. Dubey, V., Singh, G., Singh, V., Ahmad, A. & Mehta, D. S. Multispectral quantitative phase imaging of human red blood cells using inexpensive narrowband multicolor LEDs. *Applied optics* **55**, 2521–2525 (2016).

9

25. Yamauchi, T., Iwai, H., Miwa, M. & Yamashita, Y. Low-coherent quantitative phase microscope for nanometer-scale measurement of living cells morphology. *Optics express* **16**, 12227–12238 (2008).
26. Dubey, V., Singh, V., Ahmad, A., Singh, G. & Mehta, D. S. In Quantitative Phase Imaging II. 97181F (International Society for Optics and Photonics) (2016).
27. Organization, W. H. WHO laboratory manual for the examination and processing of human semen (2010).
28. Wernick, M. N., Yang, Y., Brankov, J. G., Yourganov, G. & Strother, S. C. Machine learning in medical imaging. *IEEE signal processing magazine* **27**, 25–38 (2010).
29. Wu, G., Shen, D. & Sabuncu, M. Machine Learning and Medical Imaging. (Academic Press, 2016).
30. Popescu, G. Quantitative phase imaging of cells and tissues. (McGraw Hill Professional, 2011).
31. Girshovitz, P. & Shaked, N. T. Generalized cell morphological parameters based on interferometric phase microscopy and their application to cell life cycle characterization. *Biomedical optics express* **3**, 1757–1773 (2012).
32. Ahmad, A. *et al.* Quantitative phase microscopy of red blood cells during planar trapping and propulsion. *Lab on a Chip* (2018).
33. Kim, Y. *et al.* Profiling individual human red blood cells using common-path diffraction optical tomography. *Scientific reports* **4**, 6659 (2014).
34. Whittington, K. *et al.* Reactive oxygen species (ROS) production and the outcome of diagnostic tests of sperm function. *International journal of andrology* **22**, 236–242 (1999).
35. Kao, S.-H. *et al.* Increase of oxidative stress in human sperm with lower motility. *Fertility and sterility* **89**, 1183–1190 (2008).
36. Duru, N. K., Morshedi, M. & Oehninger, S. Effects of hydrogen peroxide on DNA and plasma membrane integrity of human spermatozoa. *Fertility and sterility* **74**, 1200–1207 (2000).
37. Sanocka, D. & Kurpisz, M. Reactive oxygen species and sperm cells. *Reproductive Biology and Endocrinology* **2**, 12 (2004).
38. Tremellen, K. Oxidative stress and male infertility—a clinical perspective. *Human Reproduction Update* **14**, 243–258 (2008).
39. Storey, B. T. Biochemistry of the induction and prevention of lipoperoxidative damage in human spermatozoa. *Molecular human reproduction* **3**, 203–213 (1997).
40. De Lamirande, E. & Gagnon, C. Reactive oxygen species and human spermatozoa: I. Effects on the motility of intact spermatozoa and on sperm axonemes. *Journal of andrology* **13**, 368–378 (1992).
41. De Lamirande, E., Jiang, H., Zini, A., Kodama, H. & Gagnon, C. Reactive oxygen species and sperm physiology. *Reviews of reproduction* **2**, 48–54 (1997).
42. Liu, Y. Active learning with support vector machine applied to gene expression data for cancer classification. *Journal of chemical information and computer sciences* **44**, 1936–1941 (2004).
43. Jones, R., Mann, T. & Sherins, R. Peroxidative breakdown of phospholipids in human spermatozoa, spermicidal properties of fatty acid peroxides, and protective action of seminal plasma. *Fertility and sterility* **31**, 531–537 (1979).
44. Lopes, S., Jurisicova, A., Sun, J.-G. & Casper, R. F. Reactive oxygen species: potential cause for DNA fragmentation in human spermatozoa. *Human reproduction (Oxford, England)* **13**, 896–900 (1998).
45. Sun, J.-G., Jurisicova, A. & Casper, R. F. Detection of deoxyribonucleic acid fragmentation in human sperm: correlation with fertilization *in vitro*. *Biology of reproduction* **56**, 602–607 (1997).
46. De Iuliis, G. N. *et al.* DNA damage in human spermatozoa is highly correlated with the efficiency of chromatin remodeling and the formation of 8-hydroxy-2′-deoxyguanosine, a marker of oxidative stress. *Biology of reproduction* **81**, 517–524 (2009).
47. Barroso, G., Morshedi, M. & Oehninger, S. Analysis of DNA fragmentation, plasma membrane translocation of phosphatidylserine and oxidative stress in human spermatozoa. *Human reproduction* **15**, 1338–1344 (2000).

Acknowledgements

Author Contributions

B.S.A., D.S.M., P.B. and G.A. conceived the project and supervised this work. Most of the experiments were performed and analysed by V.D. and D.P. V.D. and A.A. developed the experimental set-up. D.P. prepared the biological cells. D.P. and P.B. designed the biological experiments. All the authors contributed towards the writing of the manuscript.

Additional Information

Supplementary information accompanies this paper at https://doi.org/10.1038/s41598-019-39523-5.

Competing Interests: The authors declare no competing interests.

Publisher's note: Springer Nature remains neutral with regard to jurisdictional claims in published maps and institutional affiliations.

Paper III

High spatially sensitive quantitative phase imaging assisted with deep neural network
for classification of human spermatozoa under stressed condition

Ankit Butola, Daria Popova, Dilip K. Prasad, Azeem Ahmad, Anowarul Habib,
Jean Claude Tinguely, Purusotam Basnet, Ganesh Acharya, Paramasivam Senthilkumaran,
Dalip Singh Mehta, Balpreet Singh Ahluwalia

SCIENTIFIC REPORTS

*nature*research

Check for updates

OPEN

High spatially sensitive quantitative phase imaging assisted with deep neural network for classification of human spermatozoa under stressed condition

Ankit Butola[1,2,8], Daria Popova[2,3,8], Dilip K. Prasad[4], Azeem Ahmad[2], Anowarul Habib[2], Jean Claude Tinguely[2], Purusotam Basnet[3,5], Ganesh Acharya[5,6], Paramasivam Senthilkumaran[7], Dalip Singh Mehta[1,7] & Balpreet Singh Ahluwalia[2,6✉]

Sperm cell motility and morphology observed under the bright field microscopy are the only criteria for selecting a particular sperm cell during Intracytoplasmic Sperm Injection (ICSI) procedure of Assisted Reproductive Technology (ART). Several factors such as oxidative stress, cryopreservation, heat, smoking and alcohol consumption, are negatively associated with the quality of sperm cell and fertilization potential due to the changing of subcellular structures and functions which are overlooked. However, bright field imaging contrast is insufficient to distinguish tiniest morphological cell features that might influence the fertilizing ability of sperm cell. We developed a partially spatially coherent digital holographic microscope (PSC-DHM) for quantitative phase imaging (QPI) in order to distinguish normal sperm cells from sperm cells under different stress conditions such as cryopreservation, exposure to hydrogen peroxide and ethanol. Phase maps of total 10,163 sperm cells (2,400 control cells, 2,750 spermatozoa after cryopreservation, 2,515 and 2,498 cells under hydrogen peroxide and ethanol respectively) are reconstructed using the data acquired from the PSC-DHM system. Total of seven feedforward deep neural networks (DNN) are employed for the classification of the phase maps for normal and stress affected sperm cells. When validated against the test dataset, the DNN provided an average sensitivity, specificity and accuracy of 85.5%, 94.7% and 85.6%, respectively. The current QPI + DNN framework is applicable for further improving ICSI procedure and the diagnostic efficiency for the classification of semen quality in regard to their fertilization potential and other biomedical applications in general.

Semen quality and male fertility potential have been continuously declining all over the world[1–4]. At the same time, biomedical and technical advances have made it possible to treat male infertility using assisted reproductive technology (ART) including intracytoplasmic sperm injection (ICSI). Evaluation of semen quality and ICSI procedure are the important steps for the successful outcome of ART. Generally, semen parameters evaluation

[1]Bio-photonics Laboratory, Department of Physics, Indian Institute of Technology Delhi, Hauz-Khas, New Delhi 110016, India. [2]Department of Physics and Technology, UiT The Arctic University of Norway, Tromsø, Norway. [3]Women's Health and Perinatology Research Group, Department of Clinical Medicine, UiT The Arctic University of Norway, Tromsø, Norway. [4]Department of Computer Science, UiT The Arctic University of Norway, Tromsø, Norway. [5]Department of Obstetrics and Gynaecology, University Hospital of North Norway, Tromsø, Norway. [6]Department of Clinical Science, Intervention and Technology Karolinska Institutet, Stockholm, Sweden. [7]Department of Physics, Indian Institute of Technology Delhi, Hauz-Khas, New Delhi 110016, India. [8]These authors contributed equally: Ankit Butola and Daria Popova. ✉email: balpreet.singh.ahluwalia@uit.no

1

and ICSI procedure are guided by the bright field microscopy and experience of laboratory personnel. Recently, computer-assisted sperm analysis (CASA) a digital microscopic technique made it possible as a machine-based analysis for semen parameters such as sperm cell concentration, sperm cell motility, kinematics, and morphology. For instance, CASA systems acquire successive images of the cells and use special software to track the motion of heads of each spermatozoon[5,6]. However, it fails to provide any supportive information regarding subcellular changes within the sperm cells which could be useful to ICSI procedure. Another powerful technique is a label free holographic imaging, for 3D reconstruction of freely moving sperm cells[7]. Apart from this, other optical as well as spectroscopic techniques have been proposed so far to determine motility of the sperm cells[8–11]. For example, fluorescence imaging and laser scanning confocal microscopy have been demonstrated to investigate the mitochondrial functionality of sperm cells[12] since the motility of the cells partially depends on the mitochondrial function[13] and get affected by cryopreservation of the cells. Semen quality is also analyzed based on Raman micro-spectroscopy which can provide the spectral features of human sperm cells[14]. Oxidative stress is also known to affect the integrity of sperm genome, result in lipid peroxidation and decrease in sperm motility, which was quantified recently using partially spatially coherent digital holographic microscopy and machine learning[15]. Additionally, smoking and alcohol consumption are negatively associated with sperm concentration and percentage of motile sperms when compared with the persons without these habits[16]. All these factors can affect the morphology, physiology and subcellular structures of the sperm cells and these changes can be investigated by extracting the quantitative information of the cells.

For label-free sperm imaging, quantitative phase imaging (QPI) is an attractive non-invasive technique to extract the quantitative information of the samples[17–21]. QPI can measure the combined information of refractive index and local thickness of the specimens with a nanometric sensitivity, which can be utilized detecting any deviations from normality[22–24]. QPI has several biological applications, such as 3D imaging of human red blood cells (RBC)[25], bovine embryo[26], bovine spermatozoa[27], tissue imaging[28], and others. Although, QPI is a potentially powerful technique as it provides morphological changes of the specimens, it has not yet been amenable to interpretation by human experts due to the lack of chemical specificity[29]. Therefore, merging QPI with artificial intelligence (AI) is a promising route to provide virtual image classification of the QPI data[29]. Recently, AI techniques have been used to differentiate between healthy and unhealthy phase images of sperm cells. In these techniques, morphological and texture features are extracted from the head part of the cells, and these features are fed to the machine learning classifier to separate them into diagnostically relevant classes[15,30,31]. However, the variations in an imaging system, and, difficulty in deriving a consistent and reliable feature out of thousands of features, base pose difficulty in applying conventional machine learning techniques for classification of the sperm cells. For example, precise segmentation of the head part is required to measure the length, width and area of the sperm head[30]. Due to the lack of chemical specificity of QPI technique, the boundary between head and mid-piece of the cell cannot be located very precisely. Secondly, measuring the length and area of the head part to differentiate between normal and stressed sperm cells depends on the human expertise and segmentation algorithm. Additionally, the actual value of morphological features such as surface area, volume, surface to volume ratio and sphericity cannot be accurately determined without decoupling the refractive index and thickness of the cells[32]. Therefore, it is beneficial to use advance machine learning technique i.e. convolutional neural network (CNN), which does not require to extract any features and can automatically generate abstract convolutional features from the training dataset. CNN/deep learning is rapidly growing as an automated technique in biomedical imaging for example disease classification[33–35], image segmentation[36], resolution enhancement[37], digital staining[18], noise reductions[38], among others[39,40].

We demonstrate the use of QPI technique assisted with deep learning for the classification of sperm cells under different stressed conditions. A total of four different classes were considered in this study, which included healthy, externally induced oxidative stressed, cryopreserved, and externally induced alcohol affected sperm cells. The four classes of sperm cells were also studied using conventional techniques to quantify and compare the progressive and the non-progressive motility of spermatozoa. Figure 1 shows the schematic representation of a partially spatially coherent digital holographic microscope (PSC-DHM) developed to acquire the interferometric images of the sperm cells as can be seen in Fig. 1b. Figure 1c,d shows the quantitative phase map of sperm cells. The PSC-DHM system offers single shot phase reconstruction of the cells especially the thinnest i.e. tail part of the sperms by utilizing partial spatial coherent properties of light source. QPI system commonly uses direct laser light (high spatially and temporally coherent) or white light (spatially and temporally incoherent). Direct laser suffers with low spatial phase sensitivity and hence accurate phase estimation of a thin sample is usually difficult. On the other hand, white light provides high spatial phase sensitivity but due to low temporal coherence it requires phase shifting technique to utilize the whole field of view of the camera. In contrast, the PSC-DHM system offers single shot phase extraction of the sample due to high temporal coherence and high spatial phase sensitivity because of its spatial incoherent nature. The details of the PSC-DHM system is provided in "Methods" section. The spatial phase sensitivity of the system developed is around ± 20 mrad which is utilized to reconstruct the phase information of the cells including the tail part. The thickness of the tail of the sperm cells are typically 100 nm and thus more challenging to image unless high spatial phase sensitivity is achieved. This is particularly useful as the tail plays an important role in progressive motility of the cells and it may change under different stressed conditions.

In this study, total 10,163 interferometric images (2,400 normal, 2,750 cryopreserved, 2,515 oxidative stressed and 2,498 alcohol affected) of the sperm cells were acquired from the PSC-DHM system. The comparison between phase measurement sensitivity of direct laser and PSC source can be found in supplementary information. The phase maps of these cells are used as input to the deep neural network (DNN) which is trained by 70% of the data and validated against the 30% testing data to check the classification accuracy of the networks. The current PSC-DHM + DNN framework has several advantages over the conventional bright field imaging techniques for sperm classification. QPI offers the quantitative information i.e. combined information of the
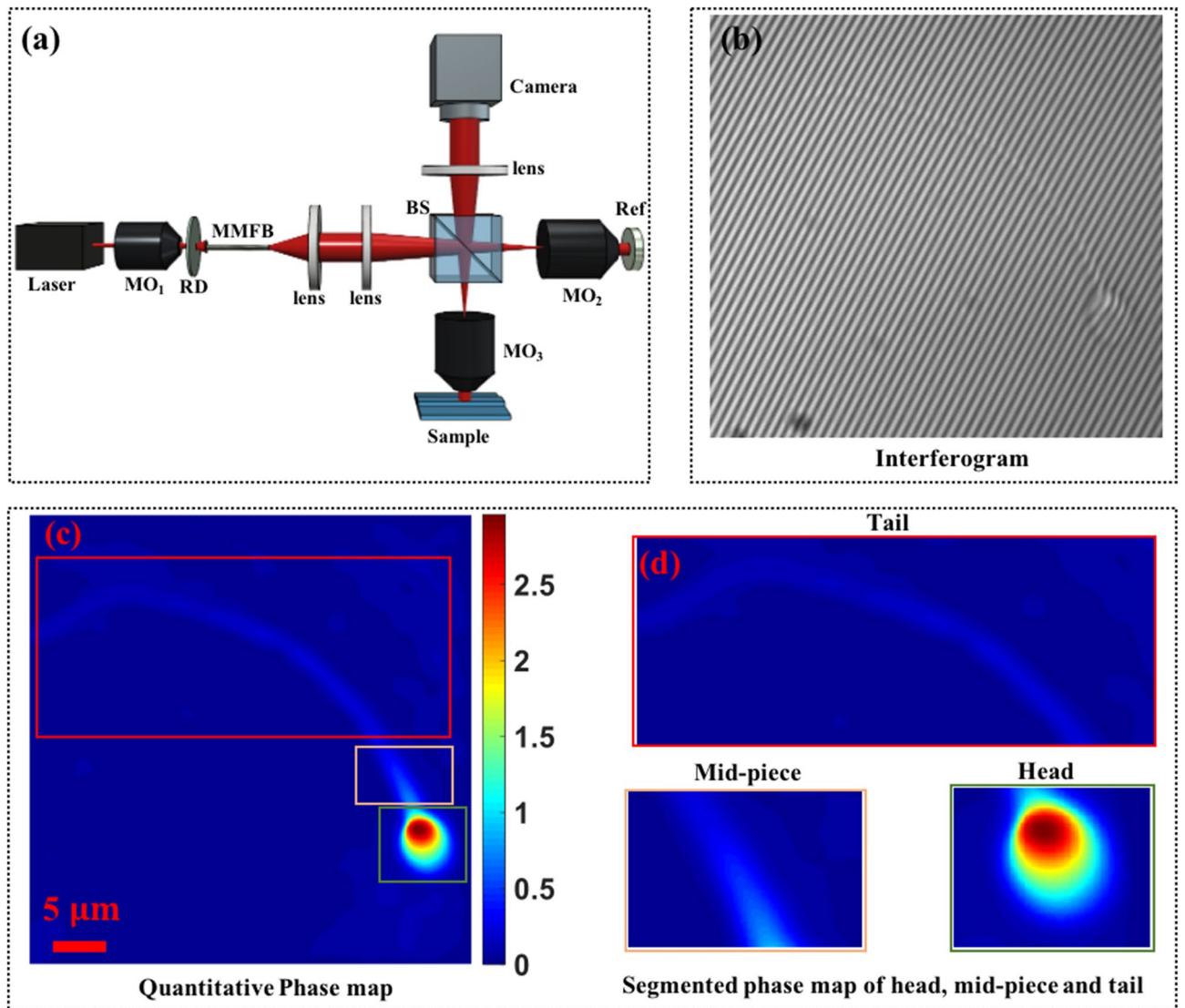
Figure 1. (**a**) Schematic diagram of the partially spatially coherent digital holographic microscope (PSC-DHM) system and (**b**) the interferometric image of the sperm cell acquired from the PSC-DHM. (RD—rotating diffuser, Ref—reference mirror, BS—Beam splitter, MO—microscope objective, MMFB—multiple multi-mode fiber bundle). Reconstructed phase map (**c**) and (**d**) the zoomed view of head, neck and tail part of the sperm cell. Color bar represents the phase map in radian.

refractive index and the local thickness of the sperm cells. This quantitative morphological information of the sperm cells is not obtained using a bright field microscopy. Additionally, the PSC-DHM system offers a label-free platform with nanometric sensitivity to detect any small sub-cellular changes in the head, mid-piece and tail of the sperm cells. These sub-cellular parts of sperm cells are influenced by the alcohol, oxidative stressed and cryopreservation of the cell. It has been shown that cryopreservation affects the mitochondrial dysfunctionality, damage of cellular membrane, failure of chromatin de-condensation and reduction in motility of the sperm cells[41–45]. Also, oxidative stressed and consumption of alcohol damage the plasma membrane, DNA and reduce the percentage of motile sperm cells[44]. Since, head contain the nucleus i.e. hold DNA of the cells, midpiece packed with mitochondria and tail play an important role in the progressive motility of the cells, therefore, PSC-DHM + DNN could be a valuable label-free tool to detect any morphological changes in these parts of the cells. Finally, DNN architectures provide automated classification of the phase map of the sperm cells. In contrast to the conventional feature extraction-based machine learning classifier[15], multiple layers in DNN architectures can automatically characterize relevant morphological and texture features to separate the samples into their relevant classes. Therefore, we believe that QPI coupled with DNN would find usage in IVF clinics in diagnosis, and for selection of healthy cells.
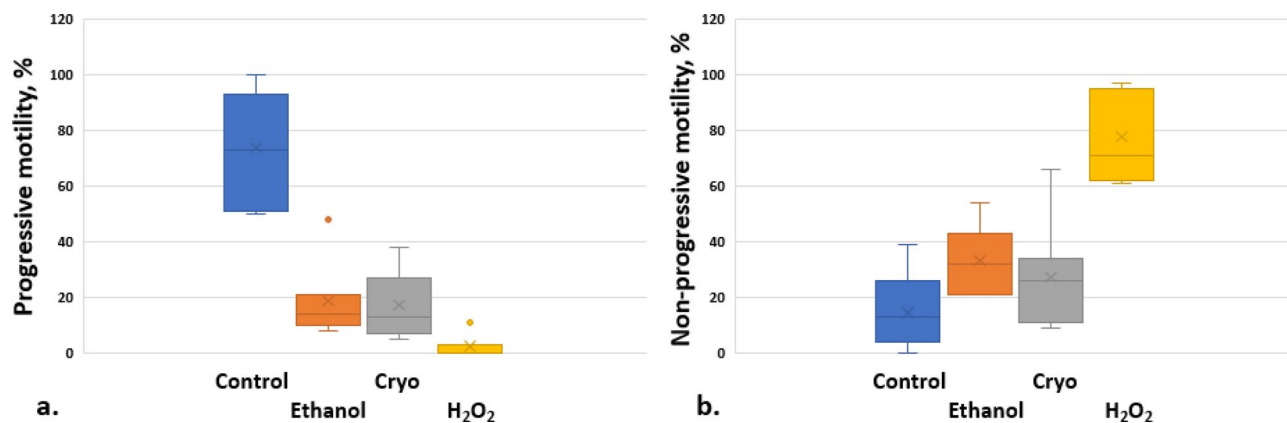
Figure 2. Progressive (**a**) and non-progressive (**b**) motility changes of sperm cells after incubation (1 h/37 °C) with ethanol, hydrogen peroxide (H_2O_2) and after cryopreservation as compared with control (n = 7, seven ejaculates from different donors). The middle line of the box represents the median, the "x" represents the mean, the whiskers extend from the ends of the box to the minimum value and maximum value. Outliers marked as dots.

Variable	Control Mean ± SD	Ethanol, 2% Mean ± SD	Cryopreservation Mean ± SD	H_2O_2, 200 µM Mean ± SD	P-value
Progressive motility (PR, %)	73.9 ± 19.5	18.7 ± 13.8	17.3 ± 11.9	2.4 ± 4.0	C/E 0.00009 C/H 0.00005 C/Cryo 0.0001
Non-progressive motility (NP, %)	14.6 ± 13.8	33.1 ± 11.9	27.1 ± 19.5	77.7 ± 16.2	C/E 0.01 C/H 0.0002 C/Cryo 0.2

Table 1. Effect of cryopreservation, ethanol and hydrogen peroxide incubation on human sperm cells motility. Analysis of the differences among group means using Paired Two Sample t-Test for Means (alpha 0,05). Values are shown as a mean ± standard deviation (SD). P-value for the analysis of the differences between the sample means of control and ethanol (C/E), control and H_2O_2 (C/H), control and cryopreserved groups (C/Cryo).

Results and discussion

Motility test of spermatozoa exposed to ethanol, hydrogen peroxide, and cryopreservation. The effect of ethanol, hydrogen peroxide and cryopreservation on progressive and non-progressive motility of spermatozoa was investigated and the results are shown in Fig. 2. Sperm motility were analyzed manually by the trained biologist from the IVF clinic using phase contrast microscope, 40× magnification with Makler counting chamber in accordance as World Health Organization (WHO) standards. Motility are categorized as progressive, non-progressive or immotile. Spermatozoa with progressive motility moves actively, linearly or in a large circle. Non-progressive motility has different patterns of trajectory without progression. The number of progressive motilities assessed first, then the number of non-progressive motility and immortality. Further, progressive and non-progressive motilities are important to count the percentage of motile sperm cells and cross-validate the effect of cryopreservation, externally induced ethanol and H_2O_2. After motility test, these sperm cells are imaged by PSC-DHM system for automated identification of normal sperm cells.

In this study, the concentration of H_2O_2 and ethanol were selected such that it triggers visible stress effect, i.e. impair the progressive motilities within 1 h. The effect of various concentration of H_2O_2 on the motility of sperm cells has been also shown in the previous study[15]. To simulate stress condition, we incubated sperm cells for 1 h in 2% ethanol or 200 µM H_2O_2. Lower concentration of ethanol or H_2O_2 did not influence the motility strongly in 1 h, at the same time higher concentrations eliminated cells with progressive motility. For cryopreservation, it is assumed that the time of storage semen mammals in liquid nitrogen at − 196 °C does not change the viability and the motility of sperm cells. For example, it is shown in the study of Ramírez-Reveco[46] that the total sperm motility of bull was not affected by long-term storage at − 196 °C. In our study thawing of human semen samples were performed in 2–5 h of freezing. Sperm cells were exposed to ethanol or hydrogen peroxide for 1 h at 37 °C. For the control group, same amount of medium as in the test group were added. Figure 2 shows the box plot of the sperm cells after different stressed conditions. After incubation for 1 h, ethanol and H_2O_2 produced a significant decrease in progressive motility of sperm cells as compared with control (Table 1): 18.7 ± 13.8% for ethanol and 2.4 ± 4.0% for H_2O_2 vs. 73.9 ± 19.5% for control cells. At the same the non-progressive motility after incubation both with ethanol and H_2O_2 increased: 33.1 ± 11.9% (ethanol) and 77.7 ± 16.2% (H_2O_2) vs. control 14.6 ± 13.8% (ANOVA, paired t-test, p < 0.05). Cryopreservation resulted in a significant decrease in progressive motility (Fig. 2, Table 1). Spermatozoa with progressive motility had a mean value before cryopreservation of 73.9 ± 19.5%, while mean value after thawing was 17.3 ± 11.9% (p < 0.01). The non-progressive motility decreased after thawing, but not significantly: 27.1 ± 19.5% vs. 14.6 ± 13.8% (p > 0.01).
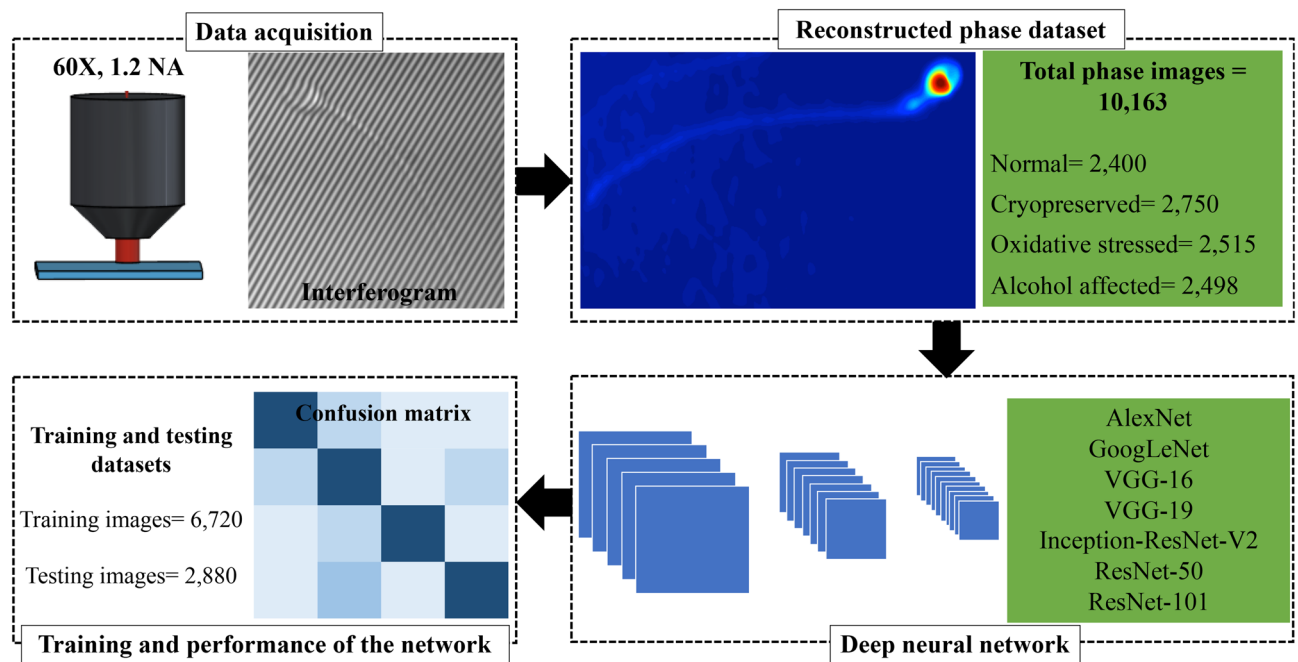
Figure 3. Workflow diagram showing the important steps for the classification of quantitative phase map of sperm cells. Phase map of the images is reconstructed by the interferogram captured using PSC-DHM system. Classification of the phase images is done by total 7 deep neural networks (DNN). Each network is trained with total 6,720 phase images and 2,880 phase images are used to test its accuracy. The final performance and sensitivity of the network is reported in term of confusion matrix.

A possible mechanism of decrease in sperm motility after treatment with ethanol is distortion of cell membrane caused by altering of membrane protein structure[47,48]. On the other hand, the principle mechanism of the effect of hydrogen peroxide on sperm motility is peroxidation of unsaturated fatty acids, which is a part of membrane lipids. As a result of peroxidation, the membrane loses flexibility and plasticity which determines disrupted tail motion[49]. The functional changes of sperm cells after cryopreservation might be influenced by oxidative stress, cryo-protector used (type and concentration), methods of cryopreservation and thawing itself, and is also dependent on original semen characteristics, such as concentration and motility[49]. In accordance with the concept of "partial survival" current procedures used for sperm freezing and thawing lead to decrease of more than 50% in motility and survival rate[50], ultrastructure and cell morphology changes[51–53], mitochondrial activity reduction[54], and damages of sperm chromatin[49].

Figure 3 shows a schematic of our framework for the selection of normal sperm cells. The interferometric image of a sperm cell is acquired from PSC-DHM using 60×, 1.2 NA objective lens. These interferometric images are processed using standard Fourier transform algorithm[55] and Goldstein phase unwrapping algorithm[56]. The details of the Fourier transform and steps for reconstruction of phase map are described in Methods section. Recently, classification of the phase map of sperm cells is performed using simple machine learning techniques[15] where texture and morphological features are extracted from the phase image. These features are fed into machine learning models to separate the corresponding phase images into their relevant classes[30]. In contrast, we develop an end-to-end deep learning approach for the classification of normal sperm cells, which does not require extraction of any features from the phase image.

The DNN takes a phase image as input and provide a diagnostically relevant class label as an output i.e. normal cells, H_2O_2 stressed cells, ethanol stressed cells, and cryopreserved cells. DNN architecture consists of difference combination of convolution layer, rectifier linear unit layer (ReLU), maxpooling layer, fully connected layer and finally softmax layer. Details of these layers can be found elsewhere[57]. A total of seven DNN, namely AlexNet, GoogLeNet, Inception-ResNet-V2, VGG-16, VGG-19, ResNet-50 and ResNet-101 are used for the classification purpose. These networks are trained by total 70% of the phase images and 30% for testing the accuracy of each model. The training time of the model increased as the number of layers (combination of convolution layer, maxpooling and ReLU layer) increased in the network. The training time and other details of each model is mentioned in the data analysis section. Accuracy of these network are shown in terms of confusion matrices. Confusion matrix shows the number of correct and incorrect prediction of the network. Further, the accuracy of DNN models are compared with total 3 different machine learning classifiers i.e. support vector machine, Naive Bayes and k nearest neighbor. For machine learning classifier, total 11 parameters are extracted from the head part of the cells. These parameters are fed into the classifier for training and testing purpose. The details of all parameters and the classification accuracy of the machine learning models can be found in supplementary information 1.

Figure 4 represents the reconstructed quantitative phase maps of human sperm cells under different stressed conditions. All interferometric images were acquired using 60×, 1.2NA (UPLSAPO 60XW, Olympus) microscopic
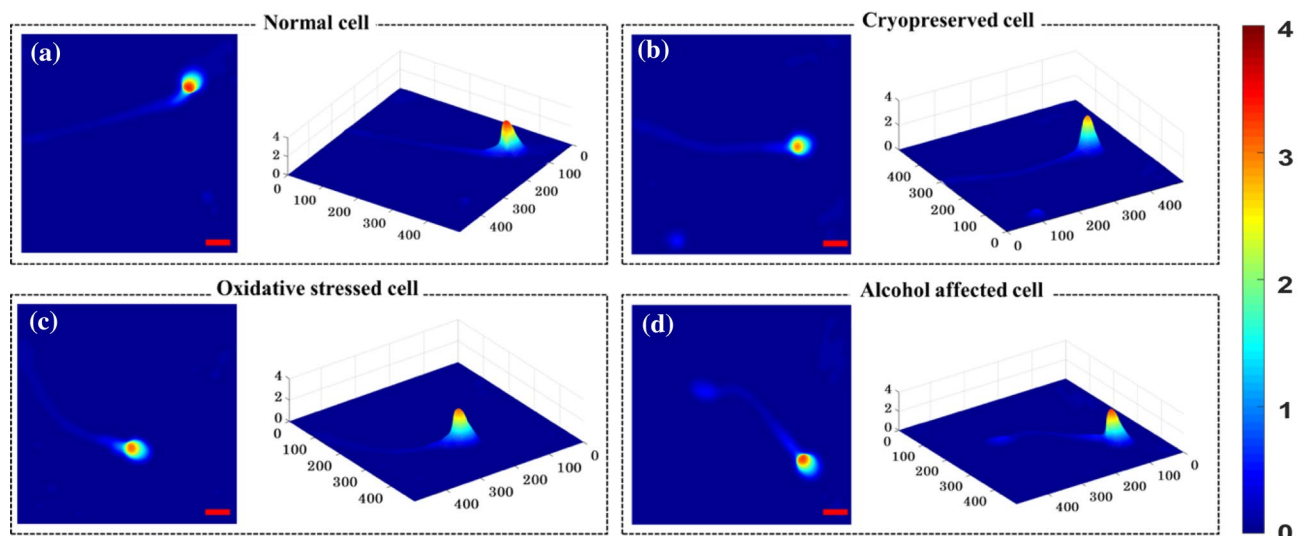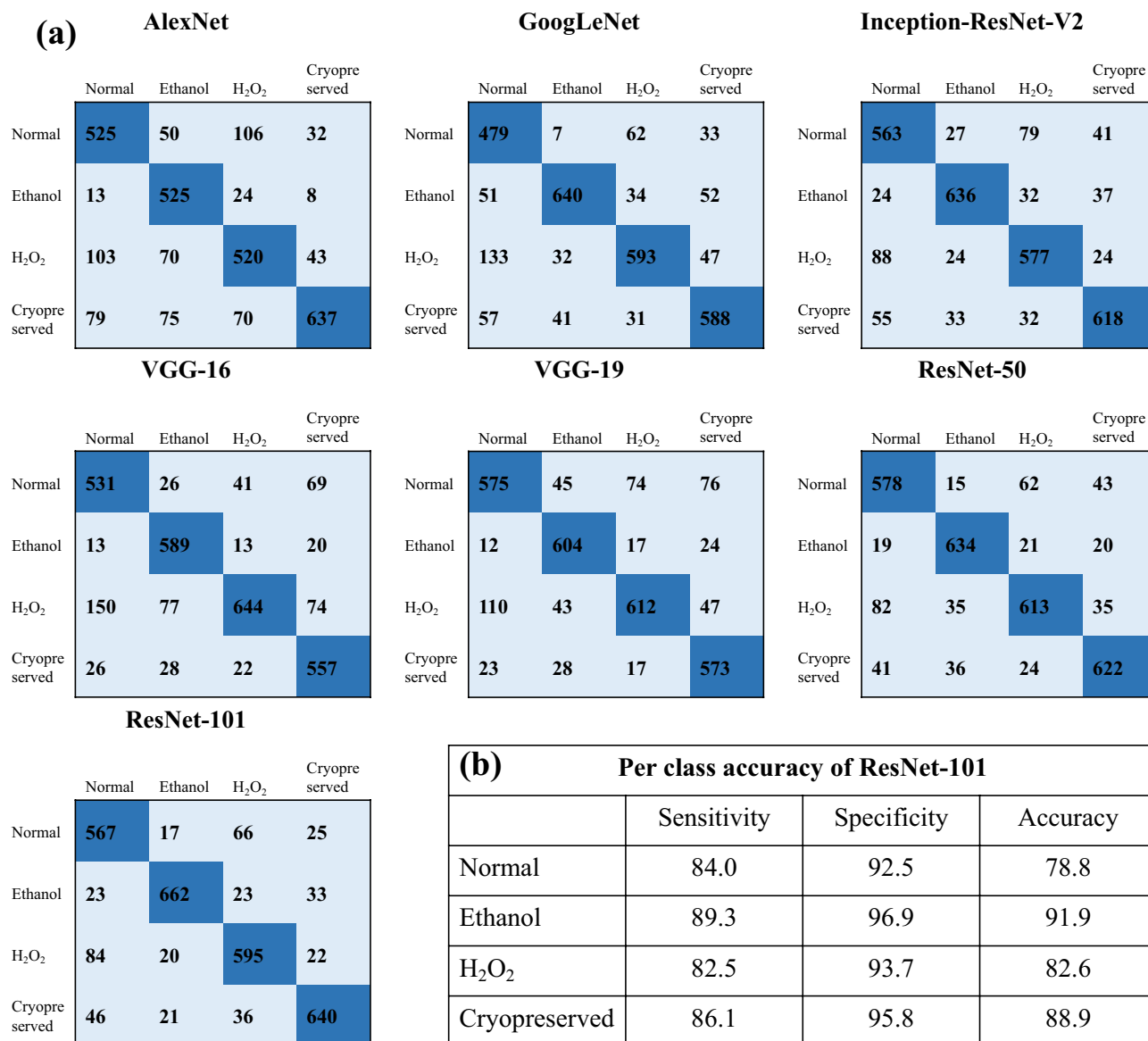
Figure 4. Quantitative phase map of human sperm cells, reconstructed from the interferogram captured by PSC-DHM system: (**a**) normal cell, (**b**) after cryopreservation, (**c**) oxidative stressed cell and (**d**) alcohol affected cell. Color bar represents the phase map in radian. Scale bar: 5 μm.

objective lens. Figure 4a–d are the quantitative phase maps of normal, cryopreserved, externally introduced ethanol and H_2O_2 sperm cells respectively. The scale bar corresponds to 5 μm distance in both x and y directions and the color bar shows the phase value in radians. A total 12,332 phase images (2,906 healthy, 2,981 cryopreserved, 3,222 ethanol and 3,223 oxidative stressed) are reconstructed from the interferometric images acquired from the proposed setup. Among the 12,332 images, only those phase images are retained which satisfy the following criteria: correct phase unwrapping, background subtraction and only one cells lies throughout the field of view. The first criterion allows for filtering of phase images that are reconstructed correctly and the later criterion is to promote accurate classification of the sperm cells using DNN. Selection of images with single cells is done automatically by converting phase image into a binary image and setting certain threshold value of white pixels. For the empirical threshold determination, a small set of images with only one cell each were hand-picked as the candidate images. The process of thresholding generally filtered away most images with multiple cells. Nonetheless, all the retained images were checked manually to assess if both the above-mentioned criteria were satisfied, so that the retained images are indeed suitable for classification purpose. A total of 10,163 phase images of sperm cells (2,400 healthy, 2,750 cryopreserved, 2,515 oxidative stressed and 2,498 alcohol affected) are thus retained.

From Fig. 4, the quantitative phase map of healthy sperm's head is found maximum as compared to the cells under different stressed conditions. The color bar represents the phase map (thickness + refractive index) in radian. Deep red indicates the maximum phase and the deep blue corresponds to zero phase. Change in phase value might indicate the change in morphology of the head of the cells under different stressed condition. However, no general trend in the maximum phase map of the cells is observed which can be explained from the progressive/non-progressive motility and number of mobile (Fig. 2) cells. Although, the number of mobile sperms get decreased as compared to the normal class, there are still some cells which are mobile. Thus, they may sustain their morphology close to normal cell and therefore, no general trend of maximum phase map is observed between these four classes.

The performance of the different DNN architectures used in this study are shown in Fig. 5. Total 70% of the data is used for the training purpose while 30% is used to test the accuracy of each model. It is important to note that sufficient training is necessary to train the network and to achieve best accuracy while validating against the test dataset. Figure 5a depicts the confusion matrices of the DNN on the testing datasets of the phase image of sperm cells. The confusion matrices show performance of the network against the testing dataset. Rows and column of the matrix indicate the predicted class and the ground truth respectively. Diagonal elements of the matrix show the correct predictions of the data while off-diagonal elements are the wrong classified data. Consider the confusion matrix of AlexNet in Fig. 5a. Total 720 phase images of the normal phase image of sperm cells are tested by the network. Out of 720, 525 phase images are predicted correctly and 13, 103 and 79 are the wrong predictions. Similarly, 525, 520 and 637 are the correct prediction by the AlexNet for Ethanol, H_2O_2 and cryopreserved cells, respectively. Performance of the GoogLeNet, Inception-ResNet-V2, VGG-16, VGG-19, ResNet-50 and ResNet-101 can be also seen in Fig. 5. Note that, the total test images are 30% of the total image (n = 9,600) i.e. 2,880 which is summation of all the elements presents in the matrix.

Figure 6 depicts the average sensitivity, specificity and classification accuracy of all deep learning architectures. Out of all DNN, ResNet-101 provides the best sensitivity, specificity and accuracy of 85.5%, 94.7%, and 85.6% respectively. Final value for ResNet-101 represents the average value of sensitivity, specificity and accuracy shown in the table of Fig. 5b. The training time for each architecture is shown in data analysis section. Though, performance of DNN classifiers is much better than the feature extraction-based machine learning classifier for the same datasets, the mismatch between ground truth and prediction of the network can be understand

(a)

AlexNet

	Normal	Ethanol	H$_2$O$_2$	Cryopre served
Normal	525	50	106	32
Ethanol	13	525	24	8
H$_2$O$_2$	103	70	520	43
Cryopre served	79	75	70	637

GoogLeNet

	Normal	Ethanol	H$_2$O$_2$	Cryopre served
Normal	479	7	62	33
Ethanol	51	640	34	52
H$_2$O$_2$	133	32	593	47
Cryopre served	57	41	31	588

Inception-ResNet-V2

	Normal	Ethanol	H$_2$O$_2$	Cryopre served
Normal	563	27	79	41
Ethanol	24	636	32	37
H$_2$O$_2$	88	24	577	24
Cryopre served	55	33	32	618

VGG-16

	Normal	Ethanol	H$_2$O$_2$	Cryopre served
Normal	531	26	41	69
Ethanol	13	589	13	20
H$_2$O$_2$	150	77	644	74
Cryopre served	26	28	22	557

VGG-19

	Normal	Ethanol	H$_2$O$_2$	Cryopre served
Normal	575	45	74	76
Ethanol	12	604	17	24
H$_2$O$_2$	110	43	612	47
Cryopre served	23	28	17	573

ResNet-50

	Normal	Ethanol	H$_2$O$_2$	Cryopre served
Normal	578	15	62	43
Ethanol	19	634	21	20
H$_2$O$_2$	82	35	613	35
Cryopre served	41	36	24	622

ResNet-101

	Normal	Ethanol	H$_2$O$_2$	Cryopre served
Normal	567	17	66	25
Ethanol	23	662	23	33
H$_2$O$_2$	84	20	595	22
Cryopre served	46	21	36	640

(b) Per class accuracy of ResNet-101

	Sensitivity	Specificity	Accuracy
Normal	84.0	92.5	78.8
Ethanol	89.3	96.9	91.9
H$_2$O$_2$	82.5	93.7	82.6
Cryopreserved	86.1	95.8	88.9

Figure 5. Performance of the deep neural networks (DNN) on the testing datasets of the phase images of sperm cells. (**a**) Confusion matrices of different DNN with number of phase images for classification of healthy and non-healthy phase map of sperm cells. Diagonal elements show number of correct predictions and the off-diagonally elements are the wrong classified observations. (**b**) Per-class sensitivity, specificity and accuracy of ResNet-101.

with following reasons. QPI offers optical thickness i.e. combine information of refractive index and thickness of the specimens but due to the lack of chemical specificity, it cannot precisely identify the changes in different organelles such as mitochondria, nucleus, DNA and the membrane of the cells. Therefore, a label free technique with high chemical specificity is required for more accurate classification of the sperm cells. Additionally, the technique must offer the quantitative changes in the sample under different stressed condition. Virtual staining[18] in the phase map of sperm cells using deep learning can improve the chemical specificity of the QPI technique. Virtual staining in the phase imaging can offer the chemical changes in the cells under different stressed condition and simultaneously the morphological changes in the cells. Therefore, combining stained information with QPI technique might improve the classification accuracy of the system.

However, a careful examination must be required during the training process and to locate the stained part i.e. head, mid-piece and tail of the cells. Any discrepancies in the training set i.e. mismatch in the correlation between stained mid-piece and phase map of mid-piece can degrade the final performance of the network. Finally, PSC-DHM can be replace with phase shifting low coherence interferometry (PS-LCI) technique[58]. PS-LCI requires multiple frames but offer superior phase sensitivity as well as lateral resolution as compare to other QPI techniques. Using, PS-LCI might help to detect the fine structural changes in the sperm cells thus will be useful to detect the healthy sperm cells with better accuracy. Nonetheless, PS-LCI requires multiple frames to
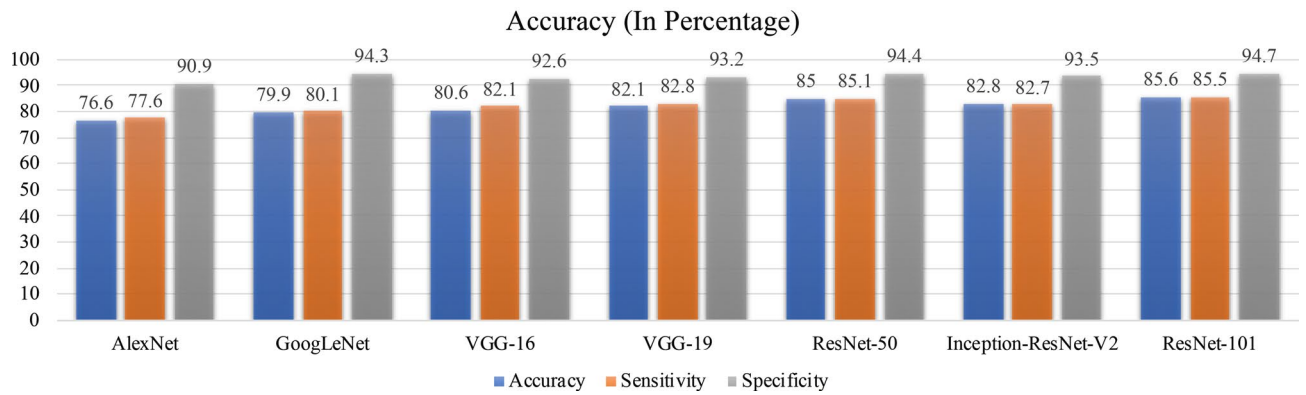
Figure 6. Sensitivity, specificity and classification accuracy of different deep neural network. The blue bar shows the average accuracy of each architectures out of which ResNet-101 provide the best accuracy (85.6%) on the testing datasets.

extract the phase map of the cells whereas PSC-DHM can extract the phase map with a single frame with high spatial phase sensitivity.

Conclusion

Our current QPI + DNN framework allows for the automated classification between normal and abnormal sperm cells. QPI is a promising technique which provides quantitative information of the sample and hence an edge over the conventional intensity-based identification of healthy cells. PSC-DHM system has been used to extract the quantitative phase map of the sperm cells enabling single shot phase reconstruction with high spatial phase sensitivity (± 20 mrad). High spatial phase sensitivity is utilized to acquire the phase map of the entire sperm cells, i.e. head, neck and tail of the sperm cells, which is otherwise difficult to image using direct laser based DHM[15]. Sperm cells after cryopreservation, oxidative stress and exposure to ethanol are imaged by the proposed setup. Previous studies show that oxidative stress initiates concentration dependent increase of DNA fragmentation because of DNA strand breaks[47]. Also, ethanol distorted the cell membrane resulting from the alteration of membrane protein structure[4]. Therefore label-free, non-invasive methods such as PSC-DHM are highly desirable to detect these changes and hence for the selection of good quality sperm for ICSI procedure that can be used to improve the success of ART however it need further clinical trials.

Quantitative analysis of sperm cells provides an opportunity to identify healthy sperm cells using deep learning approaches. Deep learning can be potentially a powerful technique for automated classification of sperm cells into normal and abnormal. Our results demonstrate that a variety of DNN architectures provide good classification accuracy to separate the 4 different type of sperm cells into their relevant classes. We also compared the proposed method with previously shown feature extraction-based machine learning models for the classification of sperm cells. However, these classifiers (SVM, Naive Bayes and KNN) provide very poor accuracy as compare to the modern DNN where ResNet-101 provided the best accuracy, i.e. 85.6%, for classification into healthy, oxidative stressed, cryopreserved and ethanol affected sperm cells. Moreover, the use of seven different network allows us to understand the capabilities of each networks and to apply best deep learning architecture for the identification of healthy cells. We applied our automated classification model for studying clinically relevant problems of semen quality in different patients attending the in-vitro fertilization clinic of University Hospital of North Norway, Norway. Fully automated classification of the sperm cells could be an intermediate tool for the expert that can be utilized for the selection of healthy sperm cells as per World Health Organization (WHO) criteria[59]. QPI + DNN framework for healthy sperm identification could be potentially used for real time selection of healthy living sperm cells that can be used for improving the success of fertilization during ART procedures.

Methods

Experimental setup. PSC-DHM is developed for quantitative phase imaging (QPI) of the sperm cells. Schematic diagram of PSC-DHM setup is shown in Fig. 1. To reduce the spatial coherence of the direct laser (He–Ne laser), it first focused by using microscopic objective lens (MO_1) and rotating diffuser is placed at the focus plane of the MO_1. Rotating diffuser scattered the light into multiple directions which captured by multi-multimode fiber bundle (MMFB). Output of MMFB consist high temporally and low spatial coherence properties and thus act as an extended light source. The extended light source coupled at an input port of the Linnik type interferometer. The light beam is first collimated and then focused by using a combination of lens L_1 (f = 50 mm) and L_2 (f = 150 mm) respectively. A beam splitter is placed to divide the focused beam into reference and sample. The sample beam is focused into the back focal plane of MO_3 (UPLSAPO 60XW, Olympus) and hence the output beam is nearly collimated to extract the accurate phase information of the sample. The light beam reflected from the sample and reference mirror, interfere at the beam splitter plane which consist the coded phase information of the sample. The interferogram is finally projected into the camera sensor (Hamamatsu ORCA-Flash4.0 LT, C11440-42U) by using a tube lens L_4 (f = 150 mm). The 2D intensity variation of an interferogram can be expressed as:

Parameter	Mean ± SD
Age (years)	34.7 ± 4.8
Semen volume (ml)	3.1 ± 1.5
Semen concentration ($\times 10^6$/ml)	51.6 ± 22.8
Total sperm count ($\times 10^6$)	166.8 ± 142.1
Progressive motility (%)	59 ± 11.9

Table 2. Age and semen quality measured before the purification by gradient method (n = 7, number of donors). Values are shown as a mean ± standard deviation (SD).

Deep neural network for classification of sperm cells	Training time (s)
AlexNet	3,222
GoogLeNet	8,359
Inception-ResNet-V2	60,992
VGG-16	5,183
VGG-19	8,783
ResNet-50	7,756
ResNet-101	16,943

Table 3. Training time of total 7 deep neural network for the classification of normal and stressed affected phase map of sperm cell.

$$I(x,y) = a(x,y) + b(x,y)\cos\left[2\pi i(f_x x + f_y y) + \phi(x,y)\right] \qquad (1)$$

where f_x and f_y are the spatial carrier frequencies of the interferogram. Background (DC) and the modulation terms are defined by $a(x,y)$ and $b(x,y)$, respectively. Phase $\phi(x,y)$ contains information of the specimen. By applying Fourier transform, the phase map of the specimen can be measured by the following expression:

$$\phi(x,y) = \tan^{-1}\left[\frac{Im(c(x,y))}{Re(c(x,y))}\right] \qquad (2)$$

where

$$c(x,y) = b(x,y)\exp(i\phi(x,y)) \qquad (3)$$

where Im and Re are the imaginary and real part of the complex signal. As the wrapped phase map lies between $-\pi$ to $+\pi$, the unwrapping is done by standard Goldstein phase unwrapping algorithm[56].

Semen preparation. The Regional Committee for Medical and Health Research Ethics of Norway (REK_nord) has approved the study. Ethical guideline was followed. At the IVF Clinic, Department of Obstetrics and Gynecology, University Hospital North Norway, Tromsø, 7 semen samples were collected from patients who were attended the IVF clinic for the service of ART. The sample were collected from the patients of age between 30 and 40 years. All patients were informed, and informed consent was obtained. The semen sample was collected according to the criteria established by the WHO[59] after 3–5 days of assistance. After liquefaction, sperm counts were evaluated using the Neubauer-improved counting chamber. All ejaculates used in the experiments meet as the good quality semen sample as per requirements of WHO 2010 (Table 2). To eliminate seminal plasma and isolate cells with good quality sperm cells, one milliliter of semen was carefully placed on each 1.5 ml of 90% and 45% gradient layers (Vitrolife, Sweeden) and centrifugated at 500g for 20 min. The resultant pellet was washed twice with human Quinn's sperm washing medium (Origio, Denmark) at 300 g for 10 min. The supernatant was discarded, and the concentration of the cells from the pellet was adjusted to 1×10^6 sperm per mL with Quinn's Advantage fertilization medium (Origio, Denmark) supplemented with 5 mg/ml Human Serum Albumin (Sigma).

To perform experiments, 96-well cell culture plates (Corning) were filled with purified sperm in a concentration of 2×10^4 cells per mL with 200 μM H_2O_2 (for oxidative stressed samples) or 2% ethanol (for alcohol affected samples), the reference chamber was filled with purified semen only. The samples were incubated for 1 h at 37 °C, 5% CO_2. After incubation evaluation of cell motility was graded according to WHO 2010 criteria as a progressive (PR) and non-progressive motility (NP). Sperm counting was performed using Neubauer-improved counting chamber and examined under the inverted phase contrast microscope at 40× magnification. Cryopreservation and thawing of purified semen were performed in accordance with Sperm Freeze medium protocol (Origio, Denmark). Motility of post-thaw spermatozoa was evaluated using Neubauer-improved counting chamber. For

the purpose of quantitative analysis by PSC-DHM the cells of each sample were transferred in a PDMS chamber on reflecting silicon. Sperm cells were immobilized by fixation with 4% PFA for 30 min at RT and washed in PBS (Phosphate-Buffer Saline, Sigma) for 5 min. Finally, fixed and attached at the surface of PDMS chamber sperm cells were mounted in PBS and covered by the cover glass of 170 μm thickness.

Data analysis. Extracting phase information from the interferogram and deep learning is implemented in MATLAB 2019a on a 64-bit Windows OS, Intel Xeon CPU E5-1650 v4 @ 3.6 GHz with 64 GB RAM and NVIDIA 2080 Ti GPU. Transfer learning is performed by using pretrained DNN and retraining them for our desired classes. Classification results are obtained by randomly assigning 70% of the images in the dataset for training and the remaining 30% for testing. The training time of each DNN can be seen in Table 3. In each training iteration, the initial learning rate is set as 10-4 and stochastic gradient descent with momentum (SGDM) is used for training. Maximum number of epochs in the learning process is set as 30.

References

1. Jouannet, P., Wang, C., Eustache, F., Kold-Jensen, T. & Auger, J. Semen quality and male reproductive health: The controversy about human sperm concentration decline. *Apmis* **109**, S48–S61 (2001).
2. Basnet, P., Hansen, S. A., Olaussen, I. K., Hentemann, M. A. & Acharya, G. Changes in the semen quality among 5739 men seeking infertility treatment in Northern Norway over past 20 years (1993–2012). *J. Reprod. Biotechnol. Fertil.* **5**, 2058915816633539 (2016).
3. Levine, H. *et al.* Temporal trends in sperm count: A systematic review and meta-regression analysis. *Hum. Reprod. Update* **23**, 646–659 (2017).
4. Virtanen, H. E., Jørgensen, N. & Toppari, J. Semen quality in the 21st century. *Nat. Rev. Urol.* **14**, 120 (2017).
5. Amann, R. P. & Waberski, D. Computer-assisted sperm analysis (CASA): Capabilities and potential developments. *Theriogenology* **81**, 5-17.e13 (2014).
6. Zinaman, M. J., Uhler, M. L., Vertuno, E., Fisher, S. G. & Clegg, E. D. Evaluation of computer-assisted semen analysis (CASA) with IDENT stain to determine sperm concentration. *J. Androl.* **17**, 288–292 (1996).
7. Daloglu, M. U. *et al.* Label-free 3D computational imaging of spermatozoon locomotion, head spin and flagellum beating over a large volume. *Light Sci. Appl.* **7**, 17121–17121 (2018).
8. Ferrara, M. A. *et al.* Label-free imaging and biochemical characterization of bovine sperm cells. *Biosensors* **5**, 141–157 (2015).
9. Henkel, R. Sperm preparation: State-of-the-art—physiological aspects and application of advanced sperm preparation methods. *Asian J. Androl.* **14**, 260 (2012).
10. Nascimento, J., Botvinick, E. L., Shi, L. Z., Durrant, B. & Berns, M. W. Analysis of sperm motility using optical tweezers. *J. Biomed. Opt.* **11**, 044001 (2006).
11. Ramalho-Santos, J. *et al.* Probing the structure and function of mammalian sperm using optical and fluorescence microscopy. *Modern Res. Educ. Topics Microsc.* **1**, 394–402 (2007).
12. Moscatelli, N. *et al.* Single-cell-based evaluation of sperm progressive motility via fluorescent assessment of mitochondria membrane potential. *Sci. Rep.* **7**, 1–10 (2017).
13. Kao, S.-H., Chao, H.-T. & Wei, Y.-H. Multiple deletions of mitochondrial DNA are associated with the decline of motility and fertility of human spermatozoa. *Mol. Human Reprod.* **4**, 657–666 (1998).
14. Da Costa, R., Amaral, S., Redmann, K., Kliesch, S. & Schlatt, S. Spectral features of nuclear DNA in human sperm assessed by Raman microspectroscopy: Effects of UV-irradiation and hydration. *PLoS ONE* **13**, e0207786 (2018).
15. Dubey, V. *et al.* Partially spatially coherent digital holographic microscopy and machine learning for quantitative analysis of human spermatozoa under oxidative stress condition. *Sci. Rep.* **9**, 1–10 (2019).
16. Martini, A. C. *et al.* Effects of alcohol and cigarette consumption on human seminal quality. *Fertil. Steril.* **82**, 374–377 (2004).
17. Di Caprio, G. *et al.* Holographic imaging of unlabelled sperm cells for semen analysis: A review. *J. Biophotonics* **8**, 779–789 (2015).
18. Rivenson, Y. *et al.* PhaseStain: The digital staining of label-free quantitative phase microscopy images using deep learning. *Light Sci. Appl.* **8**, 1–11 (2019).
19. Butola, A., Ahmad, A., Dubey, V., Senthilkumaran, P. & Mehta, D. S. Spectrally resolved laser interference microscopy. *Laser Phys. Lett.* **15**, 075602 (2018).
20. Majeed, H., Nguyen, T. H., Kandel, M. E., Kajdacsy-Balla, A. & Popescu, G. Label-free quantitative evaluation of breast tissue using Spatial Light Interference Microscopy (SLIM). *Sci. Rep.* **8**, 1–9 (2018).
21. Lee, M. *et al.* Label-free optical quantification of structural alterations in Alzheimer's disease. *Sci. Rep.* **6**, 31034 (2016).
22. Doblas, A. I., Sánchez-Ortiga, E., Martínez-Corral, M., Saavedra, G. & Garcia-Sucerquia, J. Accurate single-shot quantitative phase imaging of biological specimens with telecentric digital holographic microscopy. *J. Biomed. Opt.* **19**, 046022 (2014).
23. Sridharan, S., Macias, V., Tangella, K., Kajdacsy-Balla, A. & Popescu, G. Prediction of prostate cancer recurrence using quantitative phase imaging. *Sci. Rep.* **5**, 1–10 (2015).
24. Shan, M., Kandel, M. E. & Popescu, G. Refractive index variance of cells and tissues measured by quantitative phase imaging. *Opt. Express* **25**, 1573–1581 (2017).
25. Kim, T. *et al.* White-light diffraction tomography of unlabelled live cells. *Nat. Photonics* **8**, 256 (2014).
26. Nguyen, T. H., Kandel, M. E., Rubessa, M., Wheeler, M. B. & Popescu, G. Gradient light interference microscopy for 3D imaging of unlabeled specimens. *Nat. Commun.* **8**, 1–9 (2017).
27. Daloglu, M. U. *et al.* 3D imaging of sex-sorted bovine spermatozoon locomotion, head spin and flagellum beating. *Sci. Rep.* **8**, 1–9 (2018).
28. Park, Y., Depeursinge, C. & Popescu, G. Quantitative phase imaging in biomedicine. *Nat. Photonics* **12**, 578–589 (2018).
29. Jo, Y. *et al.* Quantitative phase imaging and artificial intelligence: A review. *IEEE J. Sel. Top. Quantum Electron.* **25**, 1–14 (2018).
30. Mirsky, S. K., Barnea, I., Levi, M., Greenspan, H. & Shaked, N. T. Automated analysis of individual sperm cells using stain-free interferometric phase microscopy and machine learning. *Cytometry Part A* **91**, 893–900 (2017).
31. Butola, A. *et al.* Volumetric analysis of breast cancer tissues using machine learning and swept-source optical coherence tomography. *Appl. Opt.* **58**, A135–A141 (2019).
32. Girshovitz, P. & Shaked, N. T. Generalized cell morphological parameters based on interferometric phase microscopy and their application to cell life cycle characterization. *Biomed. Opt. Express* **3**, 1757–1773 (2012).

33. Butola, A. *et al.* Deep learning architecture LightOCT for diagnostic decision support using optical coherence tomography images of biological samples. arXiv preprint, arXiv:1812.02487 (2018).
34. Li, F. *et al.* Deep learning-based automated detection of retinal diseases using optical coherence tomography images. *Biomed. Opt. Express* **10**, 6204–6226 (2019).
35. Fanous, M., Keikhosravi, A., Kajdacsy-Balla, A., Eliceiri, K. W. & Popescu, G. Quantitative phase imaging of stromal prognostic markers in pancreatic ductal adenocarcinoma. *Biomed. Opt. Express* **11**, 1354–1364 (2020).
36. Falk, T. *et al.* U-Net: Deep learning for cell counting, detection, and morphometry. *Nat. Methods* **16**, 67–70 (2019).
37. Wang, H. *et al.* Deep learning enables cross-modality super-resolution in fluorescence microscopy. *Nat. Methods* **16**, 103–110 (2019).
38. Choi, G. *et al.* Cycle-consistent deep learning approach to coherent noise reduction in optical diffraction tomography. *Opt. Express* **27**, 4927–4943 (2019).
39. Song, Y. *et al.* A deep learning based framework for accurate segmentation of cervical cytoplasm and nuclei. In *36th Annual International Conference of the IEEE Engineering in Medicine and Biology Society,* 2903–2906 (2014).
40. Ozaki, Y. *et al.* Label-free classification of cells based on supervised machine learning of subcellular structures. *PLoS ONE* **14**, e0211347 (2019).
41. Chaveiro, A., Machado, L., Frijters, A., Engel, B. & Woelders, H. Improvement of parameters of freezing medium and freezing protocol for bull sperm using two osmotic supports. *Theriogenology* **65**, 1875–1890 (2006).
42. Watson, P. F. The causes of reduced fertility with cryopreserved semen. *Anim. Reprod. Sci.* **60**, 481–492 (2000).
43. Wongtawan, T., Saravia, F., Wallgren, M., Caballero, I. & Rodríguez-Martínez, H. Fertility after deep intra-uterine artificial insemination of concentrated low-volume boar semen doses. *Theriogenology* **65**, 773–787 (2006).
44. Agarwal, A., Prabakaran, S. A. & Said, T. M. Prevention of oxidative stress injury to sperm. *J. Androl.* **26**, 654–660 (2005).
45. Lemma, A. Effect of cryopreservation on sperm quality and fertility. *Artif. Insemin. Farm Anim.* **12**, 191–216 (2011).
46. Ramírez-Reveco, A., Hernández, J. L. & Aros, P. Long-term storing of frozen semen at −196 °C does not affect the post-thaw sperm quality of bull semen. *Cryopreserv. Eukaryot.* 91 (2016).
47. Donnelly, E. T., McClure, N. & Lewis, S. E. Antioxidant supplementation in vitro does not improve human sperm motility. *Fertil. Steril.* **72**, 484–495 (1999).
48. Ingólfsson, H. I. *et al.* Lipid organization of the plasma membrane. *J. Am. Chem. Soc.* **136**, 14554–14559 (2014).
49. Kopeika, J., Thornhill, A. & Khalaf, Y. The effect of cryopreservation on the genome of gametes and embryos: Principles of cryobiology and critical appraisal of the evidence. *Hum. Reprod. Update* **21**, 209–227 (2015).
50. Donnelly, E. T., Steele, E. K., McClure, N. & Lewis, S. E. Assessment of DNA integrity and morphology of ejaculated spermatozoa from fertile and infertile men before and after cryopreservation. *Hum. Reprod.* **16**, 1191–1199 (2001).
51. Woolley, D. & Richardson, D. Ultrastructural injury to human spermatozoa after freezing and thawing. *Reproduction* **53**, 389–394 (1978).
52. Ozkavukcu, S., Erdemli, E., Isik, A., Oztuna, D. & Karahuseyinoglu, S. Effects of cryopreservation on sperm parameters and ultrastructural morphology of human spermatozoa. *J. Assist. Reprod. Genet.* **25**, 403–411 (2008).
53. Barthelemy, C. *et al.* Ultrastructural changes in membranes and acrosome of human sperm during cryopreservation. *Arch. Androl.* **25**, 29–40 (1990).
54. O'connell, M., McClure, N. & Lewis, S. The effects of cryopreservation on sperm morphology, motility and mitochondrial function. *Hum. Reprod.* **17**, 704–709 (2002).
55. Takeda, M., Ina, H. & Kobayashi, S. Fourier-transform method of fringe-pattern analysis for computer-based topography and interferometry. *JOSA* **72**, 156–160 (1982).
56. Goldstein, R. M., Zebker, H. A. & Werner, C. L. Satellite radar interferometry: Two-dimensional phase unwrapping. *Radio Sci* **23**, 713–720 (1988).
57. Goodfellow, I., Bengio, Y. & Courville, A. *Deep Learning* (MIT press, Cambridge, 2016).
58. Iwai, H. *et al.* Quantitative phase imaging using actively stabilized phase-shifting low-coherence interferometry. *Opt. Lett.* **29**, 2399–2401 (2004).
59. Organization, WH. *World Health Statistics 2010* (World Health Organization, Geneva, 2010).

Acknowledgements

Author contributions

B.S.A., D.S.M., P.B., G.A. and P.S. discussed the project idea. The samples were provided by P.B., who also sought the permission and ethical clearances for this study. P.B., D.P. and G.A. provided biological insights for this study. Samples were prepared by D.P. PSC-DHM system is developed by A.B., A.A. and J.C.T. AH designed and optimize the rotating diffuser and provide the sample substrate to perform the experiment. Experimental data are acquired by A.B. The support for DNN architectures, training, and performance evaluation was provided by D.K.P. in close collaboration with A.B. A.B. and D.P. prepared first draft of the manuscript and all author contributed towards writing of the manuscript. The work is supervised by P.B. and B.S.A.

Competing interests

The authors declare no competing interests.

Additional information

Supplementary information is available for this paper at https://doi.org/10.1038/s41598-020-69857-4.

Correspondence and requests for materials should be addressed to B.S.A.

Reprints and permissions information is available at www.nature.com/reprints.

Publisher's note Springer Nature remains neutral with regard to jurisdictional claims in published maps and institutional affiliations.

Paper IV

Sperm mitochondrial DNA copy numbers in normal and abnormal semen analysis: a systematic review and meta-analysis.

Daria Popova, Priya Bhide, Francesco D'Antonio, Purusotam Basnet, Ganesh Acharya

Submitted for publication

Sperm mitochondrial DNA copy numbers in normal and abnormal semen analysis: a systematic review and meta-analysis.

| Abstract: | Background:
Normal mature sperm have a considerably reduced number of mitochondria which provide the energy required for progressive sperm motility. Literature suggests that disorders of sperm motility may be linked to abnormal sperm mitochondrial number and function.
Objectives:
To summarise the evidence from literature regarding the association of mitochondrial DNA copy numbers and semen quality with a particular emphasis on the spermatozoa motility.
Search strategy:
Standard methodology recommended by Cochrane.
Selection criteria:
All published primary research reporting on differences in mitochondrial DNA copy numbers between the sperm of males with a normal and abnormal semen analysis.
Data collection and analysis:
Using standard methodology recommended by Cochrane we pooled results using a random effects model and the findings were reported as a standardised mean difference.
Main results:
We included 10 trials. The primary outcome was sperm mitochondrial |

DNA copy numbers. A meta-analysis including five studies showed significantly higher mitochondrial DNA copy numbers in abnormal semen analysis as compared to normal semen analysis(SMD 1.08, 95% CI 0.74-1.43). Three other studies not included in the meta-analysis showed a significant negative correlation between mitochondrial DNA copy numbers and semen parameters. The quality of evidence was assessed as good to very good in 60% of studies.
Conclusions:
Our review demonstrates significantly higher mitochondrial DNA in human sperm cells of men with abnormal semen analysis in comparison to men with normal semen analysis.
PROSPERO registration:
CRD42019118841
Funding
None received

SCHOLARONE™
Manuscripts

1 **Title page**

2

3 **Sperm mitochondrial DNA copy numbers in normal and abnormal**

4 **semen analysis: a systematic review and meta-analysis.**

5

6 Daria Popova[1] M.Sc, Priya Bhide[1,2] MD, FRCOG, Francesco D'Antonio[3] MD, PhD,

7 Purusotam Basnet[1] PhD, Ganesh Acharya[1,4] MD, PhD, FRCOG

8

9 [1] Women´s Health and Perinatology Research Group, Department of Clinical Medicine, UiT-

10 The Arctic University of Norway, Tromsø, Norway.

11 [2] Homerton Fertility Centre, Homerton University Hospital, London, UK.

12 [3] Department of Obstetrics and Gynecology, Centre for Fetal Care and High-risk Pregnancy,

13 University of Chieti, Italy.

14 [4] Division of Obstetrics and Gynecology, Department of Clinical Science, Intervention and

15 Technology, Karolinska Institutet and Center for Fetal Medicine, Karolinska University

16 Hospital, Stockholm, Sweden.

17

18 Corresponding author

19 Priya Bhide

20 Homerton Fertility Centre, Homerton University Hospital, London, UK.

21 +442085107660

22 priya.bhide@nhs.net

Abstract

Background:

Normal mature sperm have a considerably reduced number of mitochondria which provide the energy required for progressive sperm motility. Literature suggests that disorders of sperm motility may be linked to abnormal sperm mitochondrial number and function.

Objectives:

To summarize the evidence from literature regarding the association of mitochondrial DNA copy numbers and semen quality with a particular emphasis on the spermatozoa motility.

Search strategy:

Standard methodology recommended by Cochrane.

Selection criteria:

All published primary research reporting on differences in mitochondrial DNA copy numbers between the sperm of males with a normal and abnormal semen analysis.

Data collection and analysis:

Using standard methodology recommended by Cochrane we pooled results using a random effects model and the findings were reported as a standardised mean difference.

Main results:

We included 10 trials. The primary outcome was sperm mitochondrial DNA copy numbers. A meta-analysis including five studies showed significantly higher mitochondrial DNA copy numbers in abnormal semen analysis as compared to normal semen analysis(SMD 1.08, 95% CI 0.74-1.43). Three other studies not included in the meta-analysis showed a significant negative correlation between mitochondrial DNA copy numbers and semen parameters. The quality of evidence was assessed as good to very good in 60% of studies.

Conclusions:

Our review demonstrates significantly higher mitochondrial DNA in human sperm cells of men with abnormal semen analysis in comparison to men with normal semen analysis.

PROSPERO registration:

CRD42019118841

55   Capsule:

56   There is significantly higher mitochondrial DNA in human sperm cells of men with abnormal

57   semen analysis in comparison to men with normal semen analysis

58

Introduction

60   Mitochondria are one of the fundamental cell organelles providing the cell with energy in the

61   form of adenosine triphosphate (ATP) by the process of oxidative phosphorylation

62   (OXPHOS). The amount of mitochondria varies with cell type and function (1). The process

63   of spermatogenesis results in a drastic decrease in the number of mitochondria (2). This pre-

64   fertilisation reduction in sperm mitochondrial content is aimed to reduce/eliminate paternal

65   mitochondrial transmission in conjunction with other post-fertilisation mechanisms resulting

66   in uniparental inheritance. Mature sperm are thought to contain between 22–75 mitochondria

67   providing the energy required for progressive sperm motility (3). Sperm motility is dependent

68   on the energy provided by OXPHOS (4).

69   It has been suggested that male infertility and disorders of sperm motility may be linked to

70   abnormal sperm mitochondrial number and function. Male infertility has been reported in

71   men with mitochondrial disorders (5). Also, associations between abnormalities of sperm

72   mitochondrial DNA and abnormal sperm parameters have been reported (6). Early reports

73   available on mitochondrial DNA quantification in mammalian sperm present widely varying

74   results (2, 7). In humans, few studies report the association of mitochondrial DNA copy

75   number (mtDNAcn) with sperm motility and other semen characteristics (8-10).

76   The aim of this review is to summarize the evidence from literature regarding the association

77   of mtDNAcn and semen quality with a particular emphasis on the spermatozoa motility. This

78   aims to guide clinical practice and give direction for future research.

Materials and methods

80   Eligibility criteria:

81   Our search aimed to identify all published literature reporting on differences in mtDNAcn

82   between the sperm of males with a normal semen analysis and males with abnormal semen

83   analysis. All types of studies published as primary research were included for the review. We

84   included only those studies published in the English language, published as full manuscripts

85   (not abstracts) and those involving humans-only. We included studies where semen

86   samples were analysed based on either the WHO 1999 or 2010 criteria. The protocol for

87   undertaking the review was developed following recommendations of CRD's guidance for

88   undertaking reviews in health care (Centre for Reviews and Dissemination) (11). Results

89   were reported in accordance with PRISMA guidelines (12). The review was prospectively

90   registered with PROSPERO (CRD42019118841).

91   Assessment of study quality and the risk of bias:

92   Assessment of study quality was done using the Newcastle-Ottawa Scale (NOS) modified

93   for cross sectional studies. Further modification was used as only non-interventional

94   observational studies were included. We conducted a comprehensive search for eligible

95   studies in order to minimize the impact of reporting bias.

96   Main outcome measures

97   The primary outcome measure was sperm mitochondrial DNA copy numbers.

98   Data sources

99   DP and FD independently screened and identified studies which were relevant for the

100 review. Standard Cochrane methodology was followed comprising electronic searches and

101 hand searching. Embase Classic and Ovid MEDLINE were searched on December 07,

102 2020. The study period was from 1946 to 2020. We used the controlled vocabulary of

103 Medical Subject Headings (MeSH) terms "Male Infertility" and 17 additional keywords related

104 to or describing the participants and/or outcome (e.g. asthenospermia, oligospermia, sperm

105 quality). The detailed search strategy for MEDLINE and Embase can be found in

106 Supplementary Materials Appendix S1. We updated our search by re-conducting the search

107 1 month prior to submission of the review for publication. The reference lists of relevant

108 articles were screened to identify additional studies.

109 Data collection

110 DP and FD independently screened the title, abstract and keywords (ti,ab,kw) of the

111 retrieved articles. The full text of potentially suitable articles was retrieved. From these

112 suitable articles were finalised for inclusion for the review. Agreement regarding potential

113 relevance was reached by consensus. Inconsistencies were discussed among the reviewers

114 and resolved by discussion with a third author. Conference abstracts were excluded from the

115 quantitative analyses to avoid publication bias.

116 DP and FD reviewed all selected articles and extracted relevant data regarding study

117 characteristics independently. Data were collected on a bespoke data collection Excel sheet

118 where data were collected for study design, methodology, participant characteristics and

119 outcome variables. Multiple publications of a single study were pooled together under a

120 single study ID. All identified references were exported to EndNote X 8.2 for Windows,

121 where the list of publications was scanned for duplicates.

Data analysis and synthesis:

123 The pooled estimates for the outcome were presented as Standardised Mean Difference

124 (SMD) with 95% confidence intervals using the random effects model and inverse variance

125 method. Statistical significance was assumed when $p<0.05$. In case where the information in

126 the studies was not reported in the way appropriate for our data extraction, the authors were

127 contacted. We were able to get this information for the study Tian 2014 (10), and have

128 updated our analysis accordingly. Studies were excluded from meta-analyses if the data

129 were presented using correlation analyses and without dividing the semen of patients into

130 categories (normal/abnormal) or using different laboratory methodology.

Results

General characteristics of studies

Results of the search:

134 The search of the two electronic databases retrieved 373 full text articles after removal of

135 duplicates. No further articles were retrieved by hand searching of the reference lists. After

136 screening of the titles and abstracts, the full text of 19 studies were retrieved for further

137 review. 10 of these studies were selected for the systematic review and 9 excluded. Of the

138 10 selected studies, five were suitable for meta-analysis and included for quantitative

139 synthesis. The search and selection process are documented with a PRISMA flow chart in

140 Figure 1 and the list of included and excluded studies with reasons for exclusion provided in

141 Supplementary Materials, Table S1.

Included studies:

143 The characteristics of the included studies are detailed in Supplementary Materials, Table

144 S2.

Study design and setting:

146 The 10 studies included in this systematic review were all single-centre observational cross-

147 sectional studies conducted across eight countries. Only five studies had a sample size of

148 greater than 100 participants which we feel is satisfactory for providing good quality

149 evidence. The largest study was conducted by Diez-Sanchez 2003 (13) from Spain and

150 included 440 participants.

151 Participants:

152 Eight of the 10 studies recruited participants from fertility clinics, denoting a convenience

153 sampling strategy, with only one of these studies recruiting healthy volunteers as controls.

154 Two studies recruited volunteer donors for their studies. Only five of the 10 studies

155 accounted for confounding factors such as age, BMI and lifestyle factors in the design and/or

156 analysis stage of their studies. Hence, the comparability of the participants in the included

157 studies or within study groups cannot be estimated. The study group for five of the 10

158 studies included in the meta-analyses comprised of men with abnormal semen analysis. The

159 criteria for abnormal semen analysis however showed significant heterogeneity. Some

160 studies reported results based on the WHO 1999 criteria whereas others used the WHO

161 2010 criteria. Some studies included men with only reduced sperm motility and normal

162 sperm counts as the abnormal semen analysis for the study group. Few studies divided the

163 abnormal results into subgroups, these however were dissimilar amongst the studies and

164 hence it was not possible to conduct a subgroup analysis for a pooled estimate.

165 Outcome:

166 All studies reported the mtDNA/nuclear DNA ratio expressing the average mitochondrial DNA

167 copy number per sperm. The values for the ratio variables differed considerably between the

168 studies, which might be explained by the methodological differences in interventions. The

169 concept however remained constant across the studies. The ratios were compared between

170 patients with normal and abnormal WHO semen criteria. Two studies compared mtDNA

171 content between sperm cells from the same semen sample in addition to mtDNA content from

172 the different patients (May-Panloup 2003; Diez-Sanchez 2003).

173 Five of the 10 included studies reported the primary outcome as a mean +/- SD/SEM. Two

174 studies reported the median + IQR/range. One study which reported the mean without a SD

175 had to be excluded from the meta-analysis (9). Three studies reported the correlation between

176 sperm mitochondrial DNA with sperm parameters rather than differences amongst defined

177 groups with normal and abnormal semen parameters(13-15). One study used a different

178 methodology for estimation of DNA (16). These studies were not included in the meta-analysis.

179 Assessment of outcome:

180 The method of mtDNAcn assessment is a multistep process and varied amongst studies. The

181 time range between the first study and the last was 16 years, which can impact on the technical

182 differences between the former and the latter experiments. In general, to quantify

183 mitochondrial DNA copy number, polymerase chain reaction (PCR) assay using specific

184 primers to mitochondrial genes was used in the studies. To quantify the number of

185   spermatozoa in the sample, nuclear DNA was determined. The relative mtDNA copy number
186   was identified based on the mtDNA/nuclear DNA ratio.

187   The first step toward mtDNA quantification is a semen sample purification from the other cell
188   types, i.e., leukocytes, round cells, epithelial cells, and miscellaneous debris. The fresh semen
189   samples were purified using various methods such as a combined density gradient
190   centrifugation and a swim-up method (May-Panloup 2003) (8), only-Percoll density gradient
191   centrifugation (Amaral 2007; Bonanno 2016; Wu 2019) (14, 17, 18), Ficol-Paque fractionation
192   (Kao 2004) (16), or without washing at all (Faja 2019) (19). Tian (2014) (10) used
193   cryopreserved semen samples that have been thawed with subsequent washing in
194   phosphate-buffered saline (PBS) and sperm-wash buffer. The absence of round cells in sperm
195   preparations was checked by light microscopy in all studies. In two studies, semen samples
196   underwent osmotic shock to eliminate the non-gamete cell component (Kao 2004, Faja 2019).

197   Various commercial DNA isolation kits were used by eight of ten included studies according
198   to the manufacturer's instructions to extract total DNA. In two studies (Kao 2004 and Diez-
199   Sanchez 2003) the total DNA was extracted using the phenol-chloroform method. May-
200   Panloup 2003, Diez-Sanchez 2003, Kao 2004, Amaral 2007, and Song 2008 reported
201   supplementation with dithiothreitol (DTT) and proteinase K to dissociate mitochondria from the
202   mitochondrial sheath and disrupt the sperm nucleus disulfide bonds (20). The other three
203   studies used only proteinase K as part of commercial DNA isolation kit (Tian 2014, Wu 2018,
204   Faja 2019) or there was not any specification in the study or manufacturer's manual (Bonanno
205   2016, Zhang 2016).

206   Amplification of nuclear and mitochondrial genes was carried out by real-time PCR (qPCR) in
207   eight of ten studies to determine the amount of mtDNA relative to nDNA. The mtDNA copy
208   number per sperm cell was measured relative to a nuclear gene, for example, ß-globin gene
209   (May-Panloup 2003, Kao 2004, Amaral 2007, Tian 2014), Glyceraldehyde 3-phosphate
210   dehydrogenase - GAPDH gene (Song 2008, Bonanno 2016, Zhang 2016), calicin gene (Faja
211   2019), or gene of RNase P (Wu 2019). In the study of Diez-Sanchez (2003) mtDNAcn was
212   determined by slot-blot hybridization using specific mitochondrial (16S rRNA) and nuclear
213   probes (to 18S human rRNA). Kao and colleagues (2004) used a hot-start concurrent PCR to
214   determine the amount of mtDNA relative to nuclear DNA. PCR products of mitochondrial ND1
215   and nuclear genes ß-actin were blotted onto a membrane for relative intensity measurement.
216   This ratio was an index of the relative amount (copy number) of mtDNA with respect to nuclear
217   DNA.

218   Melting curve analyses were done to verify the accuracy and specificity of genes amplification.
219   Serial dilutions of recombinant plasmids containing mtDNA insert were used as the external

220 standard to establish a quantitative reference for mtDNA quantification (May-Panloup 2003,
221 Diez-Sanchez 2003, Kao 2004, Song 2008, Tian 2014;,Bonanno 2016). In the study of Amaral
222 2007, the external standard for qPCR was double-stranded DNA molecules. The linearity of
223 the standard curve indicated the efficiency of PCR over the whole process.

224 The relative mtDNA copy number was calculated using the formula mtDNAcn/nuclear gene
225 copy number in all studies. In the study Faja 2019, fluorescence data were converted to cycle
226 threshold (Ct) for each gene. The relative mtDNA content was obtained by calculating the ΔCt
227 (ΔCt=CtCOII − Ctcalicin) for each sample and applying the exponential function $2^{-\Delta Ct}$ (17).

Quality of evidence and the risk of bias:

229 The quality of evidence assessed by the NOS was good to very good in 6 of the 10 studies,
230 and no study was considered unsatisfactory. 70% of studies were downgraded due to the
231 use of convenience sampling and 50% for small sample sizes included. The results are
232 summarized in Supplementary Materials, Appendix S2.

Synthesis of the results:

234 Of the 10 studies reporting on differences in sperm mitochondrial DNA, five studies with 530
235 participants were included in the quantitative meta-analysis (Amaral 2007, Bonanno 2016,
236 Faja 2019, May Panloup 2003, Tian 2014)(8, 10, 17-19). The results are seen in Figure 2. A
237 significant difference in sperm mitochondrial DNA copy numbers was seen between the
238 normal and abnormal semen analysis groups (SMD 1.08, 95% CI 0.74-1.43). All five
239 included studies reported higher sperm mitochondrial DNA copy numbers in abnormal
240 semen samples as compared to normal semen samples. Significant statistical heterogeneity
241 was noted (Tau^2=0.09, Chi^2=10.23, df=4, p< 0.04, I^2=61%). Three studies reported a
242 significant negative correlation between mitochondrial DNA copy numbers and semen
243 parameters (8, 14, 15).

Subgroup analysis

245 No subgroup analysis was done due to dissimilar subgroups of abnormal semen analysis.

Discussion

Main findings:

248 Our systematic review and meta-analysis of data showed a significant difference in sperm
249 mitochondrial DNA copy numbers in human sperm cells with abnormal parameters in
250 comparison to normal sperm cells. Three studies reported a negative correlation between
251 mtDNAcn and (1) sperm motility (Tian 2014, Bonano 2016, Faja 2019), (2) total sperm count
252 (Song 2008), (3) sperm concentration per mL (Amaral 2007, Tian 2014) and (4) morphology

253 (Amaral 2007) between patients with abnormal semen parameters and control groups. Animal
254 studies also support the findings of this review, that increased mtDNAcn is associated with
255 decreased total sperm motility (21) A single study reported a large effect size but an opposite
256 direction of effect (16). This could be attributed to a different method for estimation of DNA.

257 Semen is a complex fluid containing different cell types. Besides leucocytes, immature germ
258 cells, white blood cells, and epithelial cells, there is variation in sperm population regarding
259 motility and morphology. Namely, motility within one semen sample can be graded as
260 progressive, non-progressive, and immotile. In order to eliminate seminal plasma, diploid cells
261 of different etiology, and separate sperm according to motility and morphology semen
262 purification was applied in nine of ten studies as described in the outcome assessment section.
263 Hence, the assessment of mtDNAcn was done using sperm cells selected from the best
264 fraction of semen population between different men. Moreover, in two studies by Diez-
265 Sanchez (2003) and May-Panloup (2003), they compared mtDNA content between sperm
266 cells from different populations of the same sample without taking into account the initial sperm
267 quality. It was found that cells from the semen fraction of worse quality had higher mtDNA
268 quantity than sperm cells from the fraction of better quality (8, 13).

269 The WHO criteria classifies abnormal semen analysis into three major groups;
270 asthenospermia (A), oligospermia (O), and teratospermia (T) and their different combinations
271 such as AOT, AO, OT, and AT (22). Our review indicates that those who have more than two
272 abnormal criteria have in average increased number of mtDNA copies. Amaral 2007 analyzed
273 the mtDNAcn between three male fertility groups: normal, with 1 or 2 sperm defects or more
274 than to defects (AOT). The group including three defects (AOT) as low sperm number,
275 decreased motility, and abnormal morphology statistically differed from the normal group
276 (P<0.01) and from 1- or 2- defects group (P<0.05). Comparing all groups one by one, there
277 was a significant negative correlation between mtDNAcn/sperm concentration (R=-0.561,
278 P<0.001) and mtDNAcn/sperm morphology (R=-0.467, P<0.002). At the same time, mtDNA
279 content per sperm from the group with the only motility defect did not differ significantly from
280 the sperm of normal group, but there was a trend towards correlation (R=-0.285, P=0.067).
281 This is similar to the negative correlation of mtDNAcn and motility in the study of Tian 2014
282 (r=-0.37; P<0.001). This data also corresponds to the results of May-Panloup 2003 where
283 semen with the only abnormal criteria (A or T or O) was not significantly different from the
284 mtDNAcn in the normal group. However, highly significant difference was detected between
285 patients with normal sperm and the group including multiple abnormalities (O, A, T, OA, AT,
286 OAT) (P<0.0001) (8). The results of Song 2008 are are in agreement with the studies of
287 Amaral 2007 and May-Panloup 2003 that mtDNAcn increased in the group of multiple

288　abnormalities (AOT) compared with normal semen and patients with the only abnormal semen
289　criteria (P<.05, Tukey test).

290　Two studies report mitochondrial DNA quantity specifically for asthenozoospermic patients in
291　comparison to healthy men. In the study of Bonanno 2016, the analysis was performed in 37
292　patients with idiopathic asthenospermia, i.e., with a high percentage of sperm with low motility.
293　The increased quantity of mtDNAcn was detected in 45.8% of patients, that correlated with
294　high reactive oxygen species (ROS) production. At the same time, Faja 2019 reported
295　mtDNAcn analyses on 63 asthenozoospermic samples with progressive motility less than
296　32%. There was a significant correlation between mtDNAcn and total motile spermatozoa (r=-
297　0.51, P<0.001), sperm concentration per mL (r=-0.50, P<0.001), and total sperm count per
298　ejaculate (r=-0.44, P<0.001). It is important to note that in the study of Faja 2019) there was
299　no sperm purification with cell selection regarding motility or morphology. That implies that
300　analysis was done on the general sperm population that might result in a higher level of
301　correlation rate in comparison to studies with sperm selection through semen purification.

Strengths and limitations

303　To our knowledge, the review is the first to assess the human sperm mitochondrial DNA copy
304　numbers. Despite the general trend between the studies, there is a wide range of mtDNA
305　quantities. Several possible aspects result in a wide variation of outcomes such as duplication
306　of the mitochondrial genome in nuclear DNA, the use of inappropriate primes, the bias of
307　dilution, the low efficiency of total DNA extraction (23). Among other things, accurate
308　quantification of mtDNA depends on the residual contamination of somatic cells in the
309　analyzed sample. Thus, Diez-Sanchez 2003 revealed a positive correlation between the
310　percentage of round cells in the semen sample and the relative amount of sperm mtDNA (13).
311　Considering the susceptible nature of mitochondrial DNA to degradation, there may be
312　deletions in the analyzed gene region due to oxidative stress. This may result from the
313　presence of leucocytes which active producers of extracellular ROS in semen (24). Hence, it
314　might be reasonable to determine mtDNAcn in sperm cells using several mitochondrial genes.

315　The study population may also affect the outcomes. It has been shown that the semen quality
316　depends on the geographical region, as shown for the US and Europe (25, 26). Moreover,
317　seasonal variation of sperm concentration and total sperm count has also been reported (26).
318　All these factors may cause the mtDNA count variation in sperm cells.

Interpretation

320　The mechanisms behind the association of mtDNAcn and abnormal semen parameters are
321　still unknown. Several explanations have been proposed. The mature human spermatozoa
322　contains residual quantities of mtDNA which is decreased during spermatogenesis. Rantanen

323 and Larsson proposed the hypothesis of mtDNAcn decrease during spermatogenesis through
324 downregulation of Tfam proteins in spermatids, which is known to be the transcription and
325 replication regulator of mitochondrial DNA (27-29). Adverse external factors or genetic issues
326 may affect to the process of spermatogenesis to prevent this normal reduction in mtDNA.
327 Sometimes, these changes might have a compensatory value; for instance, Jiang and
328 colleagues demonstrated on the mouse model that the increase of mtDNAcn can improve a
329 severe disease phenotype caused by mtDNA mutations in testis (30)(43). Hence, the level of
330 normal mtDNA without mutation will be higher, but the mtDNA mutation load remains the
331 same.

332 Based on the results mentioned above, the mtDNA copy number may potentially have a
333 prognostic value for fertility and ART outcomes. A few studies presented the connection
334 between mtDNAcn in sperm and clinical outcomes during ART procedures (13, 31-33) . For
335 example, Tieg 2020 reveals no relationship between live birth rates, fertilization, usable
336 blastocyst development, and blastocyst euploid rates with sperm mtDNAcn from infertile
337 patients undergoing IVF with ICSI (28). It is possible that the sperm cell selected for ICSI had
338 lower mtDNAcn than other cells from the same semen because of a heterogenic population
339 of sperm cells. Simultaneously, Tieg's 2020 analysis has confirmed the association of lower
340 relative mtDNAcn with increased sperm motility. Another study by Rosati 2020 revealed the
341 association of mtDNAcn with lower pregnancy probability within 12 months and a longer time
342 to pregnancy. The pregnancy probabilities decreased linearly with higher mtDNAcn (31). The
343 association of mtDNAcn of sperm cells and early ART outcomes was also analyzed by Wu
344 2019. The results suggest that sperm with higher mtDNAcn may result in lower odds of embryo
345 development to Day 3 and Day 5 (33).

346 Regardless of the effect on ART's clinical outcomes, the levels of mtDNAcn may be used as
347 a predictor of spermatogenic dysfunction in men. Gabriel and colleagues suggested mtDNAcn
348 as an indicator of spermatogenesis's efficiency based on the significant decrease of mtDNA
349 quantity after varicocelectomy (34). Furthermore, the mtDNA content may play a role of a
350 bioindicator of environmental pollutants such as an air pollutants exposure (35), polycystic
351 aromatic hydrocarbons (PAHs) resulted in reproductive health problems (36), and synthetic
352 organic chemicals as monocarboxy-isononyl phthalate, which were positively associated with
353 mtDNAcn (37). Prolonged exposure to SO_2 is negatively associated with mitochondrial
354 quantity (35). Another study by Luo (2012) revealed the increase of mtDNAcn with hypoxic
355 conditions at high altitudes (5.300m) (38). Given the reversible effect on sperm quality and
356 mtDNA content of environmental and some external factors such as sexual abstinence before
357 the collection of the semen, heating, cigarette smoking, and lifestyle, Wu 2019 suggests that

1

358   mtDNAcn might be suited as an indicator of male reproductive status on the ground of
359   consecutive diagnoses rather than a single abnormal sample (14).

360   ## Conclusion

361   In this review, we have demonstrated a significantly higher number of mtDNA in human sperm
362   cells of men with abnormal semen analysis in comparison to men with normal semen analysis.
363   It is important to note that the quantity of mtDNA rises with the increase in semen abnormal
364   parameters. Besides, the heterogeneous sperm cell population in the semen creates sperm
365   variation of mtDNA copy number within the same sample. These findings would seem to
366   suggest the predictive value of mitochondrial DNA quantification for male reproductive status
367   assessment.

368   ## Acknowledgments

373   ## Disclosure of interests

374   None declared. Completed disclosure of interests forms available to view online as
375   supporting information.

376   ## Contribution to authorship

377   DP and PB contributed equally to the conception, planning, execution, analysis, writing and
378   final approval of the manuscript. FD contributed to literature search, study selection, data
379   extraction and assessment of study quality. PBa revised the article critically for important
380   intellectual content. GA contributed to the conception and planning, and revised the article
381   critically for important intellectual content.

382   ## Ethical approval

383   Not needed

384   ## Funding

References

386

387   1.   Anderson S, Bankier AT, Barrell BG, de Bruijn MH, Coulson AR, Drouin J, et al.
388   Sequence and organization of the human mitochondrial genome. Nature.
389   1981;290(5806):457-65.

390   2.   Hecht NB, Liem H, Kleene KC, Distel RJ, Ho SM. Maternal inheritance of the mouse
391   mitochondrial genome is not mediated by a loss or gross alteration of the paternal
392   mitochondrial DNA or by methylation of the oocyte mitochondrial DNA. Dev Biol.
393   1984;102(2):452-61.

394   3.   Bahr GF, Engler WF. Considerations of volume, mass, DNA, and arrangement of
395   mitochondria in the midpiece of bull spermatozoa. Exp Cell Res. 1970;60(3):338-40.

396   4.   Ruiz-Pesini E, Diez C, Lapena AC, Perez-Martos A, Montoya J, Alvarez E, et al.
397   Correlation of sperm motility with mitochondrial enzymatic activities. Clin Chem. 1998;44(8
398   Pt 1):1616-20.

399   5.   Folgero T, Bertheussen K, Lindal S, Torbergsen T, Oian P. Mitochondrial disease
400   and reduced sperm motility. Hum Reprod. 1993;8(11):1863-8.

401   6.   Ruiz-Pesini E, Lapena AC, Diez C, Alvarez E, Enriquez JA, Lopez-Perez MJ.
402   Seminal quality correlates with mitochondrial functionality. Clin Chim Acta. 2000;300(1-2):97-
403   105.

404   7.   Manfredi G, Thyagarajan D, Papadopoulou LC, Pallotti F, Schon EA. The fate of
405   human sperm-derived mtDNA in somatic cells. Am J Hum Genet. 1997;61(4):953-60.

406   8.   May-Panloup P, Chretien MF, Savagner F, Vasseur C, Jean M, Malthiery Y, et al.
407   Increased sperm mitochondrial DNA content in male infertility. Hum Reprod. 2003;18(3):550-
408   6.

409   9.   Song GJ, Lewis V. Mitochondrial DNA integrity and copy number in sperm from
410   infertile men. Fertil Steril. 2008;90(6):2238-44.

411   10.   Tian M, Bao H, Martin FL, Zhang J, Liu L, Huang Q, et al. Association of DNA
412   methylation and mitochondrial DNA copy number with human semen quality. Biol Reprod.
413   2014;91(4):101.

414   11.   Systematicreviews S. CRD's guidance for undertaking reviews in health care.
415   University of York,: Centre for Reviews and Dissemination; 2009 [

416   12.   Moher D, Liberati A, Tetzlaff J, Altman DG, The PG. Preferred Reporting Items for
417   Systematic Reviews and Meta-Analyses: The PRISMA Statement. PLOS Medicine.
418   2009;6(7):e1000097.

419   13.   Diez-Sanchez C, Ruiz-Pesini E, Lapena AC, Montoya J, Perez-Martos A, Enriquez
420   JA, et al. Mitochondrial DNA content of human spermatozoa. Biol Reprod. 2003;68(1):180-5.

421   14.   Wu H, Huffman AM, Whitcomb BW, Josyula S, Labrie S, Tougias E, et al. Sperm
422   mitochondrial DNA measures and semen parameters among men undergoing fertility
423   treatment. Reprod Biomed Online. 2019;38(1):66-75.

424   15.   Zhang G, Wang Z, Ling X, Zou P, Yang H, Chen Q, et al. Mitochondrial Biomarkers
425   Reflect Semen Quality: Results from the MARCHS Study in Chongqing, China. PLoS One.
426   2016;11(12):e0168823.

427   16.   Kao SH, Chao HT, Liu HW, Liao TL, Wei YH. Sperm mitochondrial DNA depletion in
428   men with asthenospermia. Fertil Steril. 2004;82(1):66-73.

429   17.   Amaral A, Ramalho-Santos J, St John JC. The expression of polymerase gamma
430   and mitochondrial transcription factor A and the regulation of mitochondrial DNA content in
431   mature human sperm. Hum Reprod. 2007;22(6):1585-96.

432   18.   Bonanno O, Romeo G, Asero P, Pezzino FM, Castiglione R, Burrello N, et al. Sperm
433   of patients with severe asthenozoospermia show biochemical, molecular and genomic
434   alterations. Reproduction. 2016;152(6):695-704.

435   19.   Faja F, Carlini T, Coltrinari G, Finocchi F, Nespoli M, Pallotti F, et al. Human sperm
436   motility: a molecular study of mitochondrial DNA, mitochondrial transcription factor A gene
437   and DNA fragmentation. Mol Biol Rep. 2019;46(4):4113-21.

438   20.   Sutovsky P, Tengowski MW, Navara CS, Zoran SS, Schatten G. Mitochondrial
439   sheath movement and detachment in mammalian, but not nonmammalian, sperm induced
440   by disulfide bond reduction. Mol Reprod Dev. 1997;47(1):79-86.

441   21.   Hesser A, Darr C, Gonzales K, Power H, Scanlan T, Thompson J, et al. Semen
442   evaluation and fertility assessment in a purebred dog breeding facility. Theriogenology.
443   2017;87:115-23.

444   22.   WHO WHO. WHO Laboratory Manual for the Examination and Processing of Human
445   Semen. Geneva: World Health Organisation,; 2010.

446   23.   Malik AN, Czajka A. Is mitochondrial DNA content a potential biomarker of
447   mitochondrial dysfunction? Mitochondrion. 2013;13(5):481-92.

448   24.   Kang D, Hamasaki N. Mitochondrial oxidative stress and mitochondrial DNA. Clin
449   Chem Lab Med. 2003;41(10):1281-8.

450   25.   Swan SH, Brazil C, Drobnis EZ, Liu F, Kruse RL, Hatch M, et al. Geographic
451   differences in semen quality of fertile U.S. males. Environ Health Perspect. 2003;111(4):414-
452   20.

453   26.   Jorgensen N, Andersen AG, Eustache F, Irvine DS, Suominen J, Petersen JH, et al.
454   Regional differences in semen quality in Europe. Hum Reprod. 2001;16(5):1012-9.

455   27.   Rantanen A, Larsson NG. Regulation of mitochondrial DNA copy number during
456   spermatogenesis. Hum Reprod. 2000;15 Suppl 2:86-91.

457   28.   Larsson NG, Oldfors A, Garman JD, Barsh GS, Clayton DA. Down-regulation of
458   mitochondrial transcription factor A during spermatogenesis in humans. Hum Mol Genet.
459   1997;6(2):185-91.

460   29.   Larsson NG, Wang J, Wilhelmsson H, Oldfors A, Rustin P, Lewandoski M, et al.
461   Mitochondrial transcription factor A is necessary for mtDNA maintenance and
462   embryogenesis in mice. Nat Genet. 1998;18(3):231-6.

463   30.   Jiang M, Kauppila TES, Motori E, Li X, Atanassov I, Folz-Donahue K, et al. Increased
464   Total mtDNA Copy Number Cures Male Infertility Despite Unaltered mtDNA Mutation Load.
465   Cell Metab. 2017;26(2):429-36 e4.

466   31.   Rosati AJ, Whitcomb BW, Brandon N, Buck Louis GM, Mumford SL, Schisterman
467   EF, et al. Sperm mitochondrial DNA biomarkers and couple fecundity. Hum Reprod.
468   2020;35(11):2619-25.

469   32.   Tiegs AW, Tao X, Landis J, Zhan Y, Franasiak JM, Seli E, et al. Sperm Mitochondrial
470   DNA Copy Number Is Not a Predictor of Intracytoplasmic Sperm Injection (ICSI) Cycle
471   Outcomes. Reprod Sci. 2020;27(6):1350-6.

472   33.   Wu H, Whitcomb BW, Huffman A, Brandon N, Labrie S, Tougias E, et al.
473   Associations of sperm mitochondrial DNA copy number and deletion rate with fertilization
474   and embryo development in a clinical setting. Hum Reprod. 2019;34(1):163-70.

475   34.   Gabriel MS, Chan SW, Alhathal N, Chen JZ, Zini A. Influence of microsurgical
476   varicocelectomy on human sperm mitochondrial DNA copy number: a pilot study. J Assist
477   Reprod Genet. 2012;29(8):759-64.

478   35.   Zhang G, Jiang F, Chen Q, Yang H, Zhou N, Sun L, et al. Associations of ambient air
479   pollutant exposure with seminal plasma MDA, sperm mtDNA copy number, and mtDNA
480   integrity. Environ Int. 2020;136:105483.

481 36.	Ling X, Zhang G, Sun L, Wang Z, Zou P, Gao J, et al. Polycyclic aromatic

482	hydrocarbons exposure decreased sperm mitochondrial DNA copy number: A cross-

483	sectional study (MARHCS) in Chongqing, China. Environ Pollut. 2017;220(Pt A):680-7.

484 37.	Huffman AM, Wu H, Rosati A, Rahil T, Sites CK, Whitcomb BW, et al. Associations of

485	urinary phthalate metabolites and lipid peroxidation with sperm mitochondrial DNA copy

486	number and deletions. Environ Res. 2018;163:10-5.

487 38.	Luo Y, Liao W, Chen Y, Cui J, Liu F, Jiang C, et al. Altitude can alter the mtDNA copy

488	number and nDNA integrity in sperm. J Assist Reprod Genet. 2011;28(10):951-6.

489

Figure 1: PRISMA Flow chart
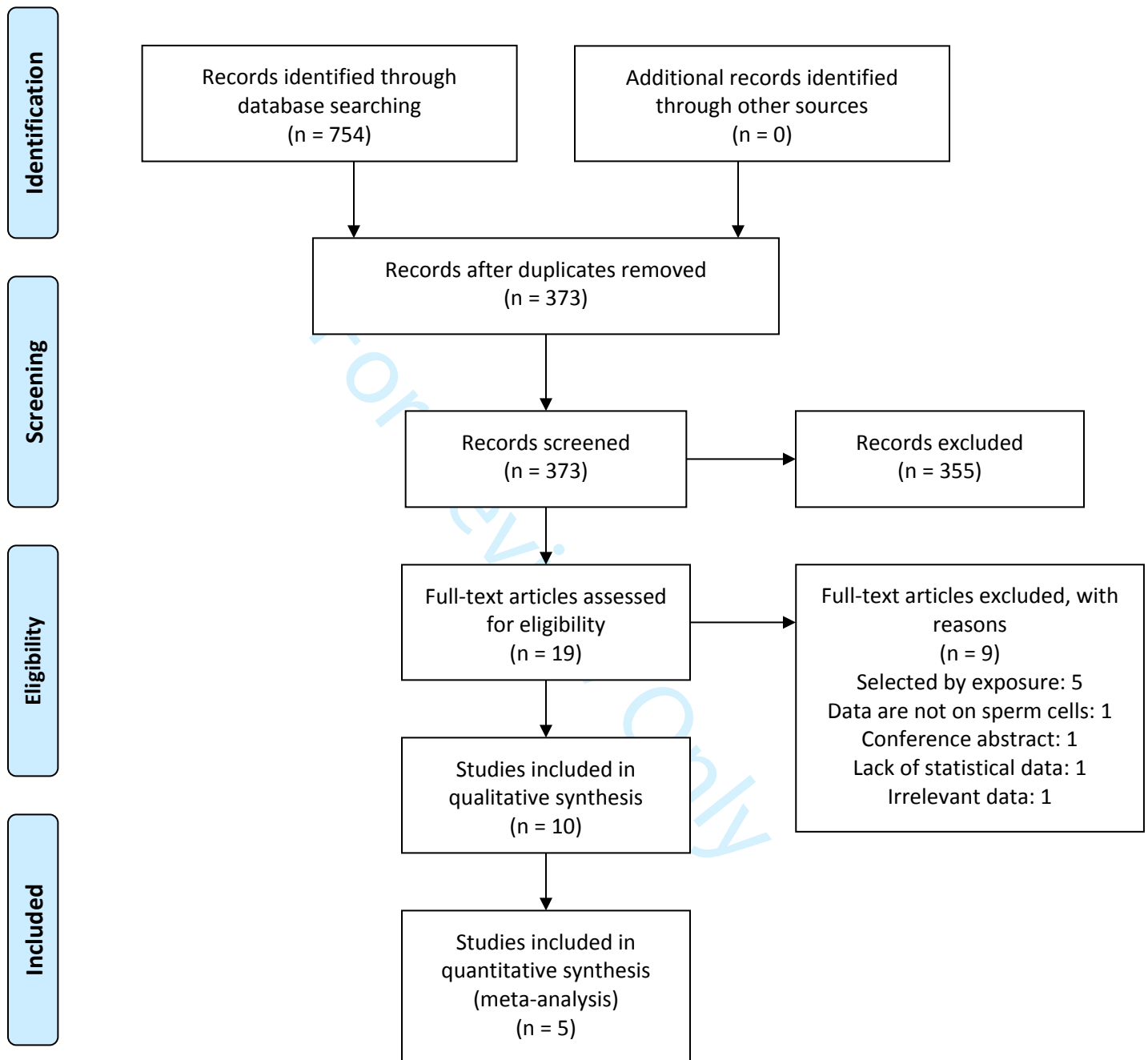
For more information, visit www.prisma-statement.org.

Figure 2: Forest plot of comparison of mtDNA between normal and abnormal semen analysis

Study or Subgroup	Abnormal semen analysis			Normal semen analysis			Weight	Std. Mean Difference IV, Random, 95% CI	Std. Mean Difference IV, Random, 95% CI
	Mean	SD	Total	Mean	SD	Total			
Amaral 2007	29	44.47	28	6.8	6.73	14	15.1%	0.59 [-0.06, 1.25]	
Bonanno 2016	18.21	14.12	37	5.69	2.33	22	17.6%	1.09 [0.53, 1.66]	
Faja 2019	73	57.6	63	29.6	23.3	63	24.2%	0.98 [0.61, 1.35]	
May–Panloup 2003	6.1	6.88	35	1.4	0.98	32	19.5%	0.93 [0.42, 1.43]	
Tian 2014	103.11	138.13	35	16.77	3.74	201	23.6%	1.63 [1.24, 2.02]	
Total (95% CI)			198			332	100.0%	1.08 [0.74, 1.43]	

Heterogeneity: Tau² = 0.09; Chi² = 10.23, df = 4 (P = 0.04); I² = 61%
Test for overall effect: Z = 6.19 (P < 0.00001)

Favours [Abnormal semen]   Favours [Normal semen an]

[Type here]